Department of Environmental, Land and Infrastructure Engineering - DIATI

MASTER'S DEGREE IN ENVIRONMENTAL AND LAND ENGINEERING

ENHANCED RETENTION OF PFAS BY AIR-SPARGING

Supervisors:

Prof. Rajandrea Sethi

Prof. Poul L. Bjerg

Annika S. Fjordbøge

Laura Morsing

Candidate:

Alessandra Pertoso

Academic Year 2024/25

TABLE OF CONTENT

LIST OF ABBREVIATIONS

6:2 FTAB: 6:2 Fluorotelomer Sulfonamide Alkylbetaine;
6:2 FTS: 6:2 Fluorotelomersulfonic Acid;
CAS: Chemical Abstract Service;
CMC: Critical Micelle Concentration;
DNAPL: Dense Non-Aqueous Phase Liquid;
LNAPL: Light Non-Aqueous Phase Liquid;
NAPL: Non-Aqueous Phase Liquid;
PFAA: Perfluoroalkyl Acids;
PFAS: per- and polyfluoroalkyl substances;
PFASAs: Perfluoroalkane Sulfonamides Acids;
PFBS: Perfluorobutanesulfonic Acid;
PFCAs: Perfluoroalkyl Carboxylic Acids;
PFHpA: Perfluoroheptanoic Acid;
PFHxA: Perfluorohexanoic Acid;
PFHxS: Perfluorohexanesulfonic Acid;
PFNA: Perfluorononanoic Acid;
PFOA: Perfluorooctanoic acid;
PFOS: Perfluorooctanesulfonic acid;
PFOSA: Perfluorooctanesulfonamide;
PFPAs: Perfluorophosphonic/-phoshoric acids;
PFPeA: Perfluoropentanoic Acid;
PFSAs: Perfluoroalkane Sulfonic Acids;
POPs: Persistent Organic Pollutants;
VOCs: Volatile Organic Compounds;
ZOI: Zone of Influence;

1. INTRODUCTION

Per- and polyfluoroalkyl substances (PFAS) are a group of more than ten thousand synthetic chemicals (ECHA, 2023), currently present either in commercial use or dispersed in the environment and characterized by a wide range of chemical and physical properties (ITRC, 2023). Recent inventory of PFAS identified more than 4,700 PFAS with Chemical Abstracts Service (CAS) Registry Numbers that may be on the global market (OECD, 2021). Some PFAS are characterized by persistence and mobility that combined with decades of extensive use in industrial applications - as for firefighting foams, galvanization, and paints - have led to their presence in natural media worldwide. First discovered in the 1950s, they have recently come to the attention of both the public and the scientific community. This renewed interest is due to findings that their levels in natural media could lead to potential human health effects, given their bioaccumulative nature and possible carcinogenicity.

In particular, the International Agency for Research on Cancer (IARC) has evaluated the carcinogenicity of perfluorooctanoic acid (PFOA) and perfluorooctanesulfonic acid (PFOS). In recent years growing concerns about PFAS contamination have prompted regulatory agencies to take action to prevent their further spread and to protect human health (Abunada et al., 2020). As a result, PFOS, PFOA, their salts and related compounds have been classified as Persistent Organic Pollutants (POPs) by the European Chemical Agency (ECHA, 2023). The European regulation establishes specific limits for the concentration of PFAS in water intended for human consumption. According to Italian regulations, the threshold limits are set for a sum of 24 PFAS, compared to 20 PFAS established by the EU. In 2021 the Danish EPA sharpened the European quality criteria for PFAS in groundwater to 2 ng/l for the sum of 4 PFAS, and to 100 ng/l for the sum of 22 PFAS (Danish EPA, 2021).

Over 15,000 potentially PFAS-contaminated sites have been identified in Denmark, representing a serious risk to the country's drinking water resources (Danske Regioner, 2024). Characterized by a chemical structure like surfactants, PFAS transport in the vadose zone is governed by solid-phase sorption and accumulation at the air-water interface, a unique feature of this contaminant compared to other pollutants. PFAS are very mobile and persistent to natural and chemical degradation, so it is highly challenging to remediate PFAS-contaminated sites (Darlington et al., 2019). Current groundwater remediation technologies capable of destroying contaminants in situ are either highly costly or less practical for addressing PFAS source zones or plumes. For example, bioremediation has not yet been successfully implemented in the field and most studies suggest that PFAS undergo only partial biotransformation into PFAA end products (Newell et al., 2021).

In situ air-sparging is a remediation technique, successfully used since 1985 (Suthersan et al., 2017), usually implemented for saturated soils and groundwater contaminated by volatile organic compounds (VOCs). Its widespread use is primarily due to its cost-effectiveness in treating large aquifer volumes due to the zones of influence (ZOI) that can be achieved for each sparge well (Newell et al., 2021). The remediation processes that occur with air-sparging are volatilization or stripping of VOCs and biodegradation of aerobically biodegradable contaminants. Its implementation for remediation of PFAS-contaminated sites has not been considered until 2021, since most PFAS aren't highly volatile and biodegradable. A study conducted by Newell et al. in 2021 exploits the partition of PFAS to the air-water interfaces through air-sparging that would concentrate PFAS directly from the aquifer to the water table. PFAS, due to their surface-active properties, exhibit partitioning to the air-water interface. During air-sparging, they are driven upwards by the buoyant force of the sparged gas and subsequently accumulate at the air-water interface in the capillary fringe (Newell et al., 2021). Then, the reduction of PFAS plume and their accumulation in the upper part of the aquifer facilitate their removal through vacuum pump or skimmers. So far, these considerations remain purely theoretical and have only been explored in laboratory settings, since the effectiveness and the feasibility of the implementation of this technology with PFAS plumes must be verified.

The overall aim of this project is to assess the potential of air-sparging for shrinking PFAS-contaminated plumes, by promoting PFAS vertical migration within the saturated zone to enhance their retention at the air-water interface in the capillary fringe. To conduct this study, column experiments in the laboratory are designed and performed, followed by sample analysis from the column and data processing of the obtained results. To fulfil the aim, the specific objectives to be reached are:

- Investigate the physical and chemical properties of PFAS, with focus on PFAS partition to the air-water interface and the potential benefit of application of an air-sparging remediation technology.
- Design a laboratory column experiment capable of replicating the capillary fringe between vadose and saturated zones, ensuring uniform air flow through sand and enabling PFAS vertical migration and retention at the air-water interface.
- Analyze differences in vertical migration of a mixture of short- and long- chained PFAS and precursors during air-sparging in different porous media, such as homogeneous fine and coarse sand using column tests in the laboratory.
- Evaluate the effectiveness of air-sparging in retaining PFAS, taking into account the differing behaviors between short- and long-chained PFAS, as well as terminal PFAS and precursors.
- Assess the feasibility of in situ air-sparging as a method for retaining PFAS within the capillary fringe, while considering the potential long-term remobilization of the concentrated PFAS layer.

2. PER- AND POLYFLUOROALKYL SUBSTANCES

2.1 CHEMICAL DESCRIPTION

In 2011, Buck et al. defined PFAS as aliphatic substances in which one or more carbon atoms have all their hydrogen substituents, present in the nonfluorinated analogues, replaced by fluorine atoms. This structural modification ensures that PFAS contain the perfluoroalkyl moiety C_nF_{2n+1}. PFAS substances are composed of perfluoroalkyl and polyfluoroalkyl substances. Perfluoroalkyl substances are defined as aliphatic substances for which all the H atoms attached to C atoms in the nonfluorinated substance have been replaced by F atoms, except those H atoms of the functional groups present. Instead in polyfluoroalkyl compounds all H atoms attached to at least one, but not all C atoms have been replaced by F atoms, in such a manner that they contain the perfluoroalkyl moiety C_nF_{2n+1}(Buck et al., 2011). A PFAS family tree with two main classes- polymers and nonpolymers- organizes this range of PFAS with various characteristics. Numerous subclasses, groups and subgroups may exist within each class; some of them are depicted in Figure 2.1.

Non-polymers	Polymers
Perfluoroalkyl substances Compounds for which all hydrogen atoms on all carbon atoms (except for carbon atoms associated with functional groups) have been replaced by fluorine atoms, such as: • Perfluoroalkyl acids **(PFAA)** - Perfluoroalkyl carboxylic acids (PFCAs) - Perfluoroalkane sulfonic acids (PFSAs) • PFAA precursors such as: - Perfluoroalkane sulfonamides (FASAs) - Perfluoroalkyl iodides (PFAIs)	**Side-chain fluorinated polymers** Non-fluorinated polymer backbone of variable composition with polyfluorinated side chains, such as: • Fluorinated acrylate and methacrylate polymers • Fluorinated urethane polymers • Fluorinated oxetane polymers • Fluorinated siloxanes polymers **Fluoropolymers** Carbon-only polymer backbone with fluorine atoms directly attached, such as: • Polytetrafluoroethylene (PTFE) • Polyvinylidene fluoride (PVDF) • Fluoroelastomer (FKM) **Perfluoropolyethers** Carbon and oxygen (ether) polymer backbone with fluorine atoms directly attached to carbon atoms
Polyfluoroalkyl substances Compounds for which all hydrogen atoms on at least one (but not all) carbon atoms have been replaced by fluorine atoms, such as: • n:2 Fluorotelomer alcohols (n:2 FTOHs) • n:2 Fluorotelomer carboxylic acids (n:2 FTCAs) • Polyfluoroalkyl phosphoric acid diesters (diPAPs)	
PFAS gases Compounds such as: • Hydrofluorocarbons (HFCs) • Perfluorocarbons (PFCs) • Hydrofluoroethers (HFEs)	
Other non-polymeric PFASs A number of PFASs in various groups such as: • Active substances in plant protection products, biocidal products and pharmaceuticals with $-CF_3$ moieties • Other side-chain fluorinated aromatics • Perfluoroalkanes (non-gaseous) • Perfluoroalkyl-tert-amines	

Figure 2.1 Overview of groups of PFASs (Buck et al., 2011; Danske Regioner, 2024; ECHA, 2023)

Perfluoroalkyl acids (PFAAs) are among the simplest PFAS molecules. They are highly persistent and do not degrade under normal environmental conditions. Many polyfluoroalkyl substances can undergo biotic and abiotic transformations, often leading to the formation of PFAAs. Because of their stability, PFAAs are sometimes referred to as “terminal PFAS” or “terminal transformation products”, meaning they do not degrade further in the environment. Polyfluoroalkyl substances that degrade into terminal PFAAs are known as “precursors”. Additionally, longer-chain PFAAs are not known to biotransform into shorter-chain PFAAs (ITRC, 2023).

The type of functional group determines industrial use, solubility in water, persistence in the environment and bioaccumulation in organisms. The three types of functional groups considered in this study are carboxylic

acids (-COOH), sulfonic acids (-SO_3H) and fluorotelomers (-CH_2CH_2-X). The first have intermediate stability and high persistence, whereas the sulfonic acids have great solubility and extremely high persistence; the former are precursors.

The functional head charge, whether it is anionic, cationic or zwitterionic, is another difference. Anionic PFAS exhibit more mobility compared to cationic or zwitterionic PFAS (Newell et al., 2022).

In this study, ten representative PFAS were selected to ensure a balanced representation of both terminal PFAS and precursors, including carboxylic, sulfonic acids and fluorotelomers, anionic and zwitterionic species, as well as a mix of long- and short-chained compounds (see Tab. 5.2).

2.2 PHYSICOCHEMICAL PROPERTIES

Understanding PFAS transport and fate requires knowledge of their physicochemical properties, which are often uncertain due to limited measured data and reliance on predictive models (ITRC, 2023). These properties vary with carbon chain length, functional group, and environmental conditions. General trends can still be identified.

2.2.1 PHYSICAL PROPERTIES

At room temperature, the majority of PFAS are solids, frequently crystalline or powdered, although shorter-chained compounds typically take on a liquid state (ITRC, 2023). It is rare for PFAS to appear in the environment as a distinct phase, such as solid PFAS, LNAPL PFAS or DNAPL PFAS, because of its great aqueous solubility (ITRC, 2023). At high concentrations, aqueous PFOA and PFOS solutions have been shown to exhibit floating separate-phase liquid layers on their surface (J. Costanza et al., 2019). However, rather than density, the tendency of PFAAs to concentrate and aggregate at air-water interfaces seems to be what drives the creation of these layers (ITRC, 2023).

Early studies on PFAAs suggested that they behave like traditional surfactants, forming both micelles and mixed micelles (Pedone et al., 1997; Downer et al., 1999). Due to the distinct behavior of hydrophilic ‘head’ and hydrophobic ‘tail’, traditional surfactants, containing hydrocarbon chain, tend to aggregate into micelles in water when their concentration exceeds a certain threshold. Surfactants can also form other supramolecular assemblies, such as hemi-micelles or mixed micelles (Fig. 2.2), either freely in solution or at phase boundaries (ITRC, 2023). Some observed properties of PFAS do not fully align with conventional micelle formation theory. For instance, certain reported critical micelle concentration (CMC) values exceed the known solubility limits of the corresponding compounds. Additionally, some researchers propose that PFAA supramolecular aggregation is far more complex in the environmental settings than the simple micelle formation observed in single-compound systems (ITRC, 2023).

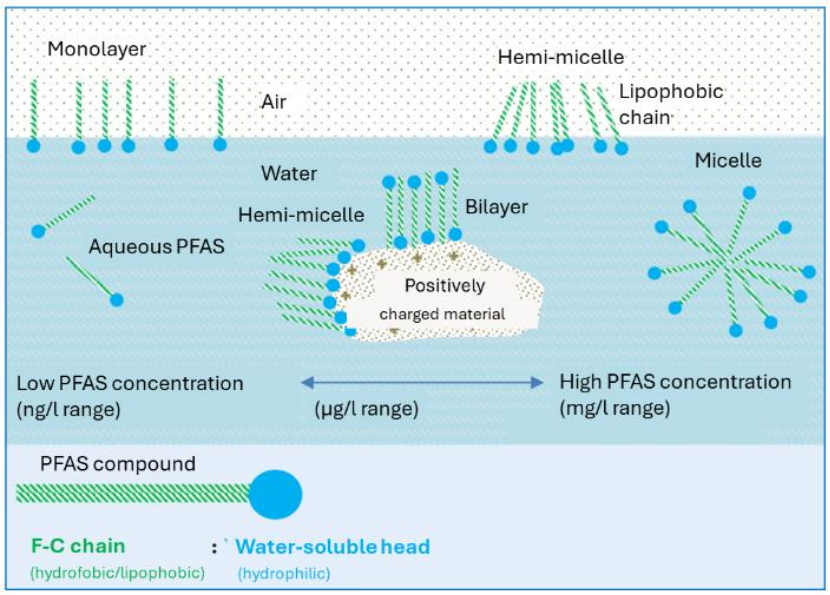

Figure 2.2 Overview of the different binding sites for PFAS; mono-layer, hemi-micelle, micelle, air-water and soil-water (VMR, 2022)

It has been hypothesized that PFAA aggregation may occur at concentrations much lower than the CMC in groundwater due to interaction with particles, co-contaminants, hemi-micelle formation, or spatially variable concentrations within soil matrices (Johnson et al., 2007; Yu et al., 2009). These complex supramolecular interactions, combined with adsorption processes at interfaces such as the air-water interface, suggest that PFAS behavior in the environment is highly intricate and not yet fully understood (ITRC, 2023).

Furthermore, the amphiphilic nature of PFAAs leads to the accumulation at fluid-fluid interfaces, such as air-water or NAPL-water boundaries, aligning themselves so that their hydrophobic tails extend into the air while their hydrophilic heads remain in the water (Fig. 2.3) (Krafft & Riess, 2015a).

Most data on solubility, vapor pressure and Henry's Law constant have been determined through extrapolation or modelling (ITRC, 2023). Reported values may vary depending on the method used to determine each property, as well as factors such pH, salinity, temperature. In many cases, PFAS exhibit high solubility, low vapor pressure and low Henry's Law constant, meaning they tend to remain in the aqueous phase without significant volatilization or stripping.

Figure 2.3 Illustration of the interfaces at which PFAS can be distributed in the unsaturated zone. The figure illustrates that PFAS can sorb to the soil, adsorb to the air-water interface, and be dissolved in the water phase (Guo et al., 2020; Morsing et al., 2025)

2.2.2 CHEMICAL PROPERTIES

The unique properties of PFAS primarily stem from the characteristics of the carbon-fluorine (C-F) bond. The high electronegativity and small atomic size of fluorine contribute to the formation of an exceptionally strong C-F bond, recognized as the strongest covalent bond in organic chemistry (Kissa E., 2001). Additionally, fluorine's low polarizability results in weak intermolecular interactions, such as Van der Waals forces and hydrogen bonding (Kissa E., 2001). These distinctive fluorine-related properties confer many PFAS dual hydro- and lipophobic nature, surfactant behavior, and remarkable thermal and chemical stability (ITRC, 2023).

2.3 SHORT- AND LONG- CHAINED PFAS

PFAS can be divided into long-chained and short-chained, considering that, according to the Organization for Economic Co-operation and Development (OECD, 2011) "long-chained" refers to

- perfluoroalkyl carboxylic acids with seven or more C-F bonds
- perfluoroalkane sulfonates with six or more C-F bonds

Short-chain PFAS are more water-soluble and hydrophilic than long-chained PFAS. Due to the strong carbon-fluorine bond, short-chain PFAAs are considered highly persistent, much like long-chained PFAAs (Parsons et al., 2008; Vierke et al., 2012). They resist both abiotic and biotic degradation under environmental conditions and are regarded as stable end-products formed from the breakdown of the precursors (D'Agostino & Mabury, 2017; Wang et al., 2013). Because of their low adsorption potential, short-chained PFAAs remain largely dissolved in the water phase and show minimal binding to particles (Brendel et al., 2018).

Table 2.1 Vapor pressure, Henry's law constant and water solubility between short- and long-chained PFAS and PFAA (Brendel et al., 2018; D'Agostino & Mabury, 2017; Li et al., 2020; Parsons et al., 2008; Vierke et al., 2012; Wang et al., 2013)

PFAS type	Vapor pressure	Henry's Law Constant	Water solubility
Long-chained PFAS	Low	Low	Low, tends to adsorb to soil's particles and sediments
Long-chained PFAA	Extremely low	Very low, tend to remain in aqueous phase	Higher, due to acidic nature
Short-chained PFAS	Higher, but lower than VOCs	Higher, but limited volatility	High, high mobility and diffusion in water
Short-chained PFAA	Low	Low, tend to remain in aqueous phase	Very high

2.4 PRECURSORS AND TERMINAL PFAS

Another distinction refers to precursors and terminal PFAAs. Some PFAS precursors degrade into terminal PFAAs that pose risks to human health (Sunderland et al., 2018). During this process, persistent intermediate compounds can also form, with different mobility and transformation behavior compared to the primary compounds (Harding-Marjanovic et al., 2015; Yi et al., 2018). Studies show that precursor biotransformation occurs more slowly under anaerobic conditions and results in different products than under oxic conditions (Yi et al., 2018; Zhang et al., 2013). The main differences between precursors and terminal PFAAs in terms of physicochemical properties relate to their stability, solubility, volatility and environmental behavior.

2.5 HEALTH EMERGENCY

Current scientific research indicates that exposure to certain PFAS may be linked to adverse health effects. Human exposure to PFAS occurs through ingestion of contaminated drinking water and food, inhalation of

indoor air, and contact with other contaminated media. The bioaccumulation tendency of PFAS is attributed to their rapid absorption, their ability to bind to plasma proteins, the absence of biotransformation (except for precursors substances), and their slow renal elimination.

Toxicological studies on laboratory animals and epidemiological research in humans suggest that long-term exposure to environmentally relevant levels of PFOA and PFOS may lead to health effects. Some outcomes, such as alterations in serum lipids, liver biomarkers, uric acid levels, thyroid function, vaccine response, and fetal growth, have been assessed across multiple studies and populations (ITRC, 2023).

Moreover, the International Agency for Research on Cancer (IARC), the cancer agency of the World Health Organization (WHO), has evaluated the carcinogenicity of PFOA and PFOS. A task force classified PFOA as carcinogenic to humans (Group 1) and PFOS as possibly carcinogenic to humans (Group 2B) (Zahm et al., 2023).

2.6 EUROPEAN LEGISLATION: FOCUS ON DANISH AND ITALIAN REGULATION

In Europe, numerous PFAS are subject to restrictions under Regulation (CE) n. 1907/2006 (REACH) and other specific sectoral provisions, with ongoing bans on the production and/or use of certain PFAS. Additionally, the Stockholm Convention on Persistent Organic Pollutant (POPs), adopted in MAY 2001 under United Nations Environment Program (UNEP), mandates various actions that have been integrated into EU legislation through Regulation (CE) n. 850/2004 to minimize global emissions of PFAS into the environment.

In 2020, the EU established a requirement for all member states to measure 20 PFAS compounds by no later than 2026, setting a quality criterion of 0.10 μg/L for the total concentration of these 20 PFAS and 0.50 μg/L for total PFAS (Directive 2020/2184) (European Union Council, 2020). Based on the Legislative Decree 18/2023, Italian threshold limits align with those established at the European level while accounting for 24 PFAS. Instead, according to the Danish Environmental Protection Agency (EPA), the threshold limits that must be met are 2 ng/L for the combined concentration of four PFAS substances (PFOS, PFNA, PFHxS, PFOA), while the total concentration for the sum of 22 PFAS present in groundwater must not exceed 100 ng/L.

While EU Directive 2020/2184 sets strict thresholds for PFAS in drinking water, it does not apply to wastewater. In response, the Piedmont Region in Italy introduced its own rules though Regional Law 25/2021 and resolution 60-5220/2022, setting binding limits for specific PFASS in surface water discharges, as PFOA maximum concentration 0.30 μg/L and discharge to soil or subsoil is strictly prohibited. Similarly, Denmark has adopted some of the strictest PFAS discharge limits in Europe, with regulatory threshold as low as 0.01 μg/L for PFOS and PFOA in industrial wastewater.

These measures place both Piedmont and Denmark among the most proactive jurisdictions in Europe regarding PFAS control.

3. PFAS TRANSPORT MECHANISMS

PFAS distribution across different media and PFAS migration within and between these media are influenced by physical, chemical, and biological mechanisms. Due to the vast diversity of PFAS, they exhibit a wide range of physical and chemical properties, which significantly impact their environmental behavior. This variability increases the complexity of fate and transport assessments.

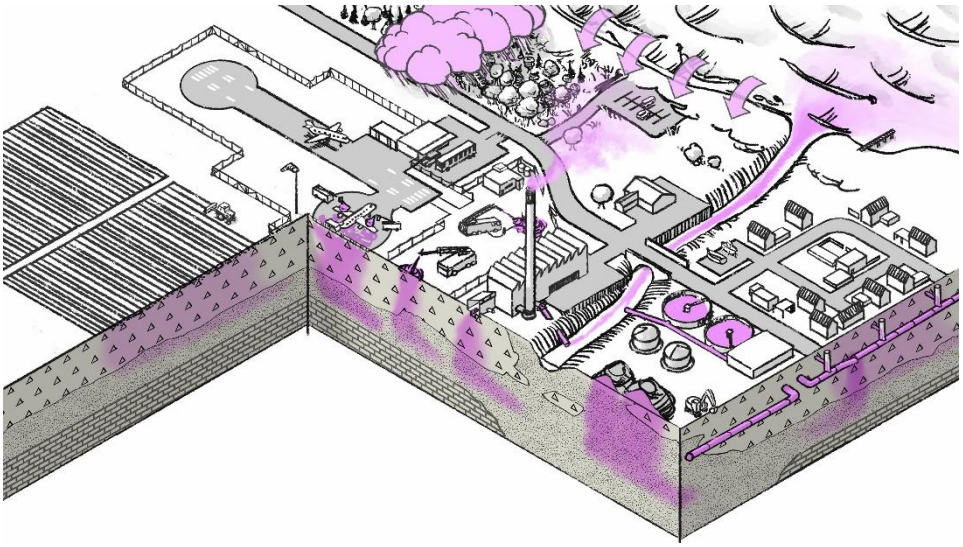

Figure 3.1 Conceptual figure illustrating potential PFAS sources and pathways in Denmark, indicating both point sources from contaminated sites and diffuse sources. The types of point sources include, among others, airfields, fire training areas, sewage treatment plants, leakage from chrome plating tanks and sewers, and landfills. The diffuse sources include, among others, PFAS from agriculture, incinerators, the sea, and precipitation (Morsing et al., 2025).

3.1 ADVECTION

Advection is the process by which a contaminant is transported by water along the flow direction at a velocity equal to the effective average velocity of groundwater (Sethi & Di Molfetta, 2019):

$$v_e = \frac{v}{n_e} = \frac{K \cdot i}{n_e} \tag{3.1}$$

In an ideal scenario where advection is the only active transport process the concentration of a pulse input would remain constant over time. For continuous contaminant sources, the concentration front would be perfectly perpendicular to the propagation direction and would advance along x at the groundwater velocity (Sethi & Di Molfetta, 2019).

3.2 HYDRODYNAMIC DISPERSION

The hydrodynamic dispersion describes the spread of solute mass flow along three main axes, resulting from molecular diffusion and kinematic dispersion, which are due to thermal motion and porous medium heterogeneities, respectively (Sethi & Di Molfetta, 2019). The hydrodynamic dispersion is described by:

$$D_L = \alpha_L \cdot v_p + D^* \tag{3.2}$$

where α_L is the dispersivity coefficient, v_p is the pore water velocity, and D* is the molecular diffusion coefficient.

Spreading along the flowline is controlled by longitudinal dispersion, whereas spreading over the flowline is controlled by transversal and vertical dispersion (Appelo & Postma, 2004; Cook, 2022).

3.3 PHASE PARTITIONING

The fate and transportation of PFAS in source zone may be influenced by retention/attenuation mechanisms. PFAS commonly found in the environment typically consist of a carbon-fluorine tail and a nonfluorinated polar head group. The tail is both hydrophobic and lipophobic, meaning it repels both water and nonpolar organic matter. In contrast, the head group is polar and hydrophilic, allowing interaction with water (Buck et al., 2011). These opposing properties influence their distribution in the environment, often leading to an uneven spread. Additionally, PFAS behavior can vary with concentration, as they may from micelles, mixed micelles, hemimicelles, or bilayer structures (Fig. 3.2) when present at high levels due to their surfactant properties (ITRC, 2023).

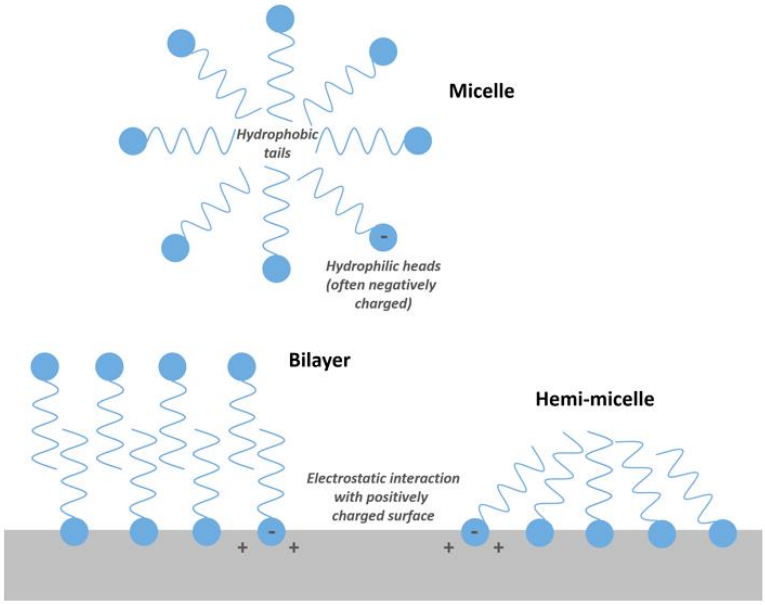

Figure 3.2 Illustration of the formation of PFAS micelles, hemi-micelles, and bilayers. Also shown is an example of aggregation at a positively charged surface. Note that the opposite effect (electrostatic repulsion of PFAS) can occur if the surface is negatively charged (ITRC, 2023)

Considering the variety of subsurface conditions, soils with varying surface charges, organic carbon, air-water interfaces, and interfaces with co-contaminants that include hydrocarbons and water, retention/attenuation mechanisms involve (Brusseau, 2018):

a. Partitioning to the soil in the vadose zone
b. Adsorption to air-water interfaces in the vadose zone
c. Partitioning (absorption) to nonaqueous-phase liquids (NAPL), accumulated in source zones (both unsaturated and saturated zones)
d. Adsorption to NAPL-water interfaces in NAPL-contaminated source zones

For PFAS, sorption is governed by two major mechanisms: solid-phase sorption and air-water interfacial adsorption. Based on these two sorption processes, the retardation factor can be derived according to the equation:

$$R = 1 + \frac{K_d \cdot \rho_b}{\theta_w} + \frac{K_{ai} \cdot A_{ai}}{\theta_w}$$

(3.3)

where K_d is the solid phase sorption coefficient, ρ_b is the bulk density, K_{ai} is the air-water interfacial coefficient, A_{ai} is the air-water interfacial area and θ_w is the water-filled porosity (Lyu et al., 2022).

3.3.1 PARTITIONING TO SOLID PHASE

Diffusive mass transfer is known to affect plume attenuation/persistence and solute transport in heterogeneous systems. PFAS transport and attenuation may be significantly impacted by the phase partitioning retention process of PFAS sorption by the solid phase of geologic medium (Brusseau, 2018). Research has demonstrated that the geochemical characteristics of the solid, especially regard to particular components present, have a significant impact on PFAS sorption by subsurface medium (Brusseau, 2018). Electrostatic interactions, based on the properties of the PFAS functional group can influence the solid-phase sorption of ionizable PFAS (Du et al., 2014; Ferrey et al., 2012; Hellsing et al., 2016; Higgins & Luthy, 2007; Johnson, Anschutz, Smolen, Simcik, & Penn, 2007; Merino et al., 2016; Zhao et al., 2014). Zwitterionic and particularly cationic species would likely have higher retention. The soil-specific distribution coefficient K_d is used to characterize sorption (Pancras et al., 2016). Hydrophobic sorption to naturally existing solid organic particles and surface sorption to charged particles and minerals, commonly referred to as electrostatic interaction, are the two primary ways by which PFAS sorption is measured overall (Pancras et al., 2016; Adamson et al., 2020).

Hydrophobic sorption refers to the interaction between a nonpolar hydrophobic compound and its tendency to bind to hydrophobic surfaces, such as soil organic carbon (Lei et al., 2023; Pancras et al., 2016). The extent to which PFAS sorb to organic carbon can be estimated using method that involves a linear relationship between K_{oc} and f_{oc} (Brusseau, 2023b):

$$K_d = K_{oc} \cdot f_{oc}$$

(3.4)

Where K_{oc} is the organic carbon normalized sorption coefficient, and f_{oc} is the fraction of organic carbon.

PFAS are amphiphilic molecules that contain fluoroalkyl groups of varying chain lengths and structures. Chain length, often used as a proxy for molecular size, has been shown to significantly influence the distribution and the fate of PFAS in the environment (Brusseau, 2023b). Several laboratory studies have investigated the relationship between chain length and PFAS sorption in soils and sediments, consistently finding that longer-chain PFAS exhibit greater sorption (Brusseau, 2023). In some cases, correlations have been established between log K_d or log K_{oc} and chain length-related properties such as molecular weight (Nguyen et al., 2020), fluorinated carbon number (Fabregat-Palau et al., 2021; Sorengard et al., 2019), and molar volume (Brusseau, 2019). However, studies have also reported deviations in the sorption behavior of short-chain PFAS, suggesting that the chain length correlations observed for long-chain PFAS may not be directly applicable. These findings indicate that a single chain length function may not be sufficient for short-chain PFAS, which has important implications for estimating sorption coefficients using the standard K_{oc} approach or other simplified models.

3.3.2 PARTITIONING TO AIR-WATER INTERFACE

The main PFAS characteristic used in this study is its propensity to partition at the air-water interfaces. For this reason, it is crucial to focus on this particular aspect.

Substances that accumulate at the air-water interface in concentrations higher than their aqueous levels and reduce water cohesion are commonly known as surfactants, a shorten term for 'surface-active agents' (J. Costanza et al., 2019).

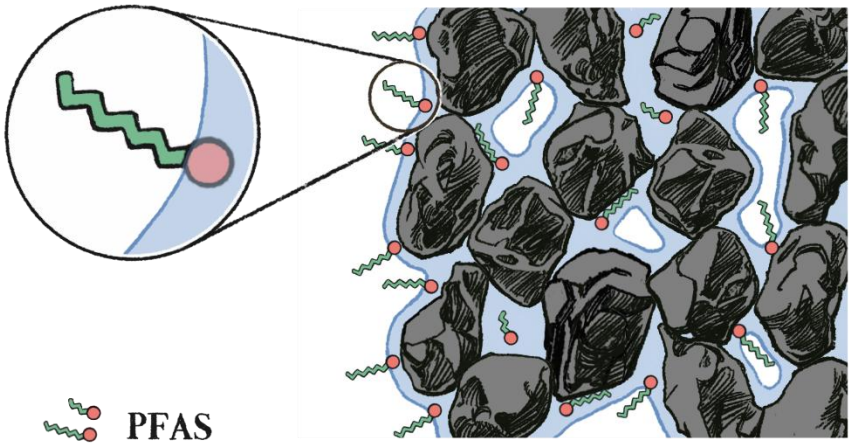

Figure 3.3 Adsorption of PFAS to the air-water interface in the unsaturated zone. At this interface, the hydrophilic head is placed in the water and the hydrophobic/lipophobic tail is placed in the air (Morsing et al., 2025)

Air-water partitioning is different from interfacial adsorption since the latter refers to the transfer of components into the bulk fluid, while the former indicates the retention at the fluid-fluid interface (Brusseau, 2018). In the transport of aqueous-phase constituents, air-water interfaces can serve as an additional domain for retention and retardation, particularly when the interface is either stationary or moves more slowly than the surrounding bulk aqueous phase (Brusseau, 2018).

Because many of them have both hydrophobic and hydrophilic characteristics, PFAS frequently behave like surfactants. Fluorinated surfactants generally exhibit greater surface activity than their hydrocarbon counterparts (e.g., Krafft & Riess, 2015b), a properly largely attributed to the distinctive characteristics of their tail groups. Like conventional hydrocarbon surfactants, the tails of fluorinated surfactants are hydrophobic due to their nonpolar and fully saturated structure (Brusseau, 2018). However, what sets them apart is that they are also lipophobic. This dual repellence arises from the low polarizability of the carbon-fluorine (C-F) bond, which reduces interactions not only with water but also with organic phases (Brusseau, 2018). They reduce the interfacial tension and preferentially form films at air-water interface, with the hydrophilic head group dissolved in the water and the hydrophobic carbon-fluorine (C-F) tail oriented toward the air (Krafft & Riess, 2015).

For solutes undergoing adsorption at the air-water interface, the R only accounting for retention due to air-water interfacial adsorption is provided as (Brusseau et al., 2007b; Kim et al., 1998):

$$R = 1 + K_{ai} * \frac{A_{ai}}{\vartheta_w} \tag{3.5}$$

where K_{ai} is the air-water interface adsorption coefficient (cm^3/cm^2), A_{ai} is the specific air-water interfacial area (cm^2/cm^3), and θ_w is volumetric water content (−).

To accurately characterize and model the transport of PFAS, it is essential to determine the air-water interfacial adsorption coefficient, K_{ai}, and understand how it changes with concentration (Brusseau, 2021). K_{ai} can be

defined in terms of surface excess (Γ), which indicates the amount of a substance adsorbed at the air-water interface, and the aqueous-phase concentration (C_w) (Brusseau & Van Glubt, 2021; Lyu et al., 2018).

$$K_{ai} = \Gamma \cdot C_w \tag{3.6}$$

K_{ai} can be estimated by measuring the surface tension as a function of the aqueous concentration and applying the Gibbs adsorption equation (Brusseau & Van Glubt, 2021). A study by Lyu et al. (Lyu et al., 2022) demonstrated that long-chained perfluorocarboxylic acids (PFCAs) have a higher adsorption to the air-water interface compared to shorter-chained PFCAs. Moreover, the results showed that interfacial adsorption predominantly influenced the retention of long-chained PFCAs, while solid-phase adsorption was the primary mechanism for the retention of short-chained PFCAs.

According to Costanza and Brusseau (2000), the compound's molecular characteristics-such as its ionic strength, pH, and temperature-affect the value of K_{ai}. Based on studies, the presence of co-occuring PFAS compounds (Vecitis et al., 2008), water chemistry characteristics like ionic composition (Downes et al., 1995), and compound chain length (Lunkenheimer et al., 2015; Psillakis et al., 2009) all affect surface activity and air-water interface adsorption potential.

The air-water interface in porous media consists of two main components: the capillary interface, which includes features where bulk air and water phases are in contact; and the film interface, which involves air in contact with thin water films coating solid surfaces (Brusseau, 2018). Experimental, theoretical, and modeling studies have demonstrated that the total air-water interfacial area (i.e. the sum of capillary and film contributions) varies with the relative amounts of water and air present (Brusseau, 2018). In particular, as water content decreases – and air content increases – the total interfacial area increases progressively (Brusseau et al., 2006, 2007a; Cary, 1994; Costanza-Robinson & Brusseau, 2002; Dalla et al., 2002; Kim et al., 1997, 1999; Oostrom et al., 2001; Or & Tuller, 1999; Peng & Brusseau, 2005; Schaefer et al., 2000). When water content becomes extremely low, the total air-water interfacial area approaches the specific area of the solid matrix (Brusseau, 2018).

An estimation method using the median grain diameter can be applied to evaluate the specific air-water interfacial area (Brusseau, 2023a)

$$A_{ai} = (-2.85 \cdot S_w + 3.6) \cdot ((1 - S_w) \cdot 3.9 \cdot {d_{50}}^{-1.2}) \tag{3.7}$$

4. AIR-SPARGING REMEDIATION TECHNIQUE

Air sparging is a remediation technology that involves injecting pressurized air below the water table through a network of vertical wells. This system can be coupled with a vapor recovery and treatment unit to capture and manage contaminants volatilized into the unsaturated zone (Sethi & Di Molfetta, 2019). The contaminant removal process relies on three primary mechanisms:

- Stripping of dissolved contaminants from the aqueous phase.
- Direct volatilization of contaminants presents in separate-phase or adsorbed states.
- Aerobic biodegradation facilitated by microbial metabolism.

The effectiveness of air sparging in removing dissolved contaminants via stripping depends largely on Henry's law constant of the compound and the way air distributes within both the saturated and unsaturated zones. In contrast, the direct volatilization mechanism is influenced by the vapor pressure of the contaminant zone (Sethi & Di Molfetta, 2019). Lastly, aerobic biodegradation is highly dependent on factors such as the type of contaminant, the presence of suitable microbial communities, and the availability of essential nutrients in sufficient quantities zone (Sethi & Di Molfetta, 2019).

Its implementation for remediation of PFAS-contaminated sites has not been considered until 2021, since most PFAS are not highly volatile and biodegradable. A study conducted by Newell et al. in 2021 exploits the partition of PFAS to the air-water interfaces through air-sparging that would concentrate PFAS directly from the aquifer to the water table (Newell et al., 2021).

The applicability of air sparging technology is highly dependent on the characteristics of both the contaminant and the porous medium. Its effectiveness relies on the ability to deliver a uniform air flow across a wide portion of the contaminated aquifer. Therefore, the site must exhibit geological homogeneity, as preferential flow paths can reduce treatment efficiency zone (Sethi & Di Molfetta, 2019).

- Low-permeability layers can trap injected air, forcing it to accumulate beneath these layers and then spread horizontally, potentially expanding the contaminant plume.
- High-permeability layers may also redirect air laterally, leading to uncontrolled vapor migration and increasing the risk of contaminant spread.

In situ air sparging has gained widespread attention due to its advantages over traditional pump-and-treat methods, such as ease of implementation, minimal wastewater generation, lower capital and operational costs and enhanced biological activity through oxygen supply to groundwater (Kim et al., 2004).

4.1 PHASES AND REMOVAL PROCESSES

The effectiveness of air sparging systems depends on understanding how air moves through saturated media (Sethi & Di Molfetta, 2019).

At low air flowrates, the buoyancy force dominates, and air flows vertically up from the air injection point in a few distinct air channels (Leeson et al., 2002). The air distribution takes on a more bush-like appearance (Fig. 4.1) as the air flowrate is increased. At some point, further increases in air injection flowrate do not yield

further expansions of the air flow zone but rather cause increases in the density of air channels and an overall desaturation of water from within the established air flow zone (Rutherford & Johnson, 1996).

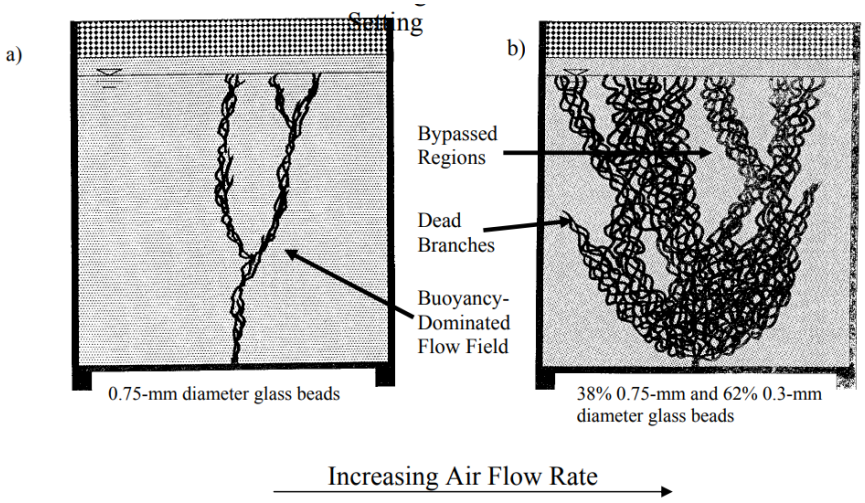

Figure 4.1 Effect of air flowrate changes on air distribution in a model homogeneous setting (Leeson et al., 2002)

During air injection into an aquifer, a temporary rise in the water table (water table mounding) may occur at the injection point (Sethi & Di Molfetta, 2019). This can pose design challenges, as it triggers radial movement of water and contaminants around the well. Numerical models (Nyer, 2000), confirmed by field measurements, indicate that air injection follows two transient phases before reaching a steady state.

Initially, air accumulates in the injection zone because the injected volume surpasses the amount transferred to unsaturated zone, leading to local expansion (Sethi & Di Molfetta, 2019). In the second phase, the water table gradually lowers as preferential air pathways form, eventually balancing the injected air with the portion escaping into the unsaturated medium (Sethi & Di Molfetta, 2019).

At steady state, the water table rise becomes negligible (Fig. 4.2, Fig. 4.3).

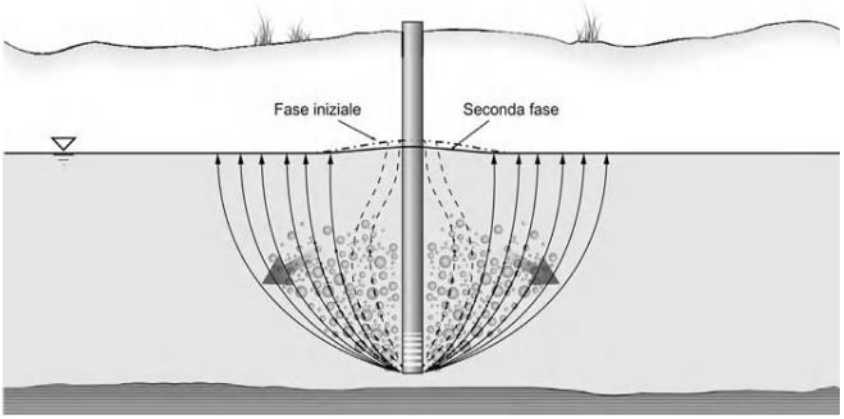

Figure 4.2 Initial phase of air injection with consequent mounding (Sethi & Di Molfetta, 2019)

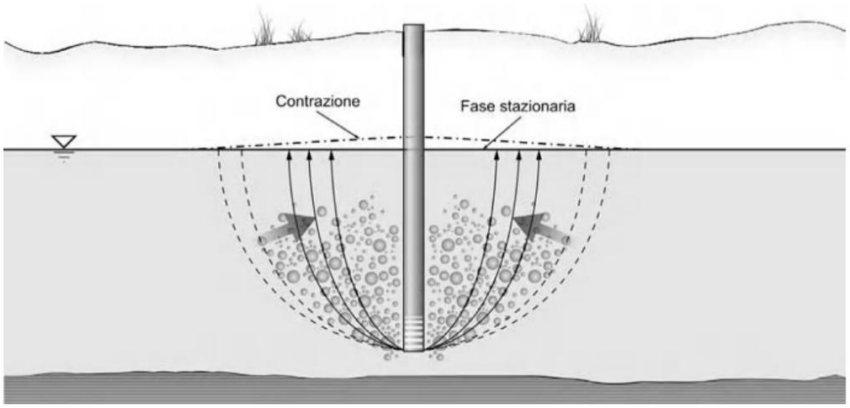

Figure 4.3 Contraction of the injection zone and achievement of steady state conditions (Sethi & Di Molfetta, 2019).

The time required to reach steady state conditions in the air-sparging system depends on the air permeability and homogeneity of the medium. Groundwater mixing during air sparging plays a crucial role in both transporting contaminants out of the aquifer and delivering oxygen into it (Sethi & Di Molfetta, 2019).

The main mechanisms driving water mixing during air sparging include (Sethi & Di Molfetta, 2019):

- Displacement caused by injected air,
- Capillary interactions between air and water,
- Shear stresses induced by rising air,
- Water movement to compensate for evaporation losses,
- Thermal convection,
- Migration of fine particles within the porous medium.

Water displacement occurs as air rises through the saturated zone during the transient phase, before preferential air pathways are established. The extent of this phenomenon is mainly determined by how long the transient phase lasts, which in turn depends on the permeability of the medium (Sethi & Di Molfetta, 2019). Specifically, lower permeability leads to a shorter transition to steady state conditions.

Pulsed air injection extends the transient phase, enhancing water mixing within the aquifer. Unlike physical mixing - which results from variations in air saturation within the pores - capillary interactions between air and water can induce groundwater movement even without changes in saturation (Sethi & Di Molfetta, 2019).

To improve air sparging effectiveness, prolonging the transient phase is beneficial. This can be achieved by cyclically adjusting the injected flow rate, optimizing mixing and contaminant removal (Sethi & Di Molfetta, 2019).

4.2 PFAS RETENTION BY AIR-SPARGING

PFAS act as surfactants and strongly partition to air-water interfaces (Brusseau, 2019; J. Costanza et al., 2019; Lyu et al., 2018). Leveraging this key property, in 2021 Newell's at al. study proposed a widely used, cost-effective groundwater remediation technique – air-sparging - could serve as a novel in situ method for remediating PFAS-contaminated plumes (Newell et al., 2021). This approach would concentrate PFAS from

the aquifer to the water table, rather than volatilizing contaminants like chlorinated solvents or promoting the biodegradation of compounds such as benzene (Newell et al., 2020).

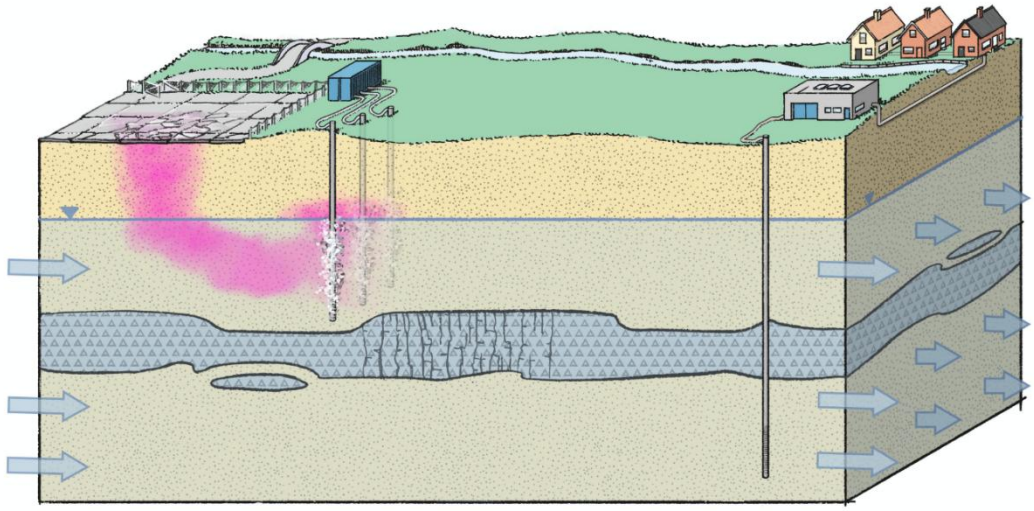

Figure 4.4 Gas sparging to concentrate per- and polyfluoroalkyl substances (PFAS) (Morsing, 2025)

When sparging gas is introduced into a groundwater treatment zone, PFAS accumulate at the air-groundwater interfaces and are drawn upward by the buoyancy of the sparged gas (Fig. 4.4) (Newell et al., 2021). While the exact mass transfer rates are not yet fully understood, it is likely that sparging will lower PFAS concentrations in the deeper parts of the sparged zone, thereby providing some level of remediation (Newell et al., 2021). The sparging process will also increase PFAS concentrations, creating a buoyant mixture of air, water, and PFAS that is less dense than water and therefore rises through the subsurface to near the top of the aquifer, sometimes following channels formed by the buoyant material or through pressure (Newell et al., 2021).

During a gas sparging application, PFAS retention is expected to occur in two primary zones within the subsurface. Within the entire sparging zone, PFAS are removed from the aqueous phase through partitioning to residual air bubbles and gas-filled channels, resulting in a reduction of the overall mass discharge of the contaminant plume (Newell et al., 2021). Simultaneously, sparging induces upward transport of PFAS-contaminated water toward the water table and the capillary fringe, where the air–water interfacial area is at its maximum (Newell et al., 2021). This upper zone acts as a secondary retention zone, where PFAS accumulation is enhanced due to the increased interfacial adsorption and reduced relative permeability of the multiphase system, further limiting PFAS mobility compared to unsparged conditions (Newell et al., 2021).

Migration makes it easier to remove PFAS by skimming the relatively small volume of groundwater with higher PFAS concentrations or by directly removing any foam or buoyant material near the water table (Newell et al., 2021). Even without the direct removal of concentrated PFAS near the water table, sparging can help concentrate and displace the PFAS away from active groundwater flow or extraction zones (Newell et al., 2021). This could effectively sequester PFAS in less used or more stagnant portions of the aquifer. The concentration of PFAS also reduces the volume of aquifer that needs to be treated, and the amount of waste generated by in situ technologies, compared to pump-and-treat (Newell et al., 2021).

The in-situ implementation of air-sparging to remediate PFAS-contaminated aquifer would provide several advantages (Newell et al., 2021):

i. Reducing the extent of contaminated plume,
ii. Limiting the volume of groundwater requiring treatment,
iii. Enhancing PFAS removal from the subsurface, and

iv. Minimizing the generation of PFAS-contaminated waste.

Regarding the reduction of the extent of the PFAS-contaminated plume, there are three different possibilities (Newell et al., 2021):

1. Extract the concentrated groundwater to remove PFAS from the formation. Examples of extraction systems include groundwater pumping wells or the installation of phytoremediation systems.
2. Extract the concentrated groundwater and any foam/buoyant material that may be present, using well point type system that removes both water, air, and foam; and
3. Rely on the strong air-water partitioning in the capillary fringe to retain the PFAS for long time scales. This is an alternative retention-based technology compared to for example injecting particulate sorbents directly into the formation.

Considering the third possibility, retention-based monitored natural attenuation (MNA) processes can offer important benefits for managing PFAS plumes in groundwater, even if they do not lead to permanent sequestration:

- Plume stabilization: in some cases, retention and dispersion are sufficient to halt plume expansion. If the source has been removed or exhausted, the plume may gradually shrink (Newell et al., 2022).
- Plume slow-down: retention processes can significantly delay plume migration, allowing more time before receptors are impacted. This enables site managers to prioritize areas with more immediate risks and evaluate cost-effective or emerging remediation technologies (Newell et al., 2022).
- Peak shaving: some retention processes exhibit hysteresis, where PFAS are absorbed quickly but released slowly. When retention capacity is high, this effect reduces peak contaminant discharge by distributing it over a longer period, effectively smoothing the plume's impact (Newell et al., 2022).

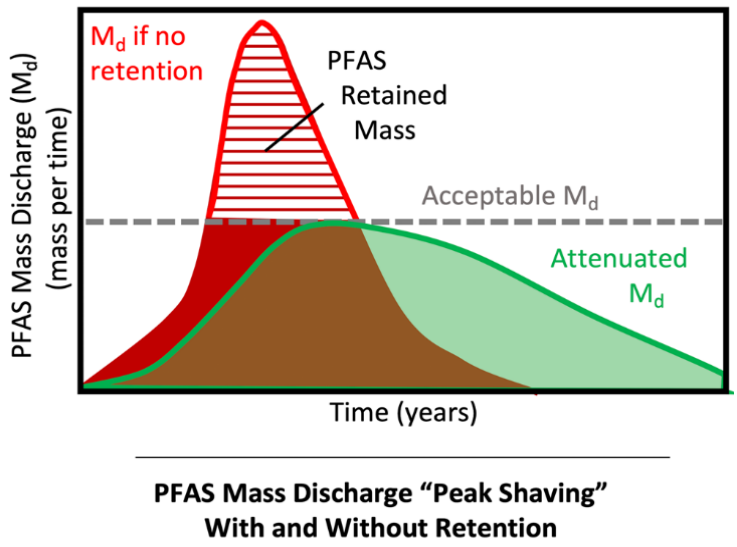

Figure 4.5 PFAS peak shaving with some retention processes (Newell et al., 2022)

However, there are key limitations to relying on retention as an attenuation strategy for PFAS plume:

- No mass destruction: retention slows PFAS migration but does not eliminate the contaminant. Since PFAAs are not known to degrade naturally, plumes may continue to grow over extended periods if the source remains active (Farhat et al., 2022)

- Regulatory acceptance: non-permanent retention may be viewed less favorably by regulatory agencies compared to remediation approaches that involve the permanent removal or destruction of PFAS (e.g. USEPA, 1999)
- Delayed but not prevent impact: although retention delays PFAS migration, if the source persists and no additional remediation is implemented, the eventual contaminant levels at downgradient discharge points (e.g. lakes) could still reach harmful concentration – only over a longer timeframe- posing similar risks to receptors (Newell et al., 2022).

In 2024, Hort et al. examined PFAS retention in the unsaturated zone above the water table using a mathematical model, MODFLOW-USG-Transport PFAS, that incorporates adsorption onto air-water interfaces, providing a more comprehensive understanding of PFAS retention near the water table and release to groundwater. This study suggested that redistributing PFOS from the saturated zone to the vadose zone (e.g., through gas sparging) could be an effective strategy for managing PFOS plumes (Hort et al., 2024). Findings that after initial redistribution via gas sparging, PFOS can persist near the water table for many years. However, certain recharge patterns and water table fluctuations influence both the amount of PFOS retained and the duration of its retention near the water table (Hort et al., 2024). Some results suggested that (Hort et al., 2024):

- Long-term PFOS retention in the vadose zone could be enhanced by limiting recharge, for example, through the installation of an impermeable cap or cover.
- Reduced long-term PFOS retention with fine sands compared to coarse sand. PFOS accumulation to air-water interfaces is reduced in presence of fine sands, which exhibit higher moisture content just above the water table and higher permeability, leading to higher PFOS concentration in the aqueous phase at and above the water table.

Air sparging can be operated in different temporal configurations depending on site-specific hydrogeological characteristics such as groundwater flow velocity, infiltration rate, and seasonal fluctuations of the water table (Newell et al., 2021). It may be applied as a semi-permanent operation, which would be significantly more cost-effective than conventional pump-and-treat systems; a periodic treatment, implemented every few months or years; or as a one-time event, sustained over weeks or months, intended to trap PFAS near the capillary fringe and maintain retention even after the sparging phase is concluded (Newell et al., 2021).

Furthermore, air-sparging, by increasing oxygen concentrations in groundwater, has the potential to stimulate the aerobic biodegradation of PFAS precursors into PFAAs, i.e. more mobile forms of PFAS in groundwater (Newell et al., 2022). However, this transformation could be managed by:

a) Using inert gas such as nitrogen for sparging (Newell et al., 2022), or
b) Implementing sparging in areas with low precursor concentrations, such as the leading edge of the PFAS plume (Adamson et al., 2020).

Alternative designs include sparging with horizontal wells, sparging in trenches (ESTCP, 2021; Newell et al., 2021) or integrating sparging with phytoremediation to extract PFAS retained near the water table (Newell et al., 2021). Also using colloidal gas aphrons – small structures formed by mixing gases, water, and surfactants with powerful sorbent properties - instead of conventional sparging may be more effective, increasing the gas-liquid interfacial area and improving PFAS transport control (Kulkarni et al., 2022).

4.2.1 COLUMN EXPERIMENTS

PFAS transport by air-sparging can be evaluated and quantified through laboratory column experiments, followed by sample analysis from the column and data processing of the obtained results. The vadose zone and the saturated zone are replicated inside the column, emphasizing the capillary fringe where PFAS may retain after sparging. Compressed air is injected into the column to determine the effectiveness of air-sparging technology in PFAS migration and retention. When conducting column experiments, it is essential to simulate real-world conditions as closely as possible to obtain realistic behaviors of the sand, water, air and contaminant. However, achieving perfect reproduction of natural conditions - such as groundwater flow, soil composition,

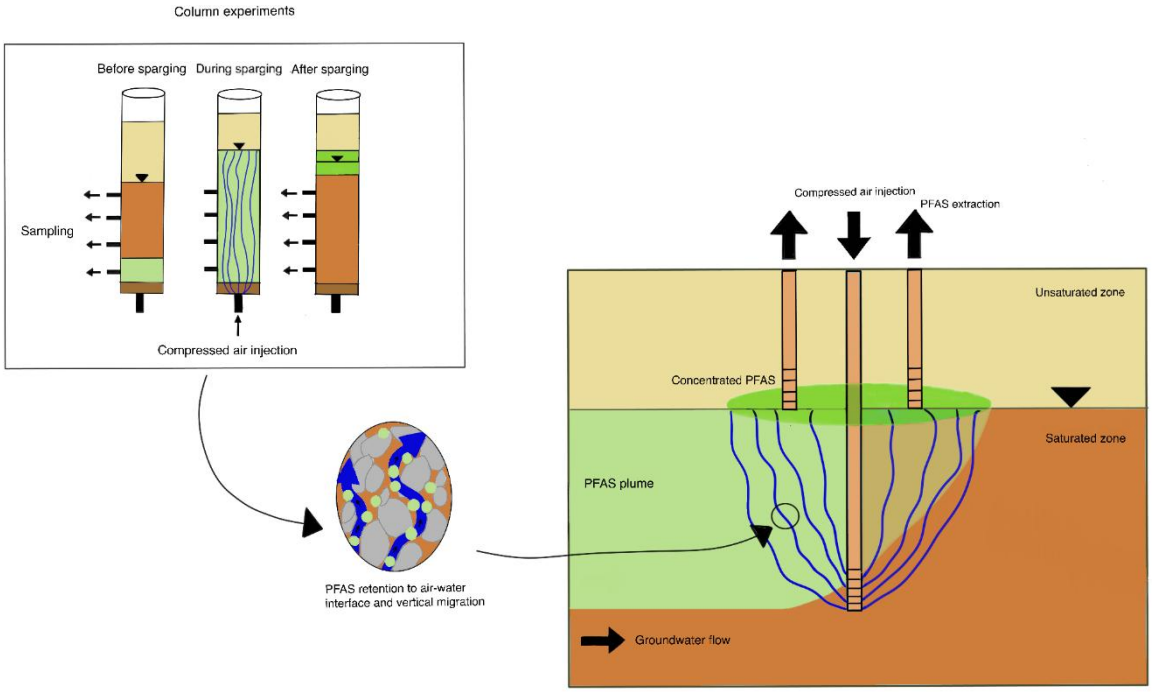

Figure 4.6 Illustration of the project's aim to highlight the correlation between column experiments and in-situ air-sparging system in retaining PFAS at the air-water interface.

granulometry and characteristics, multiple chemical substances, seasonal variation of water level - is not feasible in a laboratory setting. Understanding the limitations and deviations from natural conditions is crucial. Therefore, factors such as column size, soil grain distribution, soil homogeneity, compressed air injection, type of sparging, must be carefully analyzed.

Figure 4.5 illustrates the aim of the project: assessing the potential of air-sparging for reducing PFAS-contaminated plume, by promoting PFAS vertical migration within the saturated zone to enhance their retention at the air-water interface in the capillary fringe.

4.2.2 LABORATORY EXPERIMENTS

Column tests, while often more complex, offer a more accurate representation of environmental conditions. They allow for in-depth analysis by replication of multiple layers (contaminated, saturated and unsaturated) and enabling sampling along the column to track different parameters such as contaminant concentration trends. Column experiments provide reliable and comprehensive data for testing air sparging, as they are the most suitable method for studying it.

Furthermore, the choice of using column test experiments was followed by consultation of the study conducted by Newell et al. (2021; 2022) on PFAS concentration and removal from groundwater through gas sparging and the consequent related laboratory column experiments performed by J. Scalia, J. White and G. Dooley from

Colorado State University, E. Stockwell from GSI Environmental Inc. and J. Blotevogel from CSIRO (Commonwealth Scientific and Industrial Research Organization). Additional studies assessing the effectiveness of air-sparging were considered, particularly the works of Adams & Reddy (2003), Liu et al. (2017) and Kim et al. (2004).

4.3 OTHER REMEDIATION TECHNIQUES

Treatment technologies leverage a contaminant's chemical and physical properties to immobilize, separate, concentrate, or destroy it (ITRC, 2023). However, the unique characteristics of PFAS render many conventional treatment methods ineffective, particularly those that rely on contaminant volatilization (e.g., air stripping, soil vapor extraction) or bioremediation (e.g., biostimulation, bioaugmentation (ITRC, 2023). Even advanced approaches such as thermal and chemical oxidation may not fully degrade PFAS, often requiring a combination of technologies to address the diverse range of PFAS compounds present in contaminated sites (ITRC, 2023).

The absence of effective in-situ remediation technologies means that most PFAS plumes requiring control are managed through groundwater pump-and-trat systems, which rely on ex situ removal or destructive methods (Simon et al., 2019). While these systems are effective in preventing plume migration, experience within the groundwater remediation community has shown that they are highly inefficient for groundwater restoration. This inefficiency arises from the need to extract large volumes of low-concentration groundwater over several decades (National Research Council, 1994; Naval Facilities Engineering Command, 2001).

Currently, full-scale field applications for treating PFAS-contaminated liquids or solids are limited to sequestration methods that remove or bind PFAS rather than destroy them (ITRC, 2023). Among these, sorption techniques using granular activated carbon (GAC) and ion exchange media have demonstrated effectiveness at full scale (Regenesis, 2020).

5. MATERIALS AND METHOD: LABORATORY COLUMN EXPERIMENTS

The overall aim of this project is to assess the potential of air-sparging for shrinking PFAS-contaminated plumes, by promoting PFAS vertical migration within the saturated zone to enhance their retention at the air-water interface in the capillary fringe. To conduct this study, column experiments in the laboratory will be designed and performed, followed by sample analysis from the column and data processing of the obtained results.

5.1 DESIGN AND PRELIMINARY TESTS IN THE LABORATORY

Several laboratory tests were performed during the first month of the research to evaluate the most effective solutions for designing the experimental setup and procedure. Every step of the procedure was previously tested, from sand packing and saturation using a peristaltic pump, to the addition of tracer and detergent and the air-sparging process. All these preliminary experiments were performed without PFAS injection and in a smaller column, 30 cm high and 4 cm wide.

Figure 5.1 Picture of the preliminary test setup in the laboratory.

Different air flow rates were tested to assess the optimal rate that would avoid fracturing of the solid matrix. It was found that sparging at a lower flow rate of 60 cm^3/min effectively prevents sand fractures. To better represent the air flow conditions within the column, the volumetric air flow rate was normalized by the cross-sectional area of the column and by the fraction of pore space occupied by air, obtaining that the Darcy velocity is $v = 1.57 \cdot 10^{-4}\ \frac{m}{s}$. In these tests, Persil detergent mixed with the colored tracer Methylene Blue (Newell et al., 2021) was used to simulate PFAS behavior at the air-water interface, given the surfactant nature of Persil. As theorized by Newell et al. in 2021, Persil was observed to migrate upward in the column after air-sparging for 24 hours. Subsequently, Methylene Blue also moved upwards after approximately 2 days of sparging. Following several laboratory tests, dry sand was selected as 'unsaturated sand' layer (see Fig. 5.2) instead of

wet sand, as air flow caused water displacement that led to the accumulation of free water at the top of the column, thereby eliminating the air-water interface between saturated and unsaturated layers.

Table 5.1 List of preliminary tests in the laboratory: objectives and results

nr.	Setup	Objective	Solutions
1	Tap water + coarse sand	Fill the column	
2	Tap water + fine sand	Use of air sparging	Implementation of a flowmeter 60 cm^3/min - 300 cm^3/min
3	Tap water + coarse sand	Creation of unsaturated layer saturated from above	Implementation of PARAFILM membrane over the top of the column
4	Tap water + fine sand	Creation of unsaturated layer saturated from above	Implementation of PARAFILM membrane over the top of the column
5	Tap water + EOSIN and NaCl + fine sand	Creation of unsaturated layer with wet sand - tracer addition – calculation of residual saturation in unsaturated layer	
6	Tap water + EOSIN and NaCl + coarse sand	Creation of unsaturated layer with wet sand - tracer addition - calculation of residual saturation in unsaturated layer	
7	Tap water + EOSIN and NaCl + Persil detergent + coarse sand	Tracer and detergent addition - air sparging	As unsaturated layer, use of dry sand instead of wet sand
8	Tap water + Methylene blue + Persil detergent + coarse sand	Creation of an unsaturated layer with dry sand - tracer and detergent addition - air sparging	Dilution of Persil detergent because too dense
9	Tap water + Methylene blue + Persil detergent + coarse sand	Detergent dilution - air sparging	Reduction of the number of holes through the PARAFILM membrane to avoid evaporation of water inside the column

Further details and tests results can be found in Appendix A.

5.2 EXPERIMENTAL SETUP

Using the experience from preliminary experiments a column setup was designed. The column set up was designed by the author after discussion with supervisors and manufactured by the laboratory technicians, Jens Schaarup Sørensen, Tajs Nielsen and Erik Rønn Lange.

The experimental setup is depicted in Figure 5.2. It consists of one acrylic transparent column, 80 cm high and with an inner diameter equal to 9 cm. The column dimensions are set according to previous experience of air-sparging laboratory tests performed by to ensure uniform pathways and distribution of airflow along the column and prevent displacement or overflow of the filling material caused by its upward movement during sparging (Adams & Reddy, 2003; Liu et al., 2017; Kim et al., 2004; Newell C. and Scalia J., personal interview, 20 February 2025).

Column presents seven lateral ports made of stainless steel and silicone membranes for sampling, to avoid PFAS sorption. From the bottom of each column compressed air is injected through a tube. Air flow rate is regulated by a flowmeter (Platon 60-600 cm^3/min) and opposite water flow inside the tube is avoided through check valves.

Danish groundwater natural temperature is around 10°C. While this and light exclusion are important in degradation-sensitive experiments, PFAS are highly persistent and unaffected by these factors, so the experiments are conducted at room temperature. The column is covered at the top with Parafilm "M" by BEMIS to limit evaporation and variation of water content within the sandy sediments.

Laboratory equipment materials

Laboratory equipment – such as columns, tubing, pumps, and vials – can both adsorb and release PFAS with the extent depending on the specific compound and matrix (e.g., water or sediment) (Lath et al., 2019). Although several studies have successfully used materials like acrylic columns, glass beads, flow distributors, and polypropylene vials without observed interferences (Brusseau, 2018, 2019; Brusseau et al., 2020; Lyu et al., 2022; Yan et al., 2020), other research has shown significant PFAS sorption to both polypropylene (up to 45%) and glass (up to 24%) (Lath et al., 2019). The variability highlights that material choice can influence results and may depend on experimental conditions, supplier, and batch.

Based on these considerations, glass beads were not used as the bottom layer of the column; instead, a coarser sand was selected to avoid potential interactions with PFAS.

5.3 SOLID MATRIX

One of the objectives of this project is to analyze differences in vertical migration of a mixture of PFAS during air-sparging in different porous media, such as homogeneous fine and coarse sand using column tests in the

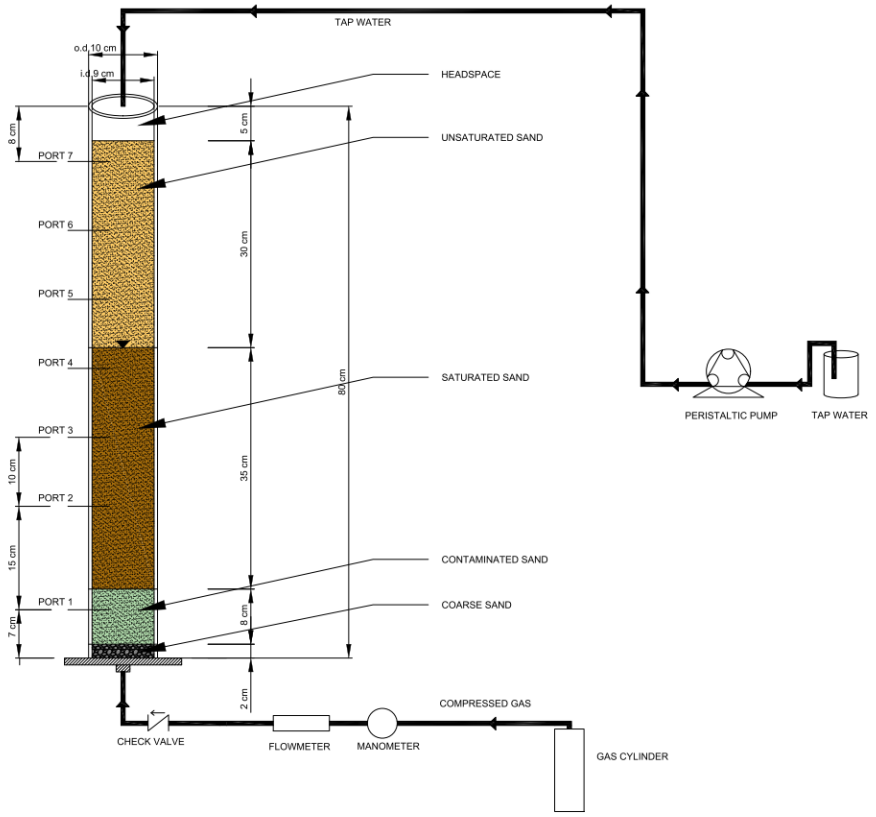

Figure 5.2 Experimental setup sketch

laboratory. Therefore, several experiments are performed to assess the effectiveness of air-sparging and consequent PFAS migration and retention across different media. Two main setups have been installed:

1. Homogeneous coarse sand (sand n.3, Φ=0.90-1.60 mm, D_{10}/D_{60}=1.5)
2. Homogeneous fine sand (sand n.0, Φ=0.40-0.80 mm, D_{10}/D_{60}=1.5)

At the bottom of the column, 2 cm of coarser sand (sand n.6, Φ=2.00-3.55 mm, D_{10}/D_{60}=1.5) is placed to allow uniform distribution of the air flow.

To ensure homogenous solid matrix in both the first and second setups, the sand was sieved to remove finer particles. The granulometry characteristics of the sand used are shown in the Appendix B.

Figure 5.3 Picture of the experimental setup in the laboratory

5.4 PFAS SOLUTION

The experiments are performed using a PFAS solution in tap water, with a concentration of each PFAS of 50µg/L. Among the various PFAS available at DTU, ten representative compounds were selected for this study, as listed in Table 5.2: PFOA, PFHpA, PFOS, PFHxS, 6:2 FTS, 6:2 FTAB, PFHxA, PFPeA, PFBS and PFOSA. The selection was made to ensure a balanced representation of both terminal PFAS and precursors, as well as a mix of long- and short-chained compounds.

These selected PFAS are also among the most frequently detected in the environment, particularly in Denmark according to "Substance flow analysis of PFAS in Denmark" final report by the Ministry of Environment of Denmark of February 2024 (Lassen et al., 2024), making them relevant for understanding contamination patterns and potential remediation strategies. The selected PFAS are also included in the sum of 22 PFAS for which threshold criteria have been established.

Table 5.2 Main characteristics of the ten selected PFAS (Brusseau, 2023b; ITRC, 2023; Lyu et al., 2022)

Compound	Chain length	Type of PFAS		Functional head charge	Main properties
PFOA	Long (C7)	Terminal	PFCA	Anionic ($–COO^-$)	Great sorption to solid phase, great adsorption to air-water interface
PFHpA	Short (C6)	Terminal	PFCA	Anionic ($–COO^-$)	Less adsorption to air-water interface, solid-phase adsorption primary mechanism
PFOS	Long (C8)	Terminal	PFSA	Anionic ($–SO_3^-$)	Great sorption to solid phase, great adsorption to air-water interface
PFHxS	Long (C6)	Terminal	PFSA	Anionic ($–SO_3^-$)	Great sorption to solid phase, great adsorption to air-water interface
6:2 FTS	Short (C6)	Precursor	Fluorotelomer sulfonic	Anionic ($–SO_3^-$)	It could degrade into PFHxA, behavior like long-chained
6:2 FTAB	Short (C6)	Precursor	Fluorotelomer	Zwitterionic	PFCA precursor, behavior like long-chained
PFHxA	Short (C5)	Terminal	PFCA	Anionic ($–COO^-$)	Less adsorption to air-water interface, solid-phase adsorption primary mechanism
PFBS	Short (C4)	Terminal	PFSA	Anionic ($–SO_3^-$)	Less adsorption to solid phase and to air-water interface
PFPeA	Short (C4)	Terminal	PFCA	Anionic ($–COO^-$)	Less adsorption to air-water interface, solid-phase adsorption primary mechanism
PFOSA	Long (C8)	Precursor	Per-fluoroalkane sulfonamides	Anionic ($–COO^-$)	PFOS precursor; lipophilic, behavior like long-chained

This selection ensures a diverse range of physicochemical behaviors, allowing for a comprehensive evaluation of their partitioning behavior and interactions within environmental systems. Other characteristics of each compound are displayed in Appendix C.

5.5 SAND LAYERS PREPARATION WITHIN THE COLUMN

The steps of the experimental procedure are shown in Appendix D.

A fine metal mesh was first placed between the bottom of the column and the first layer of sand to prevent clogging of the air injection outlet.

Then, four layers of sand are created inside the columns, as shown in Figure 5.2, to reproduce the air-water interface between vadose zone and the aquifer and to highlight the vertical migration of the contaminant:

I. Clean coarser sand: clean dry coarse sand (nr.6) packed inside the column saturated from the top through a Peristaltic pump (Watson-Marlow 502s) and a Tygon tube
II. Contaminated saturated layer: sand saturated with PFAS solution outside the column in a glass beaker, and then packed inside the column
III. Clean saturated layer: clean sand packed inside the column and saturated from the top through a Peristaltic pump (Watson-Marlow 502s 150 µg/l- 4 mg/l) and a Tygon tube
IV. Clean dry layer: clean dry sand packed inside the column

To achieve longitudinal and lateral homogeneity packing of the sand, the sand was deposited in layers of around 140 grams and compacted using a pestle. This approach was employed to minimize lateral segregation between layers and to eliminate air pockets and potential preferential flow paths. Previous studies have demonstrated that this method effectively ensures uniformity in the sand structure while preventing the formation of preferential flow channels (Oliviera et al., 1996).

5.6 TRACER ANALYSIS

In this study, sodium bromide (NaBr) was employed as a conservative tracer to investigate fluid dynamics within fine sand column undergoing air-sparging. NaBr was selected due to its well-established properties as a non-reactive, highly soluble and easily detectable tracer that reliably represents water movement without interacting with the porous medium or undergoing degradation. A preliminary evaluation was conducted to determine the optimal NaBr concentration. Different concentrations were tested, and their electrical conductivity (EC) was measured and compared to that of the tap water used to saturate the column. The calibration curve is displayed in the Appendix E, and it was used to establish the relationship between NaBr concentration and EC, allowing for the indirect estimation of tracer concentration during the column experiments. A concentration of 100 mg/L NaBr was chosen, as it resulted in an approximately 20% increase in EC relative to the background, providing a clear and distinguishable EC signal without significantly altering the physicochemical properties of the background water. After six days of continuous air-sparging, water samples were collected from multiple lateral sampling ports along the column.

5.7 PULSED AND CONTINUOUS SPARGING

The experiments were conducted using continuous air injection, as this configuration was the simplest to implement and the most feasible for potential field application. Initially, the use of pulsed air-sparging had also been considered, especially following discussions with Newell and Scalia, given its several advantages in remediating contaminated sites.

During air-sparging, the formation of preferential flow paths can reduce the effectiveness of contaminant removal and limit the treatment area (Sethi & Di Molfetta, 2019). Using pulsed air injection helps overcome this issue by preventing the development of these channels and promoting better mixing within the aquifer, thanks to the repeated opening and collapse of air pathways. Additionally, in the initial expansion phase, the zone of influence is typically larger, which further enhances the efficiency of the process (Sethi & Di Molfetta, 2019).

However, for the purposes of this study, continuous injection was selected as a more practical and straightforward approach.

5.8 POROSITY AND SATURATION

The porosity of the columns was measured prior to the start of the experiments. To determine total porosity, each column was saturated from the top using tap water to replicate the saturated zone, before adding the third layer of dry clean sand. A Tygon tube, compatible with the peristaltic pump (Watson-Marlow 502s), was connected to the top of the column to ensure consistent flow. Water was introduced at a controlled rate of 1.8 mL/min using a peristaltic pump. Once the water reached the top cap and a visible water table formed, the flow was stopped. The column was then weighed in its saturated state. Assuming full saturation with no trapped air, the resulting water-filled porosity was calculated to be 37% for both fine sand and coarse sand experiments. Calculations are available in Appendix H.1.

At the end of the six-day experiments, the column was weighed again, revealing a weight loss of approximately 50 grams. This loss was attributed to the removal of water samples during the experiment.

During both experiments, a rise in the water level was observed within the first few seconds after air injection began. This indicated an initial displacement of water, followed by a stabilization of the water level, which remained constant for the whole experiment. Since the total amount of water is known and it did not change – confirmed by the absence of evaporation – the rise in water level suggests a change in the saturation state of the column.

By comparing the final volume occupied by the water, obtained measuring the final height of the water table after six days of air-sparging, with the initial water volume, it was determined that the column reached a water saturation of 88%, meaning that 12% of the pore space was occupied by air.

For the purposes of the calculations, saturation is assumed to be constant throughout the entire column. However, it is highly likely that this assumption does not reflect actual conditions, given the potential variability in water and air distribution within the pore space over time. Such variability may be influenced both by the natural dynamics of the system and by experimental procedures, such as sample extraction. For instance, water was only recoverable from port 4 during the initial hours of the experiment with the coarse sand; subsequent changes in internal saturation, due to also daily extraction of water samples, made it impossible to collect further samples from that port.

5.9 SAMPLES COLLECTION

During each experiment, 1 ml water samples are collected in 2 ml polypropylene (PP) vials at different stages of the sparging process:

i. At the first sampling port - before saturation of the third layer (Fig. 5.2) (only in coarse sand setup)
ii. At the first, second and third ports – before starting sparging
iii. At the first, second, third and fourth port - during sparging after 1 h, 24 h, 48 h, 72 h, 96 h and 120 h
iv. At the first, second, third and fourth port – 1 h after sparging has ended (only in coarse sand setup)

No samples were collected from the portion of the column representing the vadose zone, as it remained dry throughout the entire experiment. Consequently, water sampling from this section was not possible, and it was not involved in PFAS distribution due to absence of water and a air-water interface.

Additionally, soil samples are collected after sparging, due to lack of water in the ports in correspondence of the capillary fringe. These samples are taken at different depths while the column is being emptied at the end of the experiment. Soil samples are stored in 15 ml polypropylene (PP) vials.

To sample with fine sand setup, it was necessary to stop continuous injection of compressed air to allow the extraction of water sample through the ports, since the presence of injected air within the fine porous medium created significant resistance to water flow. The small pore size in fine sand leads to higher capillary forces, which retain water more tightly and make it more difficult to displace. As a result, continuous air injection disrupts the formation of a stable water phase at the sampling ports, making it difficult to collect representative water samples unless the air flow is temporarily suspended.

5.10 INTERPRETATION OF RESULTS

A mass balance is performed to assess the fate of PFAS within the system and to verify that the total mass of PFAS remained constant within the column, despite its redistribution among the aqueous phase, the soil matrix, and the air-water interface. Since the system is closed, any changes in concentration at specific locations or times must reflect internal redistribution rather than loss, allowing for an accurate assessment of PFAS behavior and retention mechanisms. Mass loss would only be possible if precursors were transformed into terminal PFAS. However, under the conditions of this study, such transformation is unlikely, as the experimental conditions required for chemical oxidation, microbial activity, or photodegradation are not present.

The total mass M_T in the system results from the sum of its distribution across all phases: dissolved in the aqueous phase, adsorbed onto the solid matrix, and accumulated at the air-water interface.

$$M_T = C_w V_w + C_s M_s + C_{ia} A_{ia} \tag{5.1}$$

With:

- C_w pore water concentration
- $C_s = K_d C_w$ soil solids concentration
- $C_{ia} = K_{ia} C_w$ air-water interface concentration
- $V_w = V_{port} \theta_w$ pore water volume
- $M_s = \rho_b V_{port}$ soil solids mass
- A_{ia} air-water interfacial area obtained with (3.8) formula, considering that the water saturation is equal to 88% (see section 5.7) and the medium diameters d50 are displayed in Table 5.5.

All the calculations can be found in Appendix H.2.

Knowing the pore water concentration corresponding to the measured data, it is necessary to assess the solid-phase partition coefficient K_d and air-water interfacial adsorption coefficient K_{ia} to determine PFAS concentration in the other phases (soil and air-water interface). Furthermore, an analysis (see Appendix F) is carried out to evaluate the impact of the assumed port volumes on the accuracy of the mass balance calculations.

Solid-phase partition coefficient

The K_d value depends on the organic carbon fraction f_{oc}, i.e. the weight fraction of organic carbon relative to the total weight of the solid. The organic carbon fraction of the sand used in the laboratory experiments is under the detection limits, $f_{oc} < 0.01$, for both fine sand and coarse sand. To calculate the total PFAS mass in the system, two different K_d values are used: one based on experimental data obtained in the lab (5.2), and another derived from the regression curve proposed by Lyu et al., 2023 (5.3; 5.4).

$$K_d = \frac{C_0 V_0 - C_w V_w}{C_w M_s} \tag{5.2}$$

With C_0 the PFAS concentration in the stock solution, C_w pores water concentration in the column at t=0, V_0 stock solution volume added, V_w water volume related to sampling port 1, and M_s soil solid mass in the volume related to port 1 (since the two concentrations used are collected from port 1). For this calculation, the data from the first experiment, conducted with coarse sand, are selected because concentration data at time zero are available. This initial concentration is measured before any dilution effects occurred due to the addition of the clean, fully saturated sand layer.

The regression curve formulas are function of the molar volume (Lyu et al., 2023), intrinsic property of each PFAS (EPA, 2025).

$$\log K_d = 0.0114V_m - 3.76, \qquad for\ long\ chain\ PFAS \tag{5.3}$$

$$\log K_d = 0.0012V_m - 1.32, \qquad for\ short\ chain\ PFAS \tag{5.4}$$

Since the difference between the mass balances obtained using the two different results is minimal, the K_d value obtained from the laboratory experiment is considered accurate and valid and it's used for further analysis.

Table 5.3 Solid-phase partition coefficients derived from Lyu et al. (2023) regression equation and from the laboratory experiment

	K_d Lyu (l/kg)	**K_d (l/kg)**
PFBS	0.07	**0.01**
PFOA	0.09	**0.17**
PFOS	0.22	**0.22**
PFHxA	0.08	**0.12**
PFHpA	0.09	**0.13**
PFPeA	0.07	**0.12**
PFHxS	0.05	**0.19**
6:2 FTS	0.10	**0.37**
PFOSA	0.26	**0.22**
6:2 FTAB	0.10	**0.24**

It is noticed that most PFAS have the similar K_d values, comparing the two obtained results. However, the partition coefficients of 6:2 FTS, 6:2 FTAB, PFHxS are higher with respect to the values obtained by the regression curve. Since PFOSA and PFOS share similar characteristics in terms of their perfluorinated structure, environmental persistence, and potential for bioaccumulation, K_d value of PFOSA is chosen equal to the PFOS one. The adjustment was required to address the discrepancy in the calculated value, which is attributed to the anomalous behavior of PFOSA.

Air-water interfacial adsorption coefficient

The K_{ia} is determined using the QSPR (Quantitative structure-property relationship analysis) model for air-water interfacial adsorption coefficient versus molar volume, proposed by Brusseau & Van Glubt, 2021. The regression equation is

$$logK_{ia} = 0.019(\pm 0.002)V_m - 7.1(\pm 0.45) \tag{5.5}$$

Table 5.4 Air-water partition coefficients derived from regression curve proposed by Brusseau & Van Glubt (2021)

	K_{ia} (cm)
PFBS	0.0001
PFOA	0.0025
PFOS	0.0117
PFHxA	0.0002
PFHpA	0.0008
PFPeA	0.0001
PFHxS	0.0011
6:2 FTS	0.0045
PFOSA	0.0152
6:2 FTAB	0.0045

Sand properties

To perform calculations about the mass balance in the system is fundamental to describe properly the solid matrices that are used in the experiments. Table 5.5 recaps sands properties: bulk density, medium diameters, organic carbon content and air-water interfacial areas. The organic carbon fraction was determined though TOC analysis in the lab. Grain size distribution curves and further details are presented in Appendix B.

Table 5.5 Bulk density, medium diameter, organic carbon fraction and air-water interfacial area of both solid matrices used in the experiments

	ρ_b (kg/l)	D_{50} (cm)	f_{oc}	A_{ia} (cm^{-1})
Coarse sand (n.3)	1.67	0.121	<0.01	6.44
Fine sand (n.0)	1.67	0.06	<0.01	14.95

It's important to highlight in analyzing the air-water interfacial retention process that the air-water interfacial area is greater with fine sand than with coarse sand. This is related to the surface area that is greater with smaller diameters. So, it is expected greater PFAS migration and retention at the air-water interface in the fine sand experiments rather than in the experiment with coarse sand.

Sampling ports volumes

The saturated section of the column is divided into four different volumes, each corresponding to one of the four sampling ports (Fig. 5.4). Since assuming uniform concentration over such large volumes is a strong simplification and may not accurately reflect the actual spatial variability of PFAS distribution within the column, another subdivision of the volumes was considered (see Appendix F). However, the first case is selected for further calculations, as it is more practical to apply.

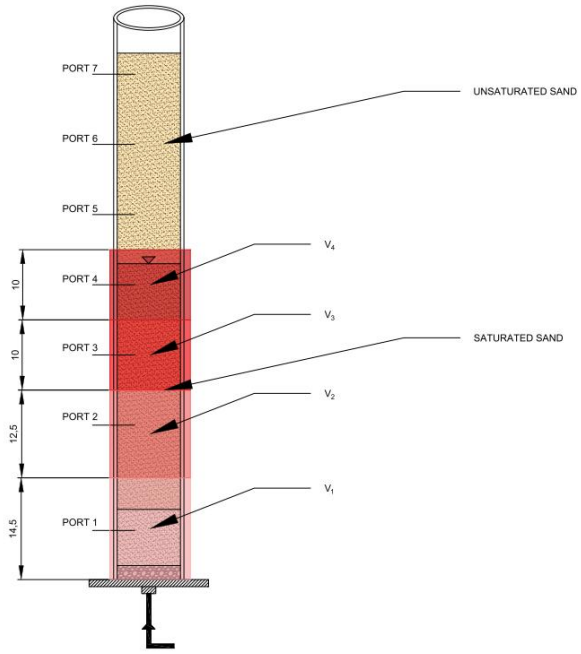

Figure 5.4 Saturated column divided in four volumes

6. RESULTS AND DISCUSSION

The effectiveness of air-sparging in moving PFAS at the air-water interface near the water table is evaluated through the analysis and interpretation of laboratory data collected during the experiments. The data provides PFAS concentrations in water samples taken at various time intervals and from different ports. These concentrations are then compared to the initial concentration of the stock solution, initially added to the column, allowing for an assessment of PFAS mass distribution and potential vertical migration, promoted by the air flow. The objective of this section is to analyze differences in behavior of short- and long- chained PFAS and precursors during air-sparging in different porous media, such as homogeneous fine and coarse sand.

6.1 PFAS CONCENTRATIONS IN TIME AND IN SPACE

To first analyze the results of this research (Appendix H.3), the normalized concentration c/c_0 - normalized with respect to the initial concentration in the stock solution - is displayed. Normalized concentrations are chosen to allow for a consistent comparison among the ten PFAS, as their initial concentrations (i.e., those in the stock solution) were not identical.

The actual pore water concentration values of each PFAS studied in the column experiments are graphically presented in Appendix G, showing the variation in concentration over time at each sampling port.

Initial conditions in the system

The experiments are performed using a PFAS solution in tap water, with a target concentration of 50µg/L for each compound. However analytical results (Appendix H.3) revealed significant deviations from the expected values: PFPeA was present at around 150 µg/L, while PFOS, PFOSA, and 6:2 FTAB were detected at concentrations equal or below 5 µg/L. These discrepancies indicate that the actual composition of the solution did not match the intended formulation.

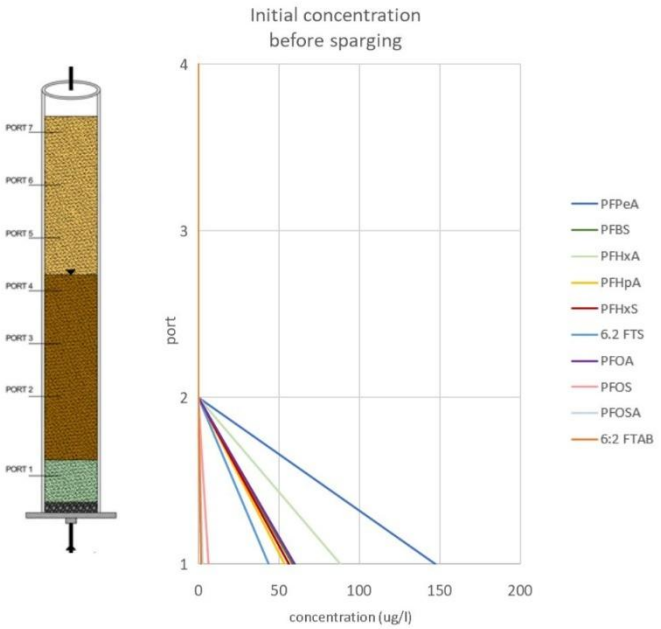

Figure 6.1 PFAS initial concentration (µg/l) before starting sparging

Tracer results

The electrical conductivity of the water samples collected was measured after six days of continuous air-sparging. Results (Fig. 6.2) showed a measurable increase in EC even at the third port, where EC rose to

approximately 960 µS/cm with respect to the background value (905 µS/cm), indicating limited but detectable vertical migration of the sodium bromide tracer. As expected, the highest EC values were observed near the bottom of the column, consistent with the expected behavior of short-chained PFAS, which consists in limited tendency to vertical migration promoted by the retention at the air-water interface of the air bubbles. The bromide concentration trend (Appendix H.3) is also similar to short-chained PFAS behavior, with a higher concentration at the bottom and a decreasing trend along the column.

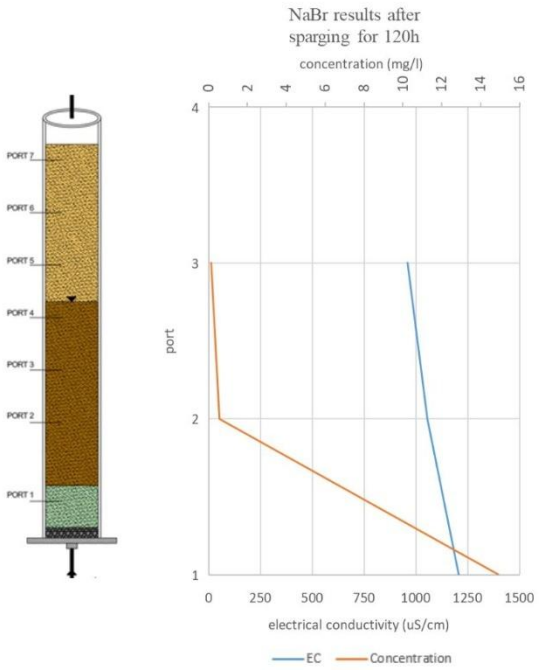

Figure 6.2 Bromide concentration trend and EC variation in presence of NaBr along the column after sparging for 120 hours in fine sand

By monitoring the transport of sodium bromide through the column, through EC and concentrations, it's assessed that water advective flow is limited, as required by this experiment. This approach is particularly relevant for distinguishing between advective water movement and the air-water interface partitioning that may influence PFAS distribution.

PFAS transport mechanism through air-sparging

The transport of PFAS within the column during air sparging may occur via two mechanisms: (1) transport by rising air bubbles, where PFAS adsorb onto the bubble surfaces and are carried upward by buoyant lift; and (2) transport along air channels, where PFAS adsorb at the air–water interface and are mobilized by viscous drag. In these experiments, air bubbles were likely generated within the porous medium, as no preferential flow paths or fractures were observed, and the solid matrix exhibited high porosity.

6.1.1 PFAS VERTICAL MIGRATION DURING AIR-SPARGING IN COARSE SAND

Data is presented from 48 hours of sparging, as during the experiment with coarse sand it was only possible to collect samples from the fourth sampling port after 24 and 48 hours. This allows for meaningful representation of the processes occurring at the water table. In contrast, at 120 hours it is not possible to characterize the behavior at the water table due to the absence of extractable water in that region.

During the first 48 hours of sparging, PFOSA showed anomalous behavior, with concentrations significantly higher than those of the stock solution, despite no additional compound being introduced in the system. As no conclusive explanation can be determined for this anomaly, PFOSA data is treated separately from the other precursors in the analysis of the first experiment.

It is particularly noteworthy that already after 48 hours, long-chained PFAS and precursors exhibited vertical migration, not driven by advective water flow, but rather driven upwards by the adsorption to the air bubbles. The hypothesis of the absence of an advective flow is supported by the limited short-chained PFAS movement during air-sparging and from bromide analysis. After sparging for 120 hours, greater PFAS removal is observed from the bottom of the column, resulting in higher normalized concentrations at the second and third sampling ports (Fig. 6.3a-b).

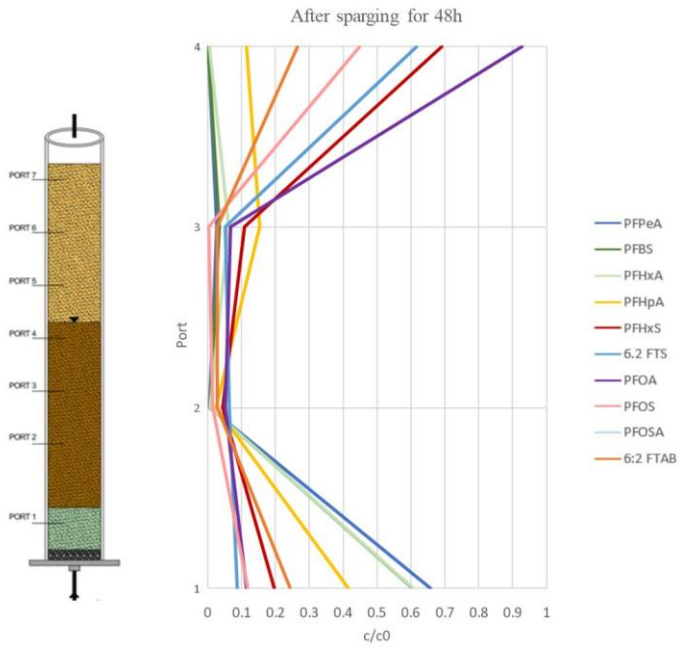

Figure 6.3a PFAS concentrations variation after sparging for 48 hours in coarse sand. PFAS concentrations is decreasing from port 1 to port 2. From port 2, they start to increase up to the port 4.

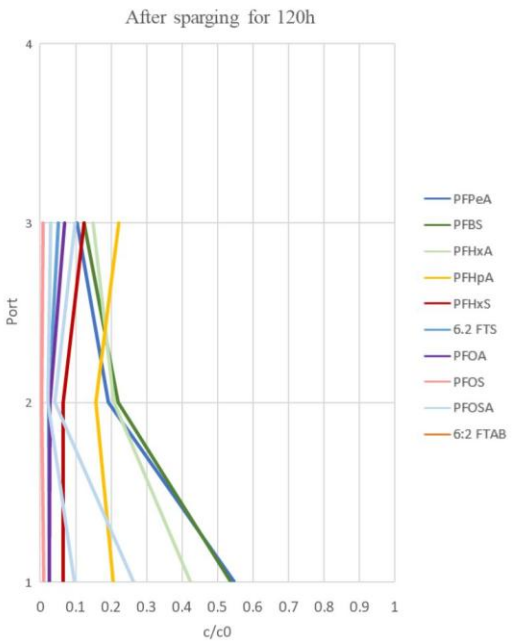

Figure 6.3b PFAS concentration variation after sparging for 120 hours in coarse sand. PFAS concentrations is decreasing from port 1 to port 2. From port 2, they start to increase up to the port 3. Sampling from the port 4 was not possible.

The variation in normalized PFAS concentrations with increasing air-sparging duration is also presented for each sampling port. The graphs are organized by PFAS type in order to highlight the different behaviors exhibited under the same experimental conditions.

Focusing on the first sampling port, at the bottom of the column, the concentrations of short-chained, long-chained PFAS and their precursors decreased relative to the initial levels (Fig. 6.4a-d).

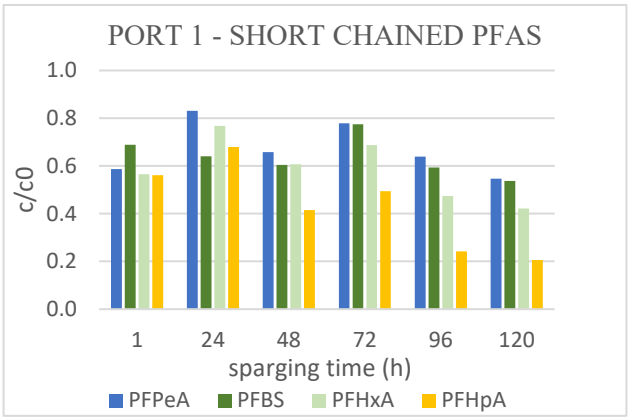

Figure 6.4a Short-chained PFAS concentration variation throughout the air-sparging process at port 1 in coarse sand. The concentrations after 24 hours of sparging increase, and then it starts to slightly decrease.

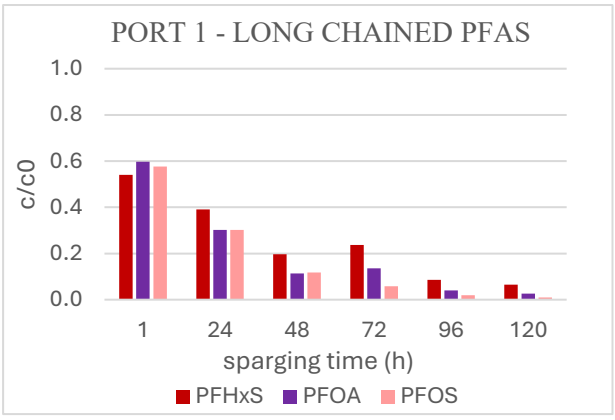

Figure 6.4b Long-chained PFAS concentration variation throughout the air-sparging process at port 1 in coarse sand. The concentrations decrease in time.

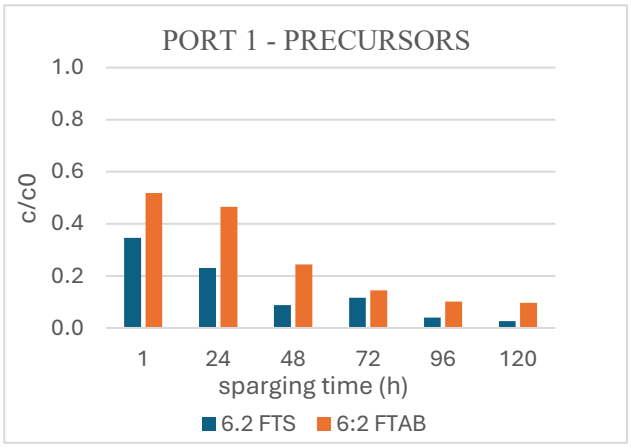

Figure 6.4c Precursors concentration variation throughout the air-sparging process at port 1 in coarse sand. The concentrations decrease in time.

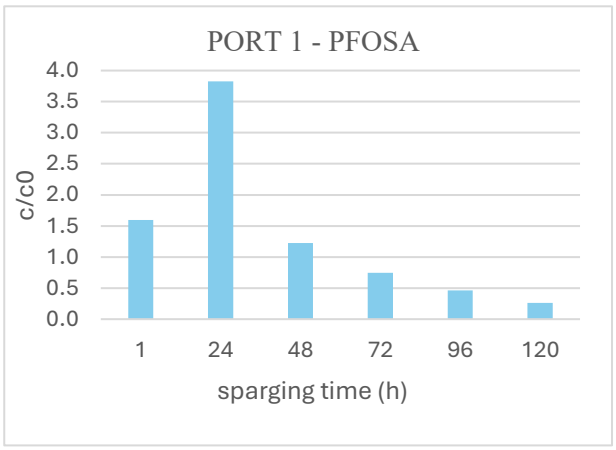

Figure 6.4d PFOSA concentration variation throughout the air-sparging process at port 1 in coarse sand. The concentration after 24 hours of sparging increase, and then it starts to decrease.

This suggests that part of the compounds initially present at the bottom of the column either migrated upwards to the air-water interface near the water table or were partially adsorbed onto the solid matrix. Long-chained PFAS and precursors exhibited more pronounced mobilization compared to short-chained PFAS, likely due to the short-chained PFAS lower tendency to adsorption at the air-water interface and to the sand. The limited movement of short-chained PFAS further supports the limited advective water flow within the column.

At the second sampling port (Fig. 6.5a-d), the concentrations trends differ from the first port. Over time the concentrations increase, mostly short-chained PFAS ones, considering their slower vertical transport due to their lower tendency to migrate attached to the air-water interface of the air bubbles. The lower concentration of long-chained PFAS and precursors is likely due to their faster vertical migration along the column, leading to their retaining near the water table after just 24 hours of air-sparging (Fig. 6.7b-c). Additionally, long-chained PFAS and precursors have higher affinity for soil adsorption that may reduce their pore water concentration.

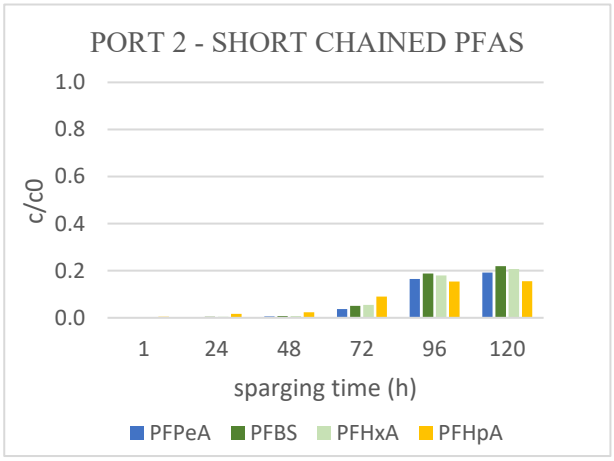

Figure 6.5a Short-chained PFAS concentrations variation throughout the air-sparging process at port 2 in coarse sand. The concentrations increase in time.

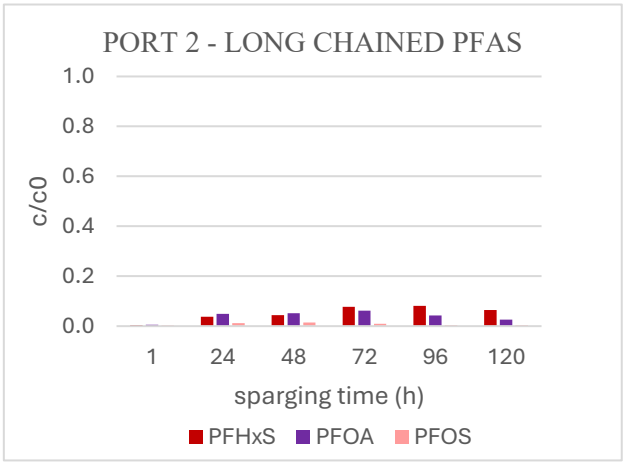

Figure 6.5b Long-chained PFAS concentrations variation throughout the air-sparging process at port 2 in coarse sand. The concentrations increase in time.

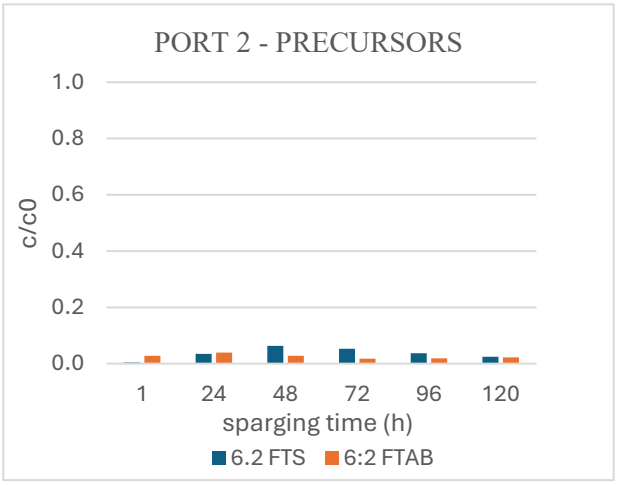

Figure 6.5c Precursors concentrations variation throughout the air-sparging process at port 2 in coarse sand. The concentrations increase in time.

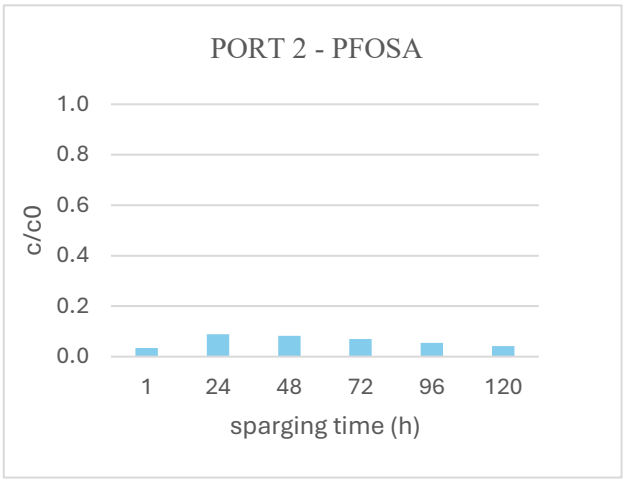

Figure 6.5d PFOSA concentration variation throughout the air-sparging process at port 2 in coarse sand. The concentrations increase in time.

The PFAS behavior exhibited at the third sampling port (Fig. 6.6a-d) is similar to the one at the second sampling port.

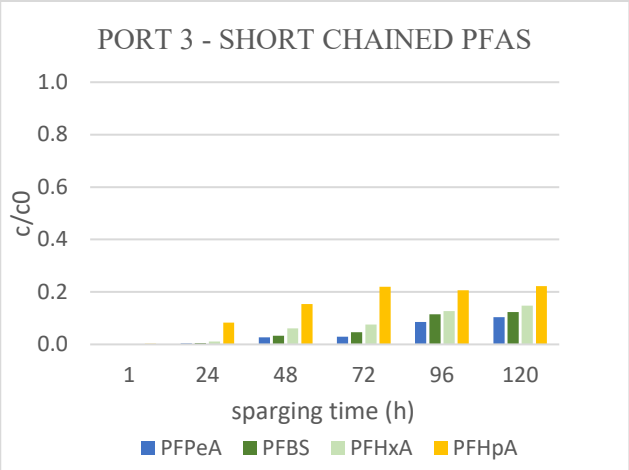

Figure 6.6a Short-chained PFAS concentrations variation throughout the air-sparging process at port 3 in coarse sand. The concentrations increase in time.

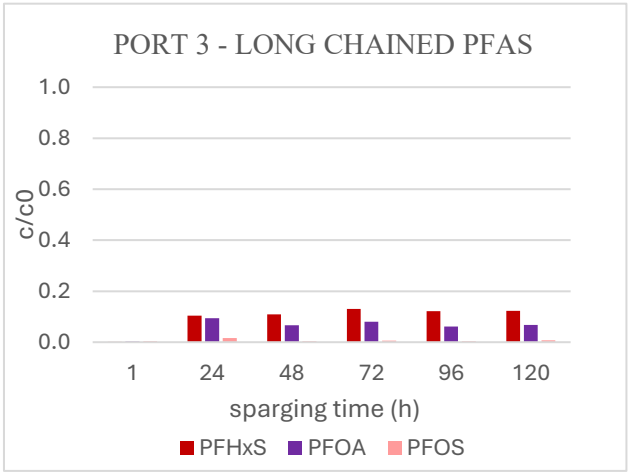

Figure 6.6b Long-chained PFAS concentrations variation throughout the air-sparging process at port 3 in coarse sand. The concentrations increase in time.

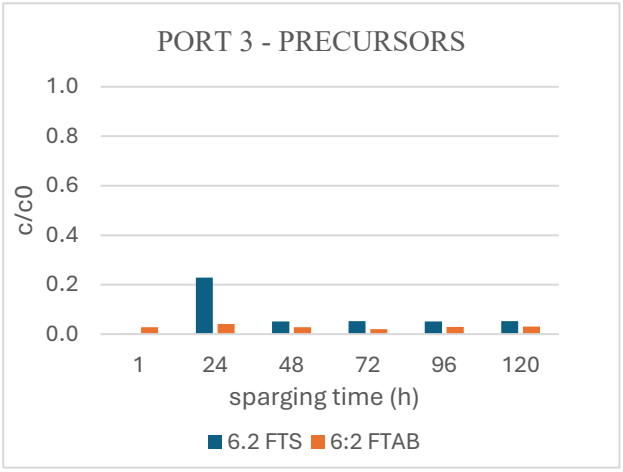

Figure 6.6c Precursors concentrations variation throughout the air-sparging process at port 3 in coarse sand. The concentrations slightly increase in time.

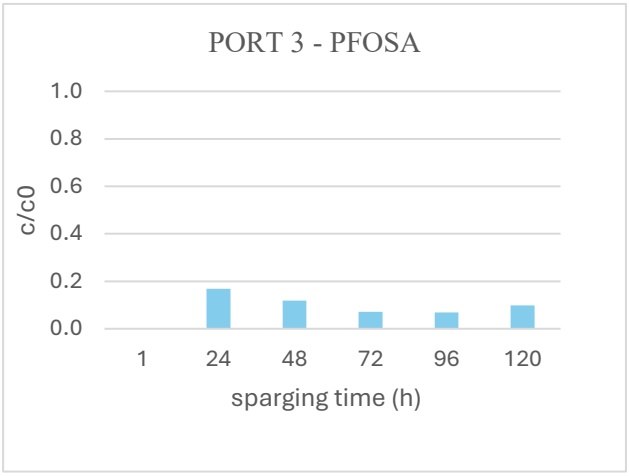

Figure 6.6d PFOSA concentrations variation throughout the air-sparging process at port 3 in coarse sand. The concentrations increase in time.

PFAS concentrations are shown also for the fourth port (Fig. 6.7a-d), located at the water table, although laboratory data are only available at 24 and 48 hours, since water was not extractable at other times due to too low saturation. It is relevant that a sharp increase in the concentrations of long-chained PFAS and precursors was observed during the initial days of air-sparging.

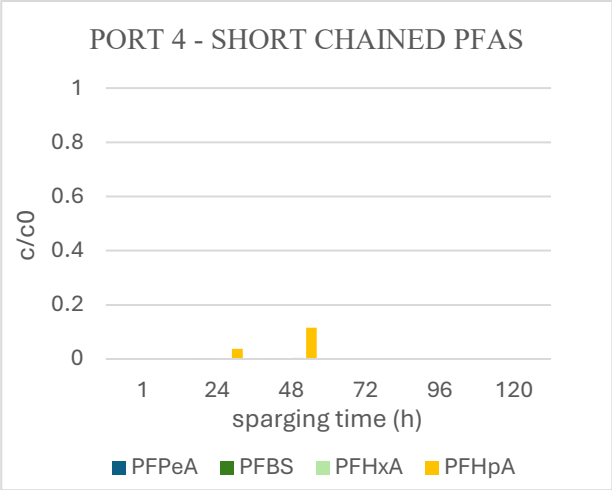

Figure 6.7a Short-chained PFAS concentrations variation after air-sparging for 24h and 48h at port 4 in coarse sand. The concentrations increase in time, mostly PFHpA.

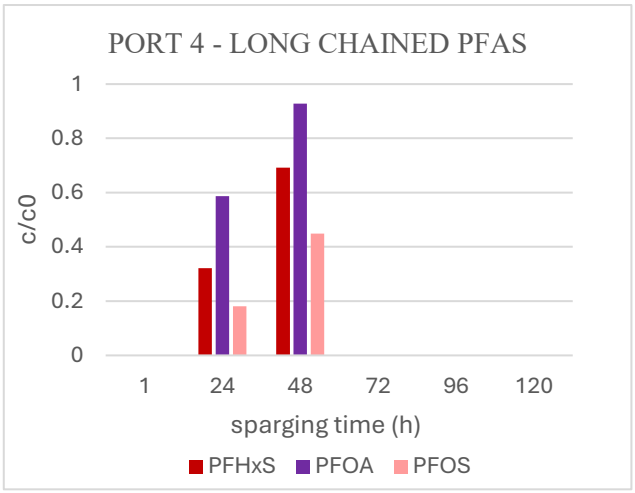

Figure 6.7b Long-chained PFAS concentrations variation after air-sparging for 24h and 48h at port 4 in coarse sand. The concentrations highly increase in time.

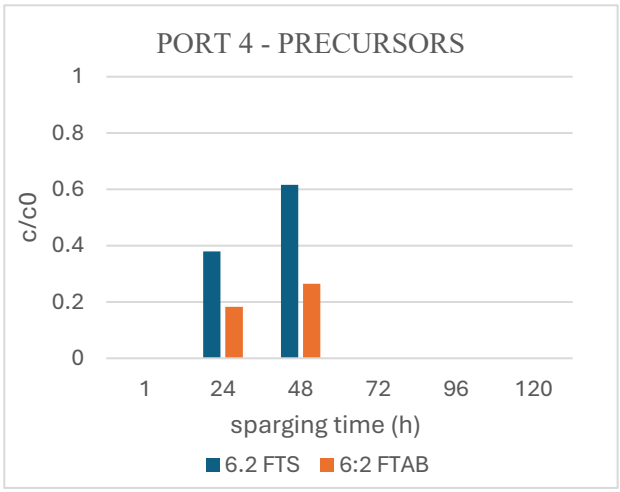

Figure 6.7c Precursors concentrations variation after air-sparging for 24h and 48h at port 4 in coarse sand. The concentrations highly increase in time.

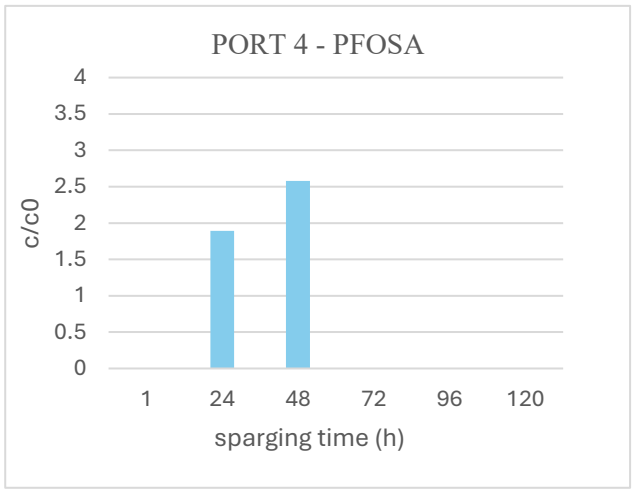

Figure 6.7d PFOSA concentration variation after air-sparging for 24h and 48h at port 4 in coarse sand. The concentrations highly increase in time.

The high concentration of long-chained PFAS and precursors detected at port 4 suggests that these compounds accumulated at the air-water interface within the water table, as early as 24 hours after the start of sparging, and likely persisted throughout the subsequent stages of the experiment. This accumulation likely explains the absence of elevated concentrations at the lower sampling ports (second (Fig. 6.5b-c) and third (Fig. 6.6b-c)), even as the experiment progressed over time. However, this hypothesis cannot be fully confirmed due to the lack of samples from port 4 during the final days of the experiment.

6.1.2 PFAS VERTICAL MIGRATION DURING AIR-SPARGING IN FINE SAND

In the second experiment, it was not possible to extract water from the fourth port corresponding to the water table area at any time, due to too low saturation in water. Normalized PFAS concentrations are shown by sampling ports after 48 and 120 hours of sparging to compare how the PFAS distribution changes in time. Over time, a decrease in concentration at the bottom of the column and a corresponding increase at the third port can be observed (Fig. 6.8a-b).

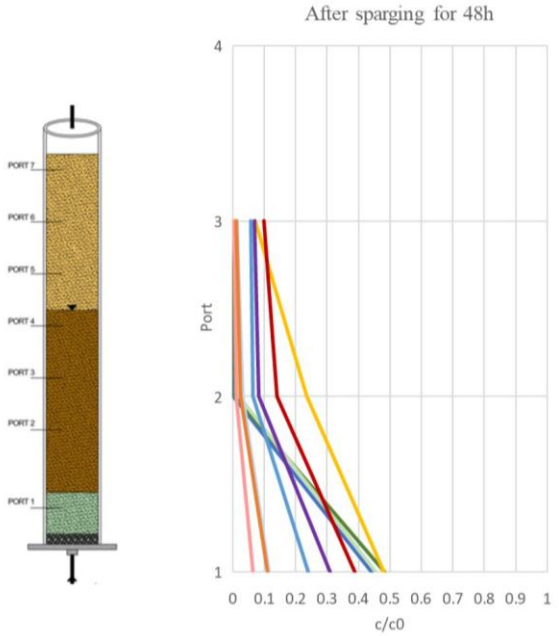

Figure 6.8a PFAS concentrations variation after sparging for 48 hours in fine sand. PFAS concentrations is decreasing from port 1 to port 2. From port 2, they start to increase up to the port 3. *Sampling from the port 4 was not possible.*

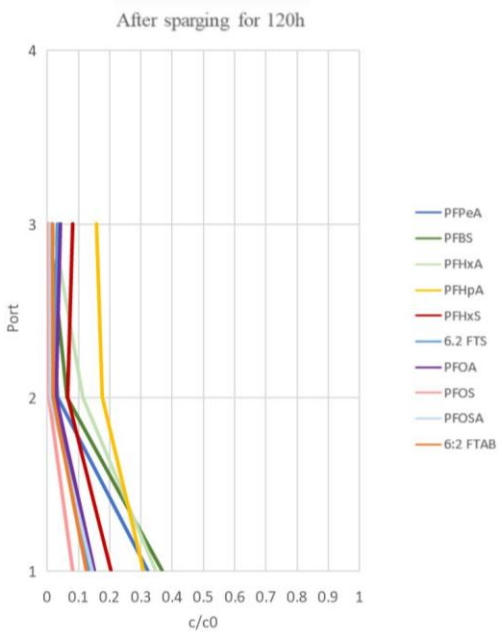

Figure 6.8b PFAS concentrations variation after sparging for 120 hours in fine sand. PFAS concentrations is decreasing from port 1 to port 2. From port 2, they start to increase up to the port 3. *Sampling from the port 4 was not possible.*

As in the previous section, temporal trends in normalized PFAS concentrations over the air-sparging duration are illustrated for each sampling port for the second experiment.

The trends at the first sampling port are shown in Fig. 6.9a-c. As in the experiment with coarse sand, the concentration at the bottom of the column is decreasing over time. However, it's important to highlight that short-chained PFAS appear more mobile in fine sand than in coarse sand. This is suggested by the lower normalized concentrations observed in fine sand in the final days of sparging, likely due to increased air-water interfacial area of fine sand (Tab. 5.5) that enhance adsorption to the air-water interface and vertical migration. Long-chained PFAS and precursors seem to exhibit less mobility in fine sand compared to coarse sand (Fig. 6.4b-c). Probably it is related to stronger adsorption to the solid matrix due to higher specific surface and/or to the air-water interface, rather than interactions with air bubbles.

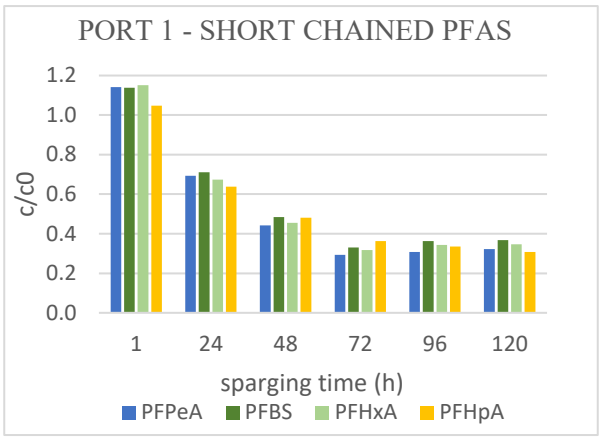

Figure 6.9a Short-chained PFAS concentrations variation throughout the air-sparging process at port 1 in fine sand. The concentrations decrease in time.

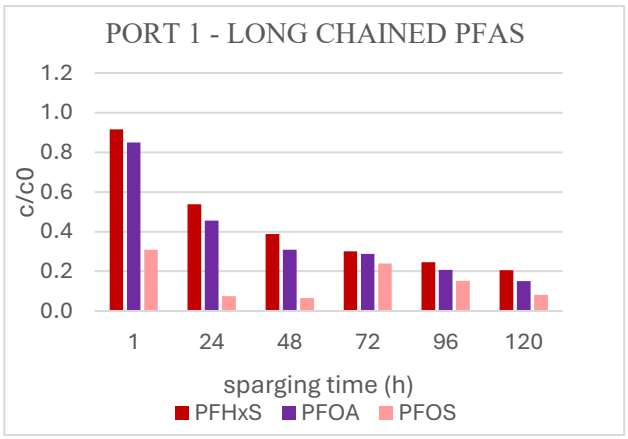

Figure 6.9b Long-chained PFAS concentrations variation throughout the air-sparging process at port 1 in fine sand. The concentrations decrease in time.

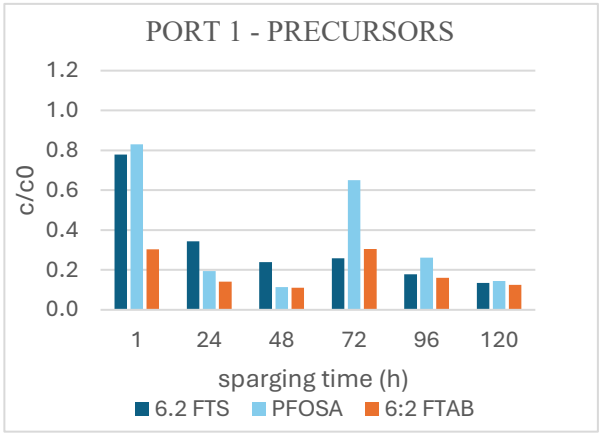

Figure 6.9c Precursors concentrations variation throughout the air-sparging process at port 1 in fine sand. The concentrations decrease in time.

At the second port (Fig. 6.10a-c), in the intermediate portion of the saturated zone, short-chained PFAS concentrations are increasing over time, while precursors and long-chained PFAS concentrations are decreasing. This is likely due to a faster vertical migration of long-chained PFAS and precursors along the column, leading to their retaining at the water table after just 24 hours of air-sparging, as previously observed in the experiment with coarse sand (see Chapter 6.1.1). As a result, the majority of these compounds are not detectable anymore in the middle of the partially saturated zone (the initial 'saturated zone', see Fig. 5.2), because they have already moved upward and retained above the fourth port, near the water table. This hypothesis is confirmed by the total concentration trends and the mass balance in Chapter 6.1.3.

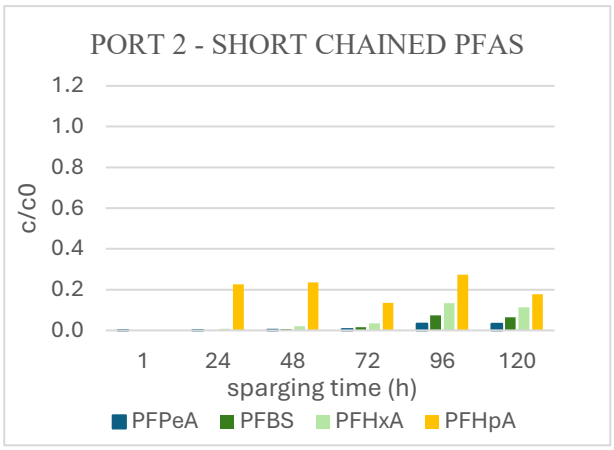

Figure 6.10a Short-chained PFAS concentrations variation throughout the air-sparging process at port 2 in fine sand. The concentrations increase in time.

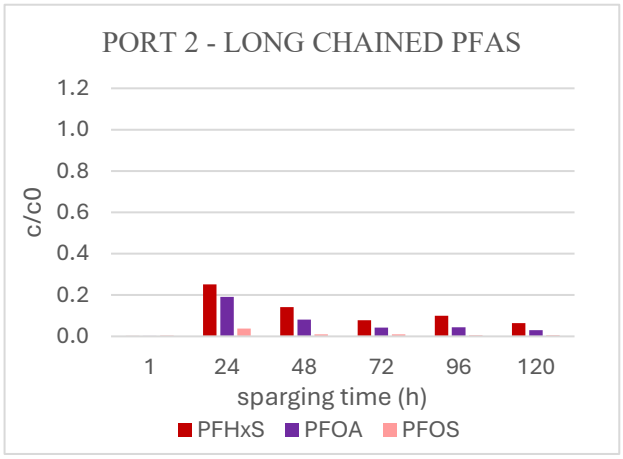

Figure 6.10b Long-chained PFAS concentrations variation throughout the air-sparging process at port 2 in fine sand. The concentrations decrease in time.

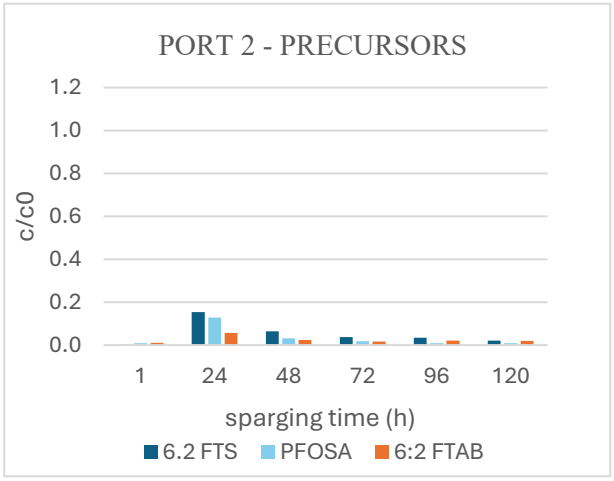

Figure 6.10c Precursors concentrations variation throughout the air-sparging process at port 2 in fine sand. The concentrations decrease in time.

The overall same PFAS behavior is observed at the third port of the column (Fig. 6.11a-c).

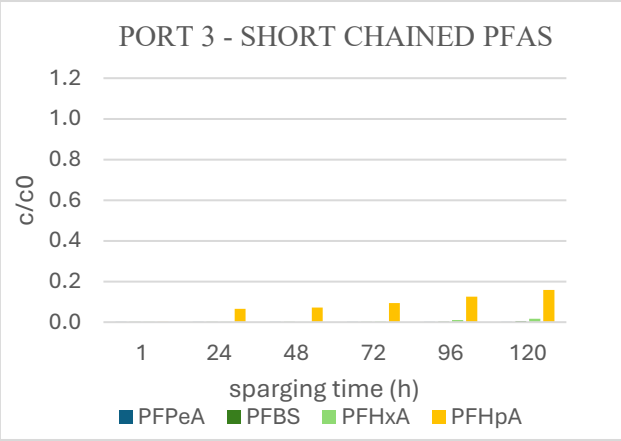

Figure 6.11a Short-chained PFAS concentrations variation throughout the air-sparging process at port 3 in fine sand. The concentrations increase in time, mostly PFHpA.

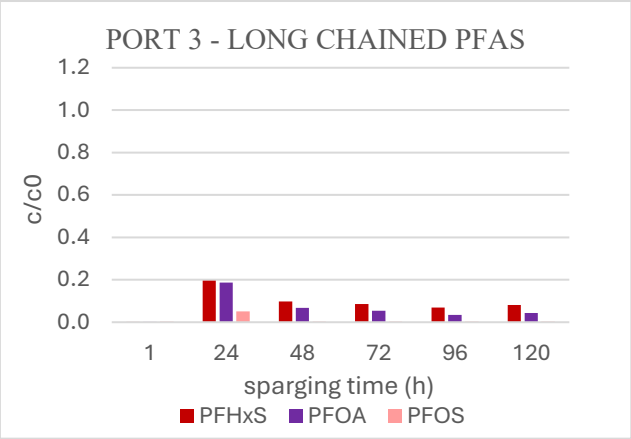

Figure 6.11b Long-chained PFAS concentrations variation throughout the air-sparging process at port 3 in fine sand. The concentrations decrease in time.

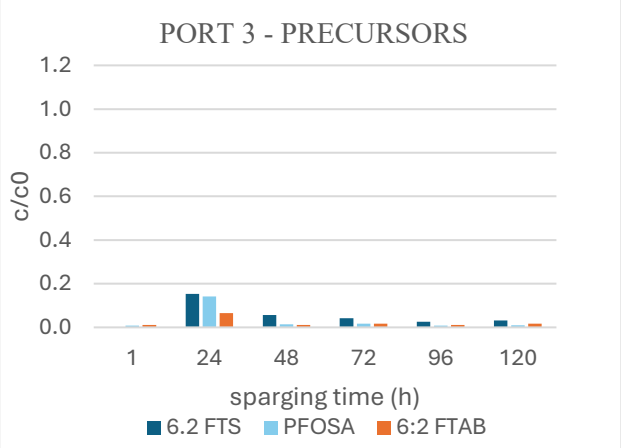

Figure 6.11c Precursors concentrations variation throughout the air-sparging process at port 3 in fine sand. The concentrations decrease in time.

6.1.3 PFAS VERTICAL MIGRATION AFTER SPARGING INTERRUPTION

Laboratory data from the sand samples show the PFAS total concentration (Appendix H.3), from port 2 to the water table above port 4, at the end of the experiment when the compressed air flow was stopped (Fig. 6.12a-b). The total concentration is comprehensive of the concentration dissolved in the pore volume and adsorbed to the sand grains. Considering these values is important to explain the distribution of the different PFAS within the three-phase system and to support the hypothesis about the adsorption to the solid matrix and migration to the water table of the long-chained PFAS and precursors.

Figure 6.12a-b highlights that all PFAS moved upwards to the water table in both the experiments because a certain concentration for each PFAS is detected above the fourth sampling port.

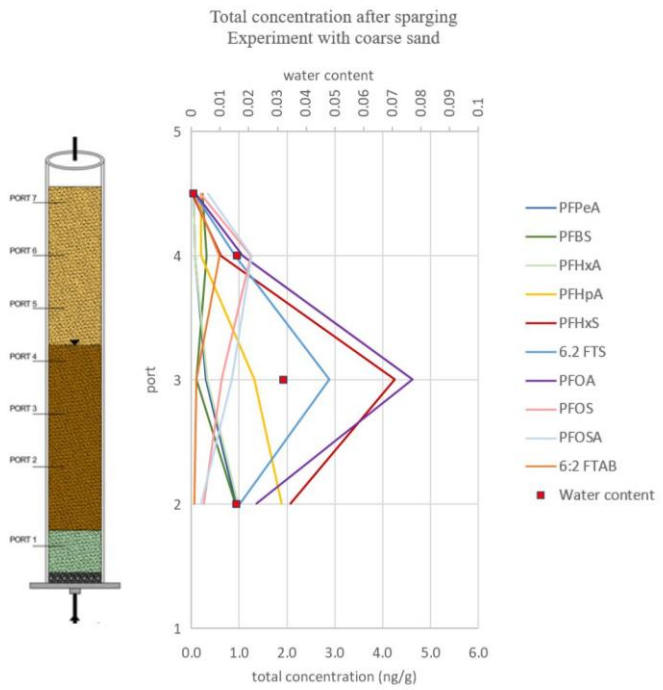

Figure 6.12a Water content and PFAS total concentrations variation after interrupting air-spanging in coarse sand. The concentrations increase up to port 3 and then start to decrease up to the water table.

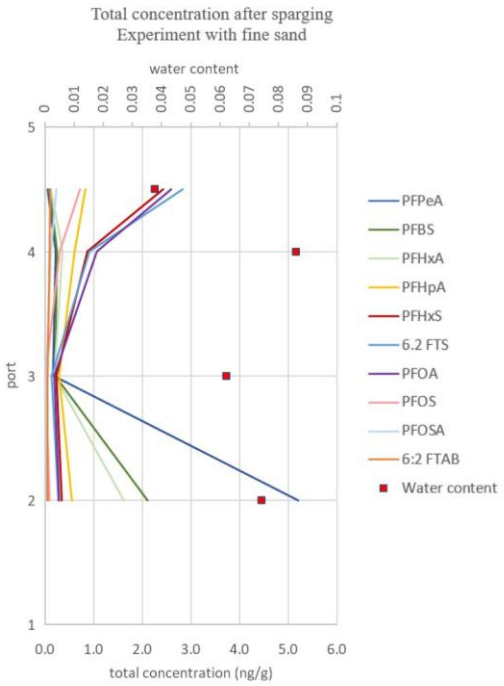

Figure 6.12b Water content and PFAS total concentrations variation after interrupting air-spanging in fine sand. PFAS total concentrations increase from port 3 up to the water table.

In the experiment with coarse sand (Fig. 6.12a), the total concentration of the majority of long- and short-chained PFAS and precursors increased until port 3 and then started to decrease towards the water table. This result was not expected since it doesn't align with pore water concentration trends obtained one hour after interrupting sparging (Fig. 6.13).

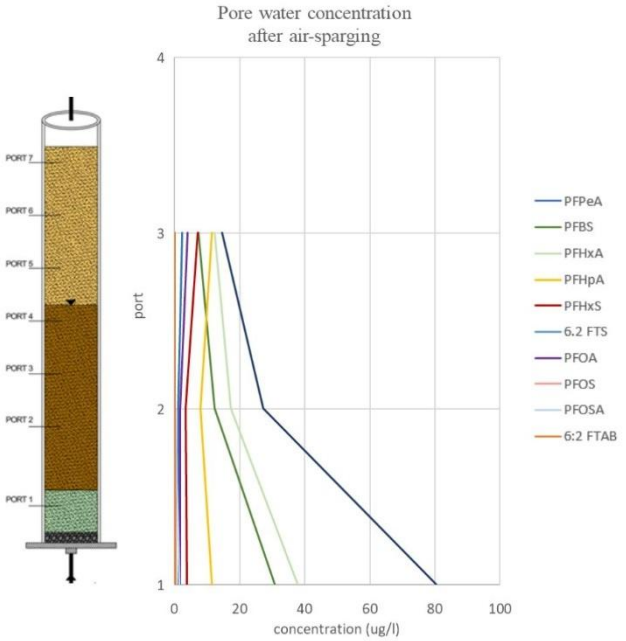

Figure 6.13 PFAS pore water concentrations variation after interrupting air-spanging in coarse sand. PFAS pore water concentrations decrease up to port 3. Sampling from the fourth port was not possible.

The water content of coarse sand has the same trend as the total PFAS concentrations, opposite with respect to the pore water concentrations (Fig. 6.13). This may be attributed to a dilution effect: in wetter zones, PFAS are more diluted in the larger volume of pore water, leading to lower aqueous concentrations despite a higher total PFAS load. In drier zones, the smaller water volume results in higher pore water concentrations even if the total PFAS is lower.

Thus, differences in water content appear to control the distribution of PFAS between the solid and liquid phases, explaining the observed trends.

At the third sampling port, particularly high is the concentration of PFHxS, PFOA and 6:2 FTS that exhibit greater mobility with respect to the other compounds. PFOS total concentration is consistent with the hypothesis made for PFOS pore water concentration, which is that the low concentrations at the second and third port are justified since its total concentration is higher around the water table. This means that PFOS is retained at the air-water interface near the water table.

Regarding the experiment with fine sand (Fig. 6.12b), the PFAS total concentration trends differ from the previous ones (Fig. 6.12a). In this case, almost all PFAS have increasing concentrations from port 3 to the water table, particularly long-chained PFAS and precursors, with a behavior very similar to the pore water concentrations (Fig. 6.8b). As a result, they have very low pore water concentrations in the middle of the partially saturated zone because they have already moved upward and retained above the fourth port, near the water table. PFPeA presents a very high concentration at the bottom of the column, likely related to its initial concentration in the stock solution that is significantly higher than the other compounds.

6.2 MASS BALANCE IN THREE-PHASE SYSTEM

Initial PFAS mass before sparging

The initial PFAS mass introduced into the column corresponds to the mass in volume of the stock solution that is added to the ‘contaminated sand’ layer (see Fig. 5.2) and then inserted in the column. As initial concentration for both the experiments, it is considered the PFAS concentration in the water sample extracted from the ‘contaminated sand’ layer of the column with coarse sand. Initial concentrations in coarse sand were also used for the mass balance calculations in fine sand, due to the lack of initial concentration data for the latter. This approach is justified by the comparable organic carbon content and porosity between the two sand types, which allows for a reasonable comparison. To calculate this initial mass, the volume of the ‘contaminated sand’ layer is used, which is fully saturated (S_w=1). Calculations are displayed in Appendix H.2. Under these conditions, the system is considered a two-phase system (water and solid) so no contribution from the air-water interface is included at this stage.

Knowing the initial PFAS mass added to the sand before starting sparging and the pore water concentration at different levels of the column, it was possible to compare the PFAS masses before and after sparging, to evaluate that total mass of PFAS remained constant within the column.

6.2.1 MASS BALANCE IN EXPERIMENT WITH COARSE SAND

The mass balance for the experiment with coarse sand is calculated considering the initial PFAS mass before sparging and the PFAS masses after air-sparging for both 48 and 120 hours. PFOSA mass balance is not discussed, due to the high inconsistency of the results (see 6.1.1).

After two days of air-sparging, the mass balance appears reasonably consistent, aside from some variability between the initial and final masses, which for most PFAS falls for most compounds within the analytical uncertainty (around 20%) reported by the laboratory. Therefore, there is no indication of significant mass loss or analytical error, except for PFOA, PFHxS and 6:2 FTS masses which increase of about 100% with sparging. Some inconsistencies could be related to the initial simplification about the sampling ports volumes (see Chapter 5.10), that may not accurately reflect the actual spatial variability of PFAS distribution within the column.

Table 6.1 PFAS mass balance between initial PFAS mass before sparging, and PFAS masses after air-sparging for both 48 and 120 hours, for the experiment with coarse sand. Differences between masses are displayed to highlight both mass loss and mass gain.

	Total mass before sparging (µg)	Total mass after sparging for 48h (µg)	Difference	Total mass after sparging for 120h (µg)	Difference
PFBS	14.469	11.551	**-20%**	14.824	**2%**
PFOA	14.848	28.990	**95%**	3.280	**-78%**
PFOS	1.482	1.884	**27%**	0.084	**-94%**
PFHxA	21.831	28.033	**28%**	29.984	**37%**
PFHpA	13.306	16.987	**28%**	13.531	**2%**
PFPeA	36.568	48.950	**34%**	56.431	**54%**
PFHxS	13.966	26.926	**93%**	7.017	**-50%**
6:2 FTS	10.763	23.480	**118%**	3.227	**-70%**
PFOSA	2.704	5.322	**97%**	0.615	**-61%**
6:2 FTAB	0.448	0.594	**32%**	0.173	**-77%**

The mass balance changes significantly if the total mass after sparging for six days is considered, due to the lack of samples from the fourth port. A high mass loss of long-chained PFAS and precursors is observed that it likely refers to the missing data from the column section near the water table. Additionally, this observed mass loss can be reasonably attributed to the PFAS distribution among the three phases (see Appendix H.2). In particular, approximately 50% of the mass of PFOA, PFOS, PFHxS, 6:2 FTS and 6:2 FTAB is adsorbed to the solid phase. Moreover, PFOA, 6:2 FTS and 6:2 FTAB show a percentage in mass – around 3% - retained at the air-water interface, PFHxS a percentage close to 1%, while PFOS exhibit a higher affinity to air-water interface, close to 10%. These data help to explain the negative mass balance (Tab. 6.1), suggesting that most PFAS remain within the system, although samples extraction, rather than actual removal or degradation.

Instead, the mass balance of short-chained PFAS still appears sufficiently consistent even after 120 hours, which corresponds with these compounds did not migrate extensively upwards and that most of their mass remained in the lower part of the column. Among the short-chained PFAS, PFHpA and PFBS exhibit the lowest mass balance compared to the compounds of the same group (Tab. 6.1). However, it is important to note that, even though the mass balance between these two compound is similar, PFHpA migrated upwards by adsorption to the air bubbles air-water interface - in fact, approximately 1% of its mass is retained at the air-water interface (see Appendix H.2) - , while PFBS, as PFPeA and PFHxA, did not exhibit any tendency to adsorb to this interface in coarse sand.

6.2.2 MASS BALANCE IN EXPERIMENT WITH FINE SAND

The mass balance for the experiment with fine sand is calculated considering the initial PFAS mass before sparging and PFAS masses after air-sparging for 48 hours and 120 hours (Tab. 6.2). This mass balance differs from the previous one (Tab. 6.1), even though it overall confirms the previous interpretation of the laboratory data about the effective vertical migration of most PFAS.

Table 6.2 PFAS mass balance between initial PFAS mass before sparging, and PFAS masses after air-sparging for both 48 and 120 hours, for the experiment with fine sand. Differences between masses are displayed to highlight both mass loss and mass gain.

	Total mass before sparging (µg)	Total mass after sparging for 48h (µg)	Difference	Total mass after sparging for 120h (µg)	Difference
PFBS	14.469	8.945	**38%**	7.779	**46%**
PFOA	14.848	15.039	**1%**	7.287	**-51%**
PFOS	1.482	0.361	**-76%**	0.419	**-72%**
PFHxA	21.831	20.236	**-7%**	19.451	**-11%**
PFHpA	13.306	20.302	**53%**	15.796	**19%**
PFPeA	36.568	31.916	**-13%**	25.238	**-31%**
PFHxS	13.966	19.929	**43%**	10.938	**-22%**
6:2 FTS	10.763	13.422	**25%**	7.058	**-34%**
PFOSA	2.704	0.294	**-89%**	0.311	**-89%**
6:2 FTAB	0.448	0.184	**-59%**	0.204	**-55%**

The difference between the total masses of short-chained PFAS before and after air-sparging falls within the analytical uncertainty (around 20%) reported by the laboratory, mostly in the first two days. Some discrepancies may be related to the initial simplifications about the initial concentration and the sampling ports volumes. After 120 hours of sparging, a negative mass balance is noticed for PFHxA. This compound, that in the experiment with coarse sand did not considerably interact with the air-water interface, exhibits a certain retention to the air-water interface and so a higher vertical transport, which makes it less detectable in the first three ports. In Appendix H.2 it is shown that 1% of the PFHxA is retained at the air-water interface, and PFHpA has a higher tendency to this retention, around 2% of its mass.

Regarding long-chained PFAS and precursors, they exhibit negative mass balance after 120 hours. This could be related to:

- Inconsistencies related to the initial simplification about the sampling ports volumes.
- Missing data from the column section near the water table, which could show PFAS mass above the fourth port (as it is displayed in Fig. 6.12b).
- Adsorption to solid phase.

It is relevant that with fine sand a greater portion of long-chained PFAS and precursors mass is partitioned to the air-water interface. In fact, approximately 7% of the total mass of PFOA, 6:2 FTS and 6:2 FTAB is retained at the air-water interface, compared to 2% for PFHxS as much as 20% for PFOS.

Therefore, it is clear that finer sand enhances the retention at the air-water interface, due to the greater air-water interfacial area.

6.3 COMPARATIVE ANALYSIS OF PFAS FUNCTIONAL GROUPS AND HEAD CHARGES

Until now, the discussion of the results has focused primarily on the influence of PFAS chain length, without considering differences related to the functional head group. This is because the most significant variations in behavior and distribution were observed among compounds differing in chain length, rather than in headgroup charge or functional group type.

However, it can be noted that 6:2 FTAB, a zwitterionic precursor, exhibited behavior very similar to 6:2 FTS, an anionic compound. Nonetheless, based on the mass balance, 6:2 FTAB showed a greater affinity for the air–water interface compared to 6:2 FTS (Appendix H.2).

As for the functional group, no clear or consistent differences were observed. PFOS, a PFSA, showed the highest retention at the air–water interface, but PFHxS, another PFSA, behaved more similarly to PFOA, a PFCA.

A similar trend was seen among short-chained compounds. PFHpA was the most mobile, primarily due to its longer chain length compared to the others, rather than its classification as a PFCA. In fact, PFPeA, which is also a PFCA, exhibited much lower mobility, likely due to weak retention at the air–water interface. Additionally, in the fine sand experiment, PFHxA (a short-chain PFCA) also exhibited some mobility, although it remained relatively limited. On the other hand, PFBS, a very short-chain PFSA, showed very low affinity for the air–water interface, despite belonging to the same class as PFOS and PFHxS.

6.4 COLUMN EXPERIMENTS: LIMITATIONS AND SUGGESTIONS

Column experiments proved to be an effective method for investigating the applicability of air sparging in PFAS transport, especially considering that results confirmed the predominant role of air–water interfacial retention in the vertical transport of most PFAS compounds. However, the experiments also presented several limitations. One of the main issues was related to sample extraction, which could only be performed at the lower sampling ports. This constraint prevented a complete quantification of PFAS distribution throughout the column during and after the air sparging phase.

The most critical limitation was the inability to maintain a clearly defined and stable water table. Upon initiating air sparging, the water level increased to an unpredictable height, making it impossible to identify or sample precisely at the interface between unsaturated and dry zones. Since the study focused on understanding PFAS behavior in correspondence with the top of the sparging zone, this uncertainty represented a significant drawback.

Moreover, the experiments could not replicate the natural horizontal groundwater flow that, under field conditions, helps maintain the treated zone saturated or interacts with the effects of air sparging. Understanding how groundwater flow influences the overall effectiveness of air sparging remains essential for in-situ applications.

Additionally, the use of pulsed air sparging should be considered as a potential improvement, as it may help overcome the formation of preferential flow paths and promote enhanced mixing within the column, which is desirable because it would homogenously distribute the treatment across the entire column and increase the likelihood of treating contaminants.

While monitoring PFAS distribution over the six-day experimental period was informative, it would have been equally valuable to investigate how concentrations evolved after the cessation of compressed air injection. This would allow us to assess whether the compounds remained retained over time or instead began to migrate downward again shortly after the end of air sparging. Such behavior would significantly limit the long-term effectiveness of air sparging as a remediation strategy for PFAS, as sustained retention near the capillary fringe is essential to achieve removal benefits.

7. FUTURE PERSPECTIVES

To further evaluate the applicability and long-term performance of air-sparging for PFAS remediation, several research directions and methodological improvements should be explored.

First, future studies should aim to simulate more realistic hydrogeological conditions by incorporating a horizontal groundwater flow, which is a key component in natural aquifer systems, e.g., in 2D or 3D tank experiments. Including this dynamic would provide more accurate insight into how air-sparging performs under field-relevant conditions, where water movement can influence PFAS mobilization, dilution, and retention.

Furthermore, the effectiveness of air-sparging is strongly dependent on the hydrogeological setting, and its applicability is mostly limited to unconfined aquifers with shallow PFAS plumes and no confining units. In confined or semi-confined aquifers, upward gas movement and interface generation may be significantly limited or unpredictable. This highlights the importance of conducting detailed site characterization before implementing air-sparging, to ensure that the subsurface conditions are compatible with gas flow and PFAS removal dynamics.

From a broader field-scale perspective, several challenges must also be considered. Fluctuations in the water table may reduce PFAS retention by altering the location and stability of the air-water interface. Moreover, sparging in geologically heterogeneous aquifers could lead to preferential gas pathways, potentially causing unwanted lateral spreading of PFAS instead of enhancing their capture.

To overcome some of these limitations, alternative designs and hybrid approaches should be considered in future work. These include:

- Sparging in trenches to improve gas distribution and allow better control over the treatment zone geometry (ESTCP, 2022).
- Coupling air sparging with phytoremediation, which could enhance long-term PFAS stabilization and uptake through plant-root interactions (Newell et al., 2021).
- The use of colloidal gas aphrons to increase gas–liquid interfacial area and improve PFAS transport control (Kulkarni et al., 2022).
- Implementing inert gases, such as nitrogen, instead of ambient air to avoid oxidative effects or promote more stable gas pathways (Newell et al., 2022).
- Limiting recharge of the aquifer by installing impermeable cap (Hort et al., 2024)

Air-sparging effectiveness in reducing the extent of the PFAS-contaminated plume and thereby facilitating PFAS removal could be significantly improved by first addressing the source of contamination. Removing or treating the source would limit the continuous input of PFAS into the subsurface, helping to slow or halt the further spreading of the plume. As a result, PFAS already present in the saturated zone would accumulate more effectively through air-sparging, allowing for a more focused and efficient remediation process.

Overall, while air-sparging shows promise as a remediation strategy for PFAS-contaminated sites, particularly due to its potential to exploit air-water interfacial retention, its in-situ application will require careful site-specific design, further validation under dynamic hydrogeological conditions, and potential integration with complementary technologies to ensure effectiveness and sustainability.

8. CONCLUSIONS

Per- and polyfluoroalkyl substances (PFAS) are persistent, surface-active compounds known for their complex behavior in subsurface environments. A key property influencing their environmental fate is their strong tendency to adsorb at the air-water interface, a phenomenon that becomes increasingly significant with the length of the fluorinated carbon chain. This property opens new perspectives for PFAS remediation techniques, particularly the use of air-sparging, which historically have been used for volatile organic compounds, but now may be used to remediate amphiphilic pollutants such as PFAS.

This study explored the effectiveness of air-sparging in shrinking PFAS-contaminated plumes, by promoting vertical migration and interfacial retention of PFAS within the transitional zone between unsaturated and saturated conditions. Two laboratory column experiments were designed and conducted over a six-days period to apply continuous compressed air flow through homogeneous solid media, coarse and fine sand. The lower part of the column was saturated with PFAS solution in tap water, containing a mixture of both short- and long-chained PFAS and precursors, including: PFBS, PFHxA, PFHpA, PFPeA, PFHxS, PFOA, PFOS, 6:2 FTS, PFOSA, and 6:2 FTAB.

Result demonstrated significant differences in mobility and retention of PFAS depending on their molecular structure and the characteristics of the porous medium:

- Long-chained PFAS and precursors, due to their stronger surface activity, showed more pronounced vertical transport through air-water interfacial adsorption, particularly evident in coarse sand. After just 24 hours of air-sparging, a sharp concentration increase was observed at the water table, suggesting rapid accumulation via interfacial migration.
- Short-chained PFAS, in contrast, were less affected by air-water interfacial processes but exhibited greater mobility in fine sand. This is likely due to the higher specific air-water interfacial area in fine-grained media, which facilitates interfacial transport.
- However, long-chained PFAS in fine sand exhibited lower mobility, possibly due to enhanced retention to the air-water interface, which may outweigh the mobilizing effect of air-sparging. The majority of these compounds were not detectable anymore in the middle of the saturated zone, likely because they have already adsorbed to the solid matrix and/or moved upward and retained near the water table.

Among individual compounds, PFOA and PFHxS displayed lower mobility than PFOS, suggesting that PFOS has a higher affinity for air-water interface adsorption. Interestingly, PFHpA, despite being a short-chained PFAS, showed significant vertical migration through interfacial retention. It is important to note that the vertical transport of PFAS was driven by adsorption at the air-water interface of rising bubbles, rather than by advective water flow, as supported by the bromide and short-chained PFAS results.

From a mass balance perspective, both column experiments maintained overall PFAS mass consistency after air-sparging, with differences within the analytical uncertainty. However, after six days, a noticeable mass loss of long-chained PFAS and precursors was observed. This may be attributed to adsorption in unsampled zones, particularly around the water table, and potential limitations in water samples extraction.

The findings suggest that air-sparging can be a viable in situ technology for promoting vertical migration and retention of PFAS at the top of the sparging zone, particularly for long-chained PFAS and precursors. However, its application is limited to unconfined aquifers and its effectiveness in retaining PFAS over long-term period is reduced by water table fluctuations. Therefore, the feasibility of using air-sparging for PFAS-contaminated sites remediation is closely linked to the hydrodynamic stability of the subsurface.

Nevertheless, the use of air-sparging to reduce the extent of PFAS-contaminated plume, by promoting their vertical migration and subsequent accumulation at the air-water interface at the water table, remains a promising remediation approach. Further studies in two- or three-dimensional laboratory conditions are needed before advancing to field pilot testing. Proper testing at field conditions is needed to assess the long-term effectiveness and scalability of air-sparging for remediation of PFAS-contaminated sites.

BIBLIOGRAPHY

Abunada, Z., Alazaiza, M. Y. D., & Bashir, M. J. K. (2020). An overview of per-and polyfluoroalkyl substances (Pfas) in the environment: Source, fate, risk and regulations. In *Water (Switzerland)* (Vol. 12, Issue 12). MDPI AG. https://doi.org/10.3390/w12123590

Adams, J. A., & Reddy, K. R. (2003). Extent of benzene biodegradation in saturated soil column during air sparging. In *Ground Water Monitoring and Remediation* (Vol. 23, Issue 3, pp. 85–94). National Ground Water Association. https://doi.org/10.1111/j.1745-6592.2003.tb00686.x

Adamson, D., Nickerson, A., Kulkarni, P., Higgins, C., Popovic, J., Field, J., Rodowa, A., Newell, C., DeBlanc, P., & Kornuc, J. (2020). Mass-Based, Field-Scale Demonstration of PFAS Retention within AFFF-Associated Source Areas. *Environmental Science & Technology*, *54*, 15768–15777. https://doi.org/10.1021/acs.est.0c04472

Appelo, C. A. J., & Postma, Dieke. (2004). *Geochemistry, groundwater and pollution*. A.A. Balkema Publishers.

Brendel, S., Fetter, É., Staude, C., Vierke, L., & Biegel-Engler, A. (2018). Short-chain perfluoroalkyl acids: environmental concerns and a regulatory strategy under REACH. *Environmental Sciences Europe*, *30*(1). https://doi.org/10.1186/s12302-018-0134-4

Brusseau, M. L. (2018). Assessing the potential contributions of additional retention processes to PFAS retardation in the subsurface. *Science of the Total Environment*, *613–614*, 176–185. https://doi.org/10.1016/j.scitotenv.2017.09.065

Brusseau, M. L. (2019). The influence of molecular structure on the adsorption of PFAS to fluid-fluid interfaces: Using QSPR to predict interfacial adsorption coefficients. *Water Research*, *152*, 148–158. https://doi.org/10.1016/j.watres.2018.12.057

Brusseau, M. L. (2023a). Determining air-water interfacial areas for the retention and transport of PFAS and other interfacially active solutes in unsaturated porous media. *Science of the Total Environment*, *884*. https://doi.org/10.1016/j.scitotenv.2023.163730

Brusseau, M. L. (2023b). Differential Sorption of Short-Chain versus Long-Chain Anionic Per- and Poly-Fluoroalkyl Substances by Soils. *Environments - MDPI*, *10*(10). https://doi.org/10.3390/environments10100175

Brusseau, M. L., Lyu, Y., Yan, N., & Guo, B. (2020). Low-concentration tracer tests to measure air-water interfacial area in porous media. *Chemosphere.* https://doi.org/10.1016/j.chemosphere.2020.126305

Brusseau, M. L., Peng, S., Schnaar, G., & Costanza-Robinson, M. S. (2006). Relationships among air-water interfacial area, capillary pressure, and water saturation for a sandy porous medium. *Water Resources Research*, *42*(3). https://doi.org/https://doi.org/10.1029/2005WR004058

Brusseau, M. L., Peng, S., Schnaar, G., & Murao, A. (2007a). Measuring Air−Water Interfacial Areas with X-ray Microtomography and Interfacial Partitioning Tracer Tests. *Environmental Science & Technology*, *41*(6), 1956–1961. https://doi.org/10.1021/es061474m

Brusseau, M. L., Peng, S., Schnaar, G., & Murao, A. (2007b). Measuring air-water interfacial areas with X-ray microtomography and interfacial partitioning tracer tests. *Environmental Science and Technology*, *41*(6), 1956–1961. https://doi.org/10.1021/es061474m

Brusseau, M. L., & Van Glubt, S. (2021). The influence of molecular structure on PFAS adsorption at air-water interfaces in electrolyte solutions. *Chemosphere*, *281*. https://doi.org/10.1016/j.chemosphere.2021.130829

Buck, R. C., Franklin, J., Berger, U., Conder, J. M., Cousins, I. T., Voogt, P. De, Jensen, A. A., Kannan, K., Mabury, S. A., & van Leeuwen, S. P. J. (2011). Perfluoroalkyl and polyfluoroalkyl substances in the environment: Terminology, classification, and origins. *Integrated Environmental Assessment and Management*, *7*(4), 513–541. https://doi.org/10.1002/ieam.258

Cary, J. W. (1994). Estimating the surface area of fluid phase interfaces in porous media. *Journal of Contaminant Hydrology*, *15*(4), 243–248. https://doi.org/https://doi.org/10.1016/0169-7722(94)90029-9

Cook, P. (2022). *Introduction to Isotopes and Environmental Tracers as Indicators of Groundwater Flow*.

Costanza, J., Arshadi, M., Abriola, L. M., & Pennell, K. D. (2019). Accumulation of PFOA and PFOS at the Air-Water Interface. *Environmental Science and Technology Letters*, *6*(8), 487–491. https://doi.org/10.1021/acs.estlett.9b00355

Costanza, M. S., & Brusseau, M. L. (2000). Contaminant vapor adsorption at the gas-water interface in soils. *Environmental Science and Technology*, *34*(1), 1–11. https://doi.org/10.1021/es9904585

Costanza-Robinson, M. S., & Brusseau, M. L. (2002). Air-water interfacial areas in unsaturated soils: Evaluation of interfacial domains. *Water Resources Research*, *38*(10), 13-1-13–17. https://doi.org/https://doi.org/10.1029/2001WR000738

D'Agostino, L., & Mabury, S. (2017). Aerobic biodegradation of 2 fluorotelomer sulfonamide-based aqueous film-forming foam components produces perfluoroalkyl carboxylates. *Environmental Toxicology and Chemistry*, *36*. https://doi.org/10.1002/etc.3750

Dalla, E., Hilpert, M., & Miller, C. T. (2002). Computation of the interfacial area for two-fluid porous medium systems. *Journal of Contaminant Hydrology*, *56*(1), 25–48. https://doi.org/https://doi.org/10.1016/S0169-7722(01)00202-9

Danish EPA. (2021). *Liste over kvalitetskriterier i relation til forurenet jord. Danish Environmental Protection Agency*.

Danske Regioner. (2024). *Stof til eftertanke - regionernes arbejde med jordforurening.Stof til eftertanke - regionernes arbejde med jordforurening.* Www.Jordforureninger.Dk.

Darlington, R., Barth, E., & McKernan, J. (2019). The challenges of PFAS remediation. *Society of American Military Engineers (SAME)*, *110*, 58–60.

Downer, A., Eastoe, J., Pitt, A. R., Penfold, J., & Heenan, R. K. (1999). Adsorption and micellisation of partially-and fully-fluorinated surfactants. In *Physicochem. Eng. Aspects* (Vol. 156). www.elsevier.nl/locate/colsurfa

Downes, N., Ottewill, G. A., & Ottewill, R. H. (1995). An investigation of the behaviour of ammonium perfluoro-octanoate at the air/water interface in the absence and presence of salts. *Colloids and Surfaces A: Physicochemical and Engineering Aspects*, *102*, 203–211. https://doi.org/https://doi.org/10.1016/0927-7757(95)03191-F

Du, Z., Deng, S., Bei, Y., Huang, Q., Wang, B., Huang, J., & Yu, G. (2014). Adsorption behavior and mechanism of perfluorinated compounds on various adsorbents—A review. *Journal of Hazardous Materials*, *274*, 443–454. https://doi.org/https://doi.org/10.1016/j.jhazmat.2014.04.038

ECHA. (2023). *List of substances subject to POPs Regulation*. Https://Echa.Europa.Eu/It/List-of-Substances-Subject-to-Pops-Regulation.

EPA. (2025). *Comptox Chemicals Dashboard*. Https://Comptox.Epa.Gov/Dashboard/.

ESTCP. (2021). *Low-Cost, Passive In Situ Treatment of PFAS-Impacted Groundwater Using Foam Fractionation In an Air Sparge Trench.*

ESTCP. (2022). *Rapid and Inexpensive Delivery off Particulate Carbon for In Situ PFAS Treatment in Groundwater*.

European Union Council. (2020). *Directive (EU) 2020/2184 of the European Parliment and of the Council of 16 December 2020 on the quality of water intended for human consumption*.

Fabregat-Palau, J., Vidal, M., & Rigol, A. (2021). Modelling the sorption behaviour of perfluoroalkyl carboxylates and perfluoroalkane sulfonates in soils. *Science of the Total Environment*, *801*. https://doi.org/10.1016/j.scitotenv.2021.149343

Farhat, S., Newell, C., Looney, B., & Falta, R. (2022). Impact of matrix diffusion on the migration of groundwater plumes for Perfluoroalkyl acids (PFAAs) and other non-degradable compounds. *Journal of Contaminant Hydrology*, *247*, 103987. https://doi.org/10.1016/j.jconhyd.2022.103987

Ferrey, M. L., Wilson, J. T., Adair, C., Su, C., Fine, D. D., Liu, X., & Washington, J. W. (2012). Behavior and Fate of PFOA and PFOS in Sandy Aquifer Sediment. *Groundwater Monitoring & Remediation*, *32*(4), 63–71. https://doi.org/https://doi.org/10.1111/j.1745-6592.2012.01395.x

Harding-Marjanovic, K., Houtz, E., Yi, S., Field, J., Sedlak, D., & Alvarez-Cohen, L. (2015). Aerobic Biotransformation of Fluorotelomer Thioether Amido Sulfonate (Lodyne™) in AFFF-Amended Microcosms. *Environmental Science & Technology*, *49*. https://doi.org/10.1021/acs.est.5b01219

Hellsing, M. S., Josefsson, S., Hughes, A. V, & Ahrens, L. (2016). Sorption of perfluoroalkyl substances to two types of minerals. *Chemosphere*, *159*, 385–391. https://doi.org/https://doi.org/10.1016/j.chemosphere.2016.06.016

Higgins, C. P., & Luthy, R. G. (2007). Modeling Sorption of Anionic Surfactants onto Sediment Materials: An a priori Approach for Perfluoroalkyl Surfactants and Linear Alkylbenzene Sulfonates. *Environmental Science & Technology*, *41*(9), 3254–3261. https://doi.org/10.1021/es062449j

Hort, H. M., Stockwell, E. B., Newell, C. J., Scalia, J., & Panday, S. (2024). Modeling and Evaluation of PFOS Retention in the Unsaturated Zone above the Water Table. *Groundwater Monitoring and Remediation*, *44*(3), 38–48. https://doi.org/10.1111/gwmr.12662

ITRC. (2023). *Per- and Polyfluoroalkyl Subastances (PFAS)*.

Johnson, R. L., Anschutz, A. J., Smolen, J. M., Simcik, M. F., & Lee Penn, R. (2007). The adsorption of perfluorooctane sulfonate onto sand, clay, and iron oxide surfaces. *Journal of Chemical and Engineering Data*, *52*(4), 1165–1170. https://doi.org/10.1021/je060285g

Johnson, R. L., Anschutz, A. J., Smolen, J. M., Simcik, M. F., & Penn, R. L. (2007). The Adsorption of Perfluorooctane Sulfonate onto Sand, Clay, and Iron Oxide Surfaces. *Journal of Chemical & Engineering Data*, *52*(4), 1165–1170. https://doi.org/10.1021/je060285g

Kim, H., Annable, M. D., & Rao, P. S. C. (1998). Influence of air-water interfacial adsorption and gas-phase partitioning on the transport of organic chemicals in unsaturated porous media. *Environmental Science and Technology*, *32*(9), 1253–1259. https://doi.org/10.1021/es970868y

Kim, H., Rao, P. S. C., & Annable, M. D. (1997). Determination of effective air-water interfacial area in partially saturated porous media using surfactant adsorption. *Water Resources Research*, *33*(12), 2705–2711. https://doi.org/10.1029/97WR02227

Kim, H., Rao, P. S. C., & Annable, M. D. (1999). Gaseous Tracer Technique for Estimating Air–Water Interfacial Areas and Interface Mobility. *Soil Science Society of America Journal*, *63*(6), 1554–1560. https://doi.org/https://doi.org/10.2136/sssaj1999.6361554x

Kim, H., Soh, H.-E., Annable, M. D., & Kim, D.-J. (2004). Surfactant-Enhanced Air Sparging in Saturated Sand. *Environmental Science & Technology*, *38*(4), 1170–1175. https://doi.org/10.1021/es030547o

Kissa E. (2001). Fluorinated Surfactants and Repellents: Second Edition, Revised and Expanded Surfactant Science Series. Volume 97. By Erik Kissa (Consultant, Wilmington, DE). Marcel Dekker: New York. 2001. xiv + 616 pp. $195.00. ISBN 0-8247-0472-X. *Journal of the American Chemical Society*, *123*(36), 8882. https://doi.org/10.1021/ja015260a

Krafft, M. P., & Riess, J. G. (2015a). Per- and polyfluorinated substances (PFASs): Environmental challenges. In *Current Opinion in Colloid and Interface Science* (Vol. 20, Issue 3, pp. 192–212). Elsevier Ltd. https://doi.org/10.1016/j.cocis.2015.07.004

Krafft, M. P., & Riess, J. G. (2015b). Selected physicochemical aspects of poly- and perfluoroalkylated substances relevant to performance, environment and sustainability—Part one. *Chemosphere*, *129*, 4–19. https://doi.org/https://doi.org/10.1016/j.chemosphere.2014.08.039

Kulkarni, P. R., Aranzales, D., Javed, H., Holsen, T. M., Johnson, N. W., Richardson, S. D., Mededovic Thagard, S., & Newell, C. J. (2022). Process to separate per- and polyfluoroalkyl substances from water using colloidal gas aphrons. *Remediation Journal*, *32*(3), 167–176. https://doi.org/https://doi.org/10.1002/rem.21716

Lassen, C., Maag, J., Krag, A., & Dau, M. S. (2024). *Publisher: Ministry of Environment of Denmark*.

Lath, S., Knight, E. R., Navarro, D. A., Kookana, R. S., & McLaughlin, M. J. (2019). Sorption of PFOA onto different laboratory materials: Filter membranes and centrifuge tubes. *Chemosphere*, *222*, 671–678. https://doi.org/https://doi.org/10.1016/j.chemosphere.2019.01.096

Leeson, A., Johnson, P. C., Johnson, R., & Hinchee, R. (2002). *Air Sparging Design Paradigm*. https://www.researchgate.net/publication/235108749

Lei, X., Lian, Q., Zhang, X., Karsili, T. K., Holmes, W., Chen, Y., Zappi, M. E., & Gang, D. D. (2023). A review of PFAS adsorption from aqueous solutions: Current approaches, engineering applications, challenges, and opportunities. In *Environmental Pollution* (Vol. 321). Elsevier Ltd. https://doi.org/10.1016/j.envpol.2023.121138

Li, Y., Barregard, L., Xu, Y., Scott, K., Pineda, D., Lindh, C. H., Jakobsson, K., & Fletcher, T. (2020). Associations between perfluoroalkyl substances and serum lipids in a Swedish adult population with contaminated drinking water. *Environmental Health: A Global Access Science Source*, *19*(1). https://doi.org/10.1186/s12940-020-00588-9

Liu, Z., Liu, S., Mao, B., & Cheng, Y. (2017). *Laboratory Remediation Test of MTBE-Contaminated Sands with Surfactant-Enhanced Air Sparging*. https://doi.org/10.1061/9780784480434.059

Lunkenheimer, K., Prescher, D., Hirte, R., & Geggel, K. (2015). Adsorption Properties of Surface Chemically Pure Sodium Perfluoro-n-alkanoates at the Air/Water Interface: Counterion Effects within Homologous Series of 1:1 Ionic Surfactants. *Langmuir*, *31*(3), 970–981. https://doi.org/10.1021/la503450k

Lyu, Y., Brusseau, M. L., Chen, W., Yan, N., Fu, X., & Lin, X. (2018). Adsorption of PFOA at the Air-Water Interface during Transport in Unsaturated Porous Media. *Environmental Science and Technology*, *52*(14), 7745–7753. https://doi.org/10.1021/acs.est.8b02348

Lyu, Y., Wang, B., & Brusseau, M. L. (2023). The influence of chain length on the sorption of C4-C10 perfluorocarboxylic acids during transport in a sand. *Journal of Hazardous Materials Letters*, *4*. https://doi.org/10.1016/j.hazl.2023.100084

Lyu, Y., Wang, B., Du, X., Guo, B., & Brusseau, M. L. (2022). Air-water interfacial adsorption of C4-C10 perfluorocarboxylic acids during transport in unsaturated porous media. *Science of the Total Environment*, *831*. https://doi.org/10.1016/j.scitotenv.2022.154905

Merino, N., Qu, Y., Deeb, R. A., Hawley, E. L., Hoffmann, M. R., & Mahendra, S. (2016). Degradation and Removal Methods for Perfluoroalkyl and Polyfluoroalkyl Substances in Water. *Environmental Engineering Science*, *33*(9), 615–649. https://doi.org/10.1089/ees.2016.0233

Morsing, L. (2025). *Concepts for remediation of PFAS contaminated sites*. DTU Sustain, Technical University of Denmark.

Morsing, L., Tsitonaki, K., Dyreborg, S., Mosthaf, K., Sidelmann, A., Rune, F., Bolette, H., Jensen, B., Baun, A., & Bjerg, P. L. (2025). *2 Miljøstyrelsen / Konceptuel model for transport og skaebne af PFAS ved forurenede grunde*.

National Research Council. (1994). *Alternatives for ground water cleanup*.

Naval Facilities Engineering Command. (2001). *Final air sparging guidance*.

Newell, C. J., Javed, H., Li, Y., Johnson, N. W., Richardson, S. D., Connor, J. A., & Adamson, D. T. (2022). Enhanced attenuation (EA) to manage PFAS plumes in groundwater. *Remediation*, *32*(4), 239–257. https://doi.org/10.1002/rem.21731

Newell, C. J., Kulkarni, P. R., & Adamson, D. T. (2021). In situ gas sparging for concentration and removal of per- and polyfluoroalkyl substances (PFAS) from groundwater. *Remediation*, *31*(4), 35–47. https://doi.org/10.1002/rem.21696

Nguyen, T. M. H., Bräunig, J., Thompson, K., Thompson, J., Kabiri, S., Navarro, D. A., Kookana, R. S., Grimison, C., Barnes, C. M., Higgins, C. P., Mclaughlin, M. J., & Mueller, J. F. (2020). Influences of Chemical Properties, Soil Properties, and Solution pH on Soil-Water Partitioning Coefficients of Per- And Polyfluoroalkyl Substances (PFASs). *Environmental Science and Technology*, *54*(24), 15883–15892. https://doi.org/10.1021/acs.est.0c05705

Nyer. (2000). *In Situ Treatment Technology* (E. K. Nyer, Ed.). CRC Press. https://doi.org/10.1201/9781420032642

OECD. (2011). *PFCS: Outcome of the 2009 Survey – Survey on the Production, Use and Release of PFOS, PFAS, PFOA, PFCA, Their Related Substances and Products/Mixtures Containing These Substances*. Http://Www.Oecd.Org/Officialdocuments/Publicdisplaydocumentpdf/?Cote=env/Jm/Mono(2011)1&doclanguage=en.

OECD. (2021). *Reconciling Terminology of the Universe of Per- and Polyfluoroalkyl Substances: Recommendations and Practical GuidanceReconciling Terminology of the Universe of Per- and Polyfluoroalkyl Substances: Recommendations and Practical Guidance*. Https://One.Oecd.Org/Document/ENV/CBC/MONO(2021)25/En/Pdf.

Oliviera, I. B., Demond, A. H., & Salehzadeh, A. (1996). Packing of Sands for the Production of Homogeneous Porous Media. *Soil Science Society of America Journal*, *60*(1), 49–53. https://doi.org/https://doi.org/10.2136/sssaj1996.03615995006000010010x

Oostrom, M., White, M. D., & Brusseau, M. L. (2001). Theoretical estimation of free and entrapped nonwetting–wetting fluid interfacial areas in porous media. *Advances in Water Resources*, *24*(8), 887–898. https://doi.org/https://doi.org/10.1016/S0309-1708(01)00017-3

Or, D., & Tuller, M. (1999). Liquid retention and interfacial area in variably saturated porous media: Upscaling from single-pore to sample-scale model. *Water Resources Research*, *35*(12), 3591–3605. https://doi.org/https://doi.org/10.1029/1999WR900262

Pancras, T., Schrauwen, G., Held, T., Baker, K., Ross, I., & Slenders, H. (2016). *Environmental fate and effects of poly-and perfluoroalkyl substances (PFAS) Prepared for the Concawe Soil and Groundwater Taskforce (STF/33)*.

Parsons, J., Saez, M., Dolfing, J., & De Voogt, P. (2008). Biodegradation of Perfluorinated Compounds. *Reviews of Environmental Contamination and Toxicology*, *196*, 53–71. https://doi.org/10.1007/978-0-387-78444-1_2

Pedone, L., Chillura Martino, D., Caponetti, E., Floriano, M. A., & Triolo, R. (1997). *Determination of the Composition of Mixed Hydrogenated and Fluorinated Micelles by Small Angle Neutron Scattering*. https://pubs.acs.org/sharingguidelines

Peng, S., & Brusseau, M. (2005). Impact of soil texture on air-water interfacial areas in unsaturated sandy porous media. *Water Resources Research - WATER RESOUR RES*, *41*. https://doi.org/10.1029/2004WR003233

Psillakis, E., Cheng, J., Hoffmann, M. R., & Colussi, A. J. (2009). Enrichment Factors of Perfluoroalkyl Oxoanions at the Air/Water Interface. *The Journal of Physical Chemistry A*, *113*(31), 8826–8829. https://doi.org/10.1021/jp902795m

Regenesis. (2020). *Plumestop liquid activated carbon*. Https:// Regenesis.Com/En/Remediation-Products/Plumestop-Liquidactivated-Carbon/.

Rutherford, K. W., & Johnson, P. C. (1996). Effects of Process Control Changes on Aquifer Oxygenation Rates During In Situ Air Sparging in Homogeneous Aquifers. *Groundwater Monitoring & Remediation*, *16*(4), 132–141. https://doi.org/https://doi.org/10.1111/j.1745-6592.1996.tb01180.x

Schaefer, C. E., DiCarlo, D. A., & Blunt, M. J. (2000). Experimental measurement of air-water interfacial area during gravity drainage and secondary imbibition in porous media. *Water Resources Research*, *36*(4), 885–890. https://doi.org/10.1029/2000WR900007

Sethi, R., & Di Molfetta, A. (2019). *Groundwater Engineering: A Technical Approach to Hydrogeology, Contaminant Transport and Groundwater Remediation* (1st ed. 2019.). Springer Nature. https://doi.org/10.1007/978-3-030-20516-4

Simon, J. A., Abrams, S., Bradburne, T., Bryant, D., Burns, M., Cassidy, D., Cherry, J., Chiang, S.-Y. (Dora), Cox, D., Crimi, M., Denly, E., DiGuiseppi, B., Fenstermacher, J., Fiorenza, S., Guarnaccia, J., Hagelin, N., Hall, L., Hesemann, J., Houtz, E., … Wice, R. (2019). PFAS Experts Symposium: Statements on regulatory policy, chemistry and analytics, toxicology, transport/fate, and remediation for per- and polyfluoroalkyl substances (PFAS) contamination issues. *Remediation Journal*, *29*(4), 31–48. https://doi.org/https://doi.org/10.1002/rem.21624

Sorengard, M., Kleja, D. B., & Ahrens, L. (2019). Stabilization of per- and polyfluoroalkyl substances (PFASs) with colloidal activated carbon (PlumeStop®) as a function of soil clay and organic matter content. *Journal of Environmental Management*, *249*. https://doi.org/10.1016/j.jenvman.2019.109345

Sunderland, E., Hu, X., Dassuncao, C., Tokranov, A., Wagner, C., & Allen, J. (2018). A Review of the Pathways of Human Exposure to Poly- and Perfluoroalkyl Substances (PFASs) and Present

Understanding of Health Effects. *Journal of Exposure Science & Environmental Epidemiology*, *29*. https://doi.org/10.1038/s41370-018-0094-1

Suthersan, S. S., Horst, J., Scnobrich, M., Welty, N., & McDonough, J. (2017). *REMEDIATION ENGINEERING Design Concepts Second Edition*. https://doi.org/https://doi.org/10.1201/9781315367088

USEPA. (1999). *Use of Monitored Natural Attenuation at Superfund, RCRA Corrective Action, and Underground Storage Tank Sites*.

Vecitis, C. D., Park, H., Cheng, J., Mader, B. T., & Hoffmann, M. R. (2008). Enhancement of Perfluorooctanoate and Perfluorooctanesulfonate Activity at Acoustic Cavitation Bubble Interfaces. *The Journal of Physical Chemistry C*, *112*(43), 16850–16857. https://doi.org/10.1021/jp804050p

Vierke, L., Staude, C., Biegel-Engler, A., Drost, W., & Schulte, C. (2012). *Perfluorooctanoic acid (PFOA)-main concerns and regulatory developments in Europe from an environmental point of view*. http://www.enveurope.com/content/24/1/16

Wang, Z., Cousins, I. T., Scheringer, M., & Hungerbühler, K. (2013). Fluorinated alternatives to long-chain perfluoroalkyl carboxylic acids (PFCAs), perfluoroalkane sulfonic acids (PFSAs) and their potential precursors. *Environment International*, *60*, 242–248. https://doi.org/https://doi.org/10.1016/j.envint.2013.08.021

Yan, N., Ji, Y., Zhang, B., Zheng, X., & Brusseau, M. (2020). Transport of GenX in Saturated and Unsaturated Porous Media. *Environmental Science & Technology*, *54*. https://doi.org/10.1021/acs.est.9b07790

Yi, S., Harding-Marjanovic, K. C., Houtz, E. F., Gao, Y., Lawrence, J. E., Nichiporuk, R. V, Iavarone, A. T., Zhuang, W.-Q., Hansen, M., Field, J. A., Sedlak, D. L., & Alvarez-Cohen, L. (2018). Biotransformation of AFFF Component 6:2 Fluorotelomer Thioether Amido Sulfonate Generates 6:2 Fluorotelomer Thioether Carboxylate under Sulfate-Reducing Conditions. *Environmental Science & Technology Letters*, *5*(5), 283–288. https://doi.org/10.1021/acs.estlett.8b00148

Yu, Q., Zhang, R., Deng, S., Huang, J., & Yu, G. (2009). Sorption of perfluorooctane sulfonate and perfluorooctanoate on activated carbons and resin: Kinetic and isotherm study. *Water Research*, *43*(4), 1150–1158. https://doi.org/10.1016/j.watres.2008.12.001

Zahm, S., Bonde, J., Chiu, W., Hoppin, J., Kanno, J., Abou-Elwafa Abdallah, M., Blystone, C., Calkins, M., Dong, G.-H., Dorman, D., Fry, R., Guo, H., Haug, L., Hofmann, J., Iwasaki, M., Machala, M., Mancini, F., Maria-Engler, S., Møller, P., & Schubauer-Berigan, M. (2023). Carcinogenicity of perfluorooctanoic acid and perfluorooctanesulfonic acid. *The Lancet Oncology*, *25*. https://doi.org/10.1016/S1470-2045(23)00622-8

Zhang, S., Szostek, B., McCausland, P., Wolstenholme, B., Lu, X., Wang, N., & Buck, R. (2013). 6:2 and 8:2 Fluorotelomer Alcohol Anaerobic Biotransformation in Digester Sludge from a WWTP under Methanogenic Conditions. *Environmental Science and Technology*, *47*. https://doi.org/10.1021/es4000824

Zhao, L., Bian, J., Zhang, Y., Zhu, L., & Liu, Z. (2014). Comparison of the sorption behaviors and mechanisms of perfluorosulfonates and perfluorocarboxylic acids on three kinds of clay minerals. *Chemosphere*, *114*, 51–58. https://doi.org/https://doi.org/10.1016/j.chemosphere.2014.03.098

APPENDIX A: Preliminary tests in the laboratory

In Figure A.1 the list of preliminary tests of air-sparging is presented. In particular, there is a description of the substances used in these tests, the sand types, the sparging time, the main objectives, the results obtained from the tests and then the solutions found to solve problems related to the experimental setup.

PRELIMINARY TEST IN THE LABORATORY

nr.	date	substances	sand type	sparging hours	main objective	results	solutions
1	24/02/2025	Tap water	Coarse sand with heterogeneities		Sand packing - saturation - porosity calculation		
2	28/02/2025	Tap water	Fine sand with heterogeneities		Implementation of air sparging	Too high flowrate without flowmeter so fractures in the solid matrix	Implementation of a flowmeter 60 cm3/min - 300 cm3/min
3	03/03/2025	Tap water	Homogeneous coarse sand		Creation of unsaturated layer saturated from above	After 24 h water evaporation because column without covering	Implementation of PARAFILM membrane over the top of the column
4	03/03/2025	Tap water	Homogeneous fine sand		Creation of unsaturated layer saturated from above	After 24 h water evaporation because column without covering	Implementation of PARAFILM membrane over the top of the column
5	07/03/2025	Tap water + EOSIN and NaCl	Homogeneous fine sand		Creation of unsaturated layer with wet sand - tracer addition - calculation of residual saturation in unsaturated layer		
6	07/03/2025	Tap water + EOSIN and NaCl	Homogeneous coarse sand		Creation of unsaturated layer with wet sand - tracer addition - calculation of residual saturation in unsaturated layer		
7	13/03/2025	Tap water + EOSIN and NaCl + Persil detergent	Homogeneous coarse sand	17 h	Tracer and detergent addition - air sparging	Concentration of free water above the sand column. Sand no more completely saturated.	As unsaturated layer, use of dry sand instead of wet sand
8	25/03/2025	Tap water + Methylene blue + Persil detergent	Homogeneous coarse sand	20 h	Creation of unsaturated layer with dry sand - tracer and detergent addition - air sparging	Detergent not completely migrated upwards because Persil detergent too dense	Dilution of Persil detergent
9	31/03/2025	Tap water + Methylene blue + Persil detergent	Homogeneous coarse sand	72 h	Detergent dilution - air sparging	Detergent and tracer migration but evaporation of water	Reduction of number of holes through the PARAFILM membrane

Figure A.1 Specifications on preliminary tests in the laboratory

The substances used in preliminary tests are shown in Fig. A.2-4.

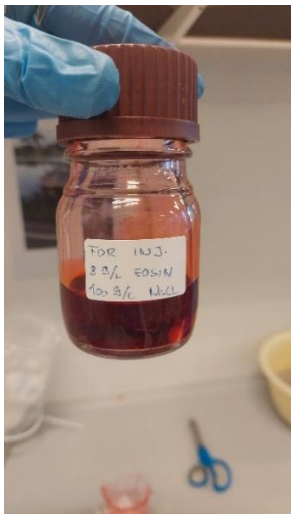

Figure A.2 Tracer EOSIN and NaCl

Figure A.3 Tracer Methylene Blue

Figure A.4 Persil detergent

The following pictures illustrate the issues encountered during the test due to setup errors (Fig. A.5-7).

Figure A.5 Fractures in the column caused by too high air flowrate. Test nr.2 on date 28/02/25.

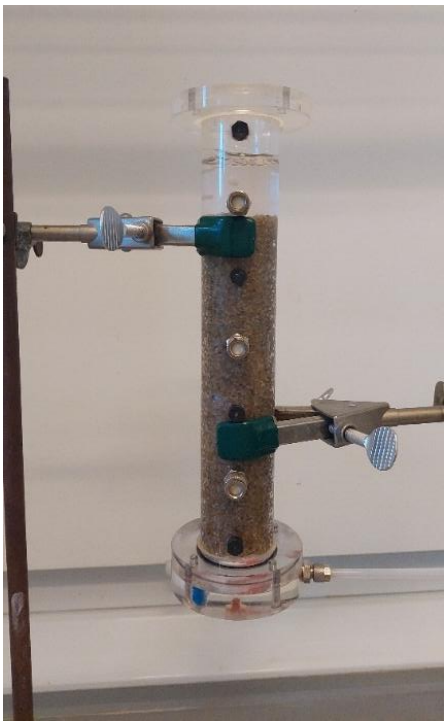

Figure A.6 Free water above the sand, caused by too much amount of water in the system. Test nr.7 on date 13/03/25.

Figure A.7 Persil detergent mostly concentrated at the bottom of the column because too dense. Certain migration of the detergent attached to air bubbles. No migration of Methylene blue showing no advective water flux. Test nr.8 on date 25/03/25.

APPENDIX B: Solid matrices properties

Egenskaber	Prøvningsmetode	Typisk værdi	Variationsbånd
Bulk densitet . Kg/m³	EN 12902	1586	1530-1620
Kornulighedskoefficient - D60/D10	EN 12902	1,3	<1,5
Chloridindhold - %	DS/EN 1744-1	0,012	

Sigestørrelse - mm	1	0,9	0,8	0,71	0,63	0,5	0,4	0,355	0,315	0,25	0,125	0,063
Gennemfald - vægt-%	100	99,6	96,3	86,1	63,8	9,7	1,1	0,5	0,3	0,0	0,0	0,0

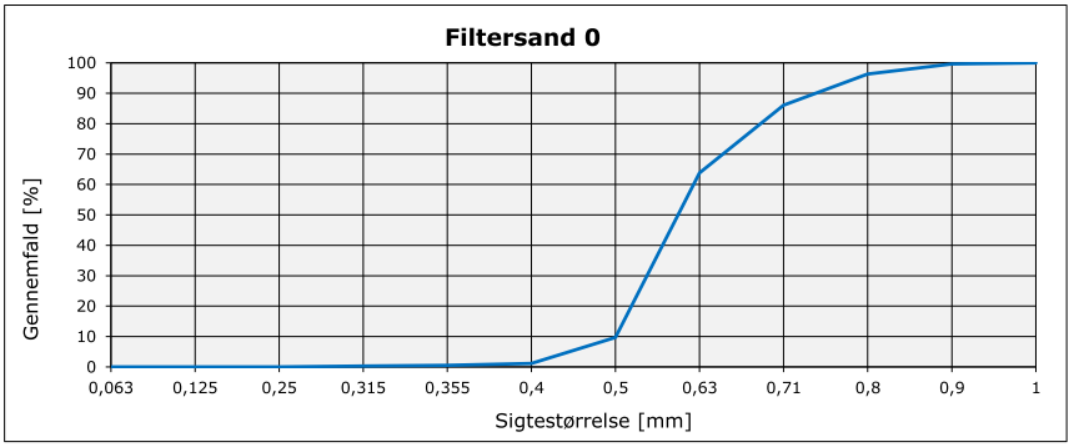

Kemisk analyse						
Type	Fe_2O_3	Al_2O_3	K_2O	CaO	Na_2O	SiO_2
vægt-%	0,117	0,805	0,365	0,068	0,15	98,11

Figure B.1 Grain size distribution curve of fine sand nr.0.

Egenskaber	Prøvningsmetode	Typisk værdi	Variationsbånd
Bulk densitet . Kg/m³	EN 12902	1630	1580-1650
Kornulighedskoefficient - D60/D10	EN 12902	1,4	<1,5
Chloridindhold - vægt %	DS/EN 1744-1	0,012	-
Hydraulisk ledningsevne - K (m/s)	DS 415	8,4 X 10^{-3}	-

Sigestørrelse - mm	2,5	2,24	2	1,8	1,6	1,4	1,25	1,12	1	0,9	0,8	0,71
Gennemfald - vægt-%	100	100	100	99	92	74	56	37	18	7	3	1

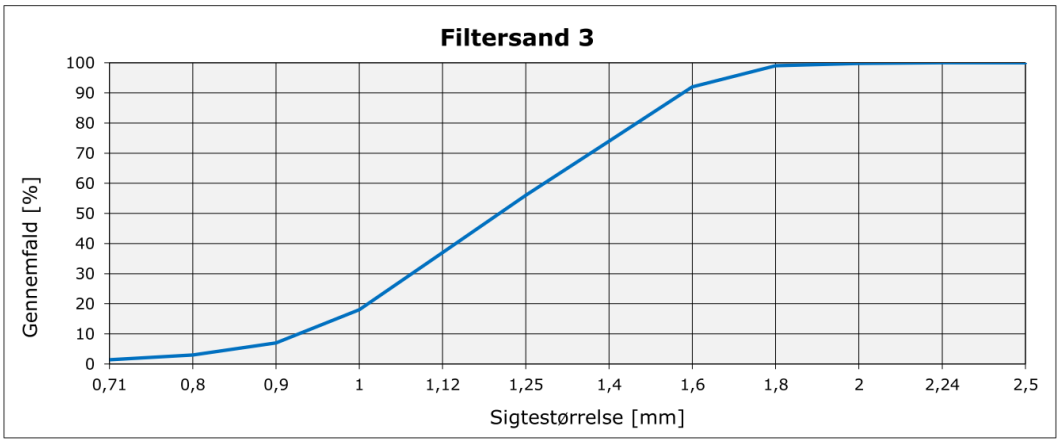

Kemisk analyse						
Type	Fe_2O_3	Al_2O_3	K_2O	CaO	Na_2O	SiO_2
vægt-%	0,123	0,544	0,215	0,076	0,107	98,56

e

Figure B.2 Grain size distribution curve of coarse sand nr.3.

Egenskaber	Prøvningsmetode	Typisk værdi	Variationsbånd
Bulk densitet . Kg/m³	EN 12902	1582	1530-1630
Kornulighedskoefficient - D60/D10	EN 12902	1,4	<1,5
Chloridindhold - vægt %	DS/EN 1744-1	0,0	-
Hydraulisk ledningsevne - K (m/s)	DS 415	$4{,}02 \times 10^{-2}$	-

Sigestørrelse - mm	7,1	6,3	5,6	5	4,5	4	3,55	3,15	2,8	2,5	2,24	2
Gennemfald - vægt-%	100	100	100	100	100	99	92	72	47	26	15	9

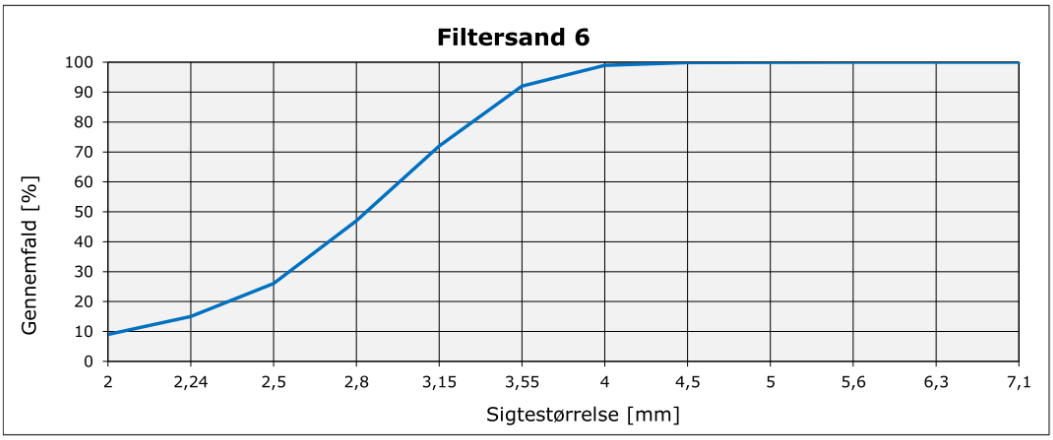

Kemisk analyse						
Type	Fe_2O_3	Al_2O_3	K_2O	CaO	Na_2O	SiO_2
vægt-%	1,0341	2,8842	0,8417	0,9263	0,6961	92,106

Figure B.3 Grain size distribution curve of coarser sand nr.6, used at the bottom of the column to homogenously distribute the air flow.

TOC analysis results are also displayed in Fig. B.4

Controls (n=3)	**TOC - g/kg**
ERM - CC144 - Ref. value (g/kg)	360
Cert Ref Standard, soil (%RSD)	3%
Cert Ref Standard, soil (%Recovery)	95%
SampleIdentity	**TOC - g/kg**
B1 – fine sand (nr.0)	< 10 mg/g
B2 – coarse sand (nr.3)	<10 mg/g
B3 – coarse sand (nr.6)	<10 mg/g

Figure B.4 TOC analysis results

APPENDIX C: PFAS characteristics

PFAS details and chemical characteristics are displayed in Figure C.1. These data were collected through the CompTox Chemicals Dashboard by EPA (United States Environmental Protection Agency). Instead, the partition coefficients to solid phase and to air-water interface values were calculated as shown in Chapter 5.10 and Appendix H.2.

Compound	CAS number	Complete name	Molecular formula	Chain length	Type of PFAS	Polarity of functional head	Functional head group	Molecular weight (g/mol)	Molar volume (cm3/mol)	Kd (l/kg)	Kia (cm-1)
PFOA	335-67-1	Perfluorooctanoic acid	C8HF15O2	Long	Terminal	Anionic	Perfluorocarboxylic acid	414.07	237	0.17	0.0025
PFHpA	120885-29-2	Perfluoroheptanoic acid	C7F13O2	Short	Terminal	Anionic	Perfluorocarboxylic acid	363.05	210	0.13	0.0008
PFOS	1763-23-1	Perfluorooctanesulfonic acid	C8HF17O3S	Long	Terminal	Anionic	Perfluorosulfonic acid	500.13	272	0.22	0.0117
PFHxS	355-46-4	Perfluorohexanesulfonic Acid	C6HF13O3S	Long	Terminal	Anionic	Perfluorosulfonic acid	400.11	217	0.19	0.0011
6:2 FTS	27619-97-2	6:2 Fluorotelomersulfonic acid	C8H5F13O3S	Short	Precursor	Anionic	Fluorotelomer sulfonic acid	428.16	250	0.37	0.0045
6:2 FTAB	34455-29-3	6:2 Fluorotelomer sulfonamide betaine	C15H19F13N2O4S	Short	Precursor	Zwitterionic	Fluorotelomer	570.37	250	0.24	0.0045
PFHxA	92612-52-7	Perfluorohexanoate	C6F11O2	Short	Terminal	Anionic	Perfluorocarboxylic acids	313.05	182	0.12	0.0002
PFPeA	2706-90-3	Perfluoropentanoic acid	C5HF9O2	Short	Terminal	Anionic	Perfluorocarboxylic acid	264.05	155	0.12	0.0001
PFBS	45187-15-3	Perfluorobutanesulfonate	C4F9O3S	Short	Terminal	Anionic	Perfluorosulfonic acids	299.09	162	0.01	0.0001
PFOSA	754-91-6	Perfluorooctanesulfonamide	C8H2F17NO2S	Long	Precursor	Anionic	Perfluoroalkane sulfonamides	499.15	278	0.07	0.0152

Figure C.1 PFAS details and chemical characteristics

Solid-phase extraction and LCMSMS analysis of PFAS.

Mikael Olsson

DTU Sustain

20250618

The samples were extracted by solid phase extraction using mix mode graphitized carbon black/weak-anion-exchange cartridges (Oasis GCB/WAX 50 mg / 200 mg / 6ml, Waters corp). The cartridges were conditioned using 1 % Ammonia in Methanol (15ml) followed by 0.3 M Formic acid (5ml). 1000 ml sample were loaded at 5 ml/min and water (10ml was used to wash the cartridge. After vacuum-drying, the PFAS were eluted by 0.1 M Formic acid in Methanol (10 ml) followed by 1% Ammonia in Methanol. The eluates were combined and dried under a gentle stream of Nitrogen until near dryness and re dissolved in 1 ml Methanol:water (50:50).

The PFAS were analyzed by High Performance liquid Chromatography – Triple Quadrupole Mass Spectrometry (8045 LC-MS, Shimadzu corp).

Chromatographic separation was achieved on a 2.1 x 50 mm, 1.6 µm PS 100Å reversed phase column (Luna Omega , Phenomenex), with 10 mM Ammonium acetate pH 4 as aqueous phase (A) and 95 % Methanol with 10 mM Ammonium acetate pH 4 (B) using the following gradient: 80% A for 0.5 min, then up to 30% B in 1.5 min, then up to 90 % B in 5 min, then up to 100% B in 0.5 min and held for 1.5 min with a column regeneration time of 3 min. The flow is kept at 0.7 ml/min and the column temperature at 40 °C. Between the pump and injector a delay column was fitted (4.6 x 50 mm, 3 µm Eclipse Plus C18, Agilent Technologies). 20 µl sample was injected at 5 µl/s.

Detection was achieved by Multiple Reaction Monitoring (MRM) with the interface temperature kept at 190 °C with 3 l/min nebulizer gas flow and 15 ml/min heating gas flow. The desolvation temperature was kept at 337 °C with the DL temperature at 200 °C and drying gas flow at 5 l/min. Collision energy (CE), dwell time and pre bias voltage for Q1 and Q3 were optimized for each compound. The interface voltage were kept at +/- 1 kV for all compounds.

Table C.1 MRM settings

Compound Name	Type	CE (V)	ESI +/-	m/z	RT range (min)

AMPR	MRM	-36	+	485.00>85.05	5.800-6.600
NTAmP	MRM	-39	+	499.00>60.05	5.800-6.700
6 2 FTAB	MRM	-32	+	571.20>104.20	6.300-7.000
PFBA 13C3	MRM	9	-	215.90>172.10	1.200-2.500
PFBA	MRM	9	-	212.90>169.00	1.200-2.500
PFPeA	MRM	8	-	263.10>219.00	3.700-4.800
PFPeA 13C5	MRM	8	-	267.90>223.00	3.700-4.900
PFBS 13C4	MRM	31	-	303.00>98.90	4.100-4.700
PFBS	MRM	30	-	298.90>99.00	4.100-4.700
FBSA	MRM	26	-	297.90>78.05	5.000-5.800
PFPS	MRM	37	-	349.00>99.00	5.300-6.000
PFHxA 13C6	MRM	10	-	318.50>274.10	5.400-6.200
PFHxA	MRM	9	-	312.90>269.00	5.400-6.200
PFHpA 13C7	MRM	17	-	370.00>172.00	6.100-6.900
PFHpA	MRM	18	-	363.00>169.00	6.100-6.900
PFHxS 13C6	MRM	51	-	405.00>80.00	6.100-6.900
PFHxS	MRM	50	-	399.00>80.00	6.100-6.900
62 FTS	MRM	23	-	427.00>407.00	6.450-7.250
62 FTS C2, D4	MRM	26	-	433.00>412.00	6.450-7.250
FHxSA	MRM	31	-	397.50>77.95	6.500-7.100
PFHpS	MRM	43	-	449.00>99.00	6.550-7.350
PFOA	MRM	10	-	413.00>369.00	6.600-7.400
PFOA C13	MRM	12	-	421.00>376.00	6.600-7.400
PFOS	MRM	52	-	498.80>80.00	6.900-7.700
PFOS C13	MRM	44	-	507.00>99.00	6.900-7.700
PFNA 13C9	MRM	12	-	472.00>427.00	7.000-7.800
PFNA	MRM	11	-	463.00>418.90	7.000-7.800
82 FTS	MRM	28	-	526.80>506.80	7.000-8.200
PFNS	MRM	52	-	548.80>98.90	7.220-8.000
PFDA 13C9	MRM	12	-	522.00>477.00	7.300-8.100
PFDA	MRM	12	-	513.00>468.90	7.300-8.100
PFOSA 13C8	MRM	39	-	506.00>78.00	7.300-8.100
PFOSA	MRM	39	-	498.00>78.00	7.300-8.100
PFDS	MRM	53	-	598.90>80.00	7.500-8.300
PFUdA 13C	MRM	14	-	572.00>528.00	7.600-8.400
PFuDA	MRM	12	-	562.90>519.00	7.600-8.400
PFUnDS	MRM	55	-	648.90>80.00	7.750-8.550
PFDoA 13C12	MRM	13	-	625.00>580.10	7.800-8.600
PFDoA	MRM	11	-	613.00>569.00	7.800-8.600
PFDoDS	MRM	54	-	698.90>80.00	7.950-8.750
PFTrDA	MRM	13	-	663.00>619.00	8.100-8.800
PFTrDS	MRM	55	-	748.90>80.00	8.120-8.900
PFTeDA 13C2	MRM	15	-	715.00>669.90	8.200-9.000
PFTeDA	MRM	15	-	713.10>669.00	8.200-9.000

Commercial mixes for calibration standards and 13C labelled internal standards are used.

Calibration standards

https://www.lgcstandards.com/DK/en/PFAS-Mixture-Food-Testing-EU-2022-1431-10-g-mL-in-Methanol-Water/p/DRE-A30000074MW

Internal standards

https://www.lgcstandards.com/DK/en/Method-8327-Surrogate-Spiking-Mixture-Methanol-w-4-Molar-Equivalents-NaOH-/p/CIL-ES-5643-A

APPENDIX D: Experimental procedure

This appendix contains step-by-step descriptions of the key stages of the experimental procedure for column preparation, prior to the start of the air sparging process. The experimental procedure consists of four main steps (see Chapter 5.5). After each addition of material (sand or water), the column is weighed (Fig. D.1).

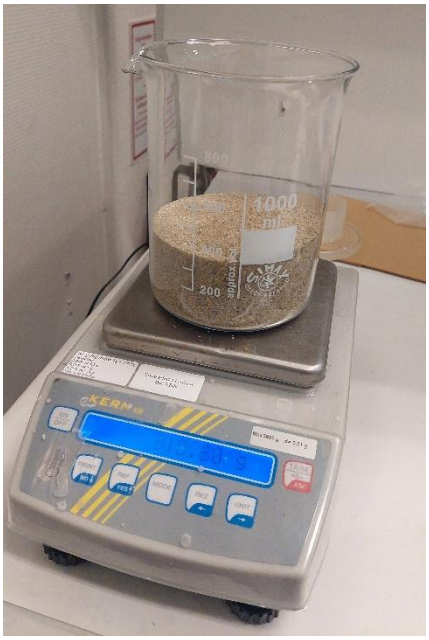

Figure D.1 Weighing sand layer

The first step involves placing a fine metal mesh and a layer of coarse sand at the bottom of the column. Next, the PFAS solution (Fig. D.2) is prepared by adding it to a pre-measured volume of clean sand in a glass beaker (Fig. D.3) and thoroughly mixing the two to achieve full saturation (Fig. D.4).

Figure D.2 Beaker with PFAS solution

Figure D.3 Adding PFAS solution to clean dry sand

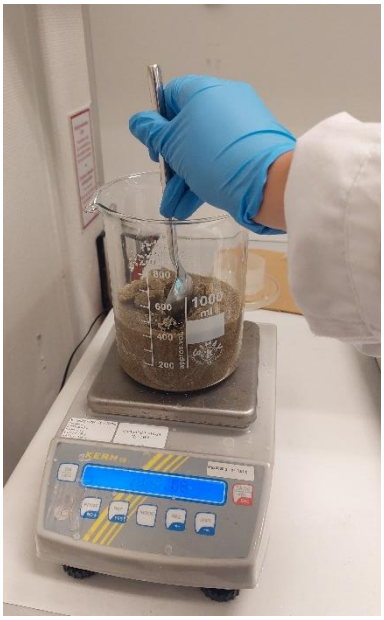

Figure D.4 Mixing PFAS solution with the sand to achieve homogeneous distribution of PFAS

The now-contaminated sand is then packed into the column using a pestle. Afterward, a layer of clean, dry sand is added up to the height of the fourth sampling port and compacted with the pestle (Fig. D.5).

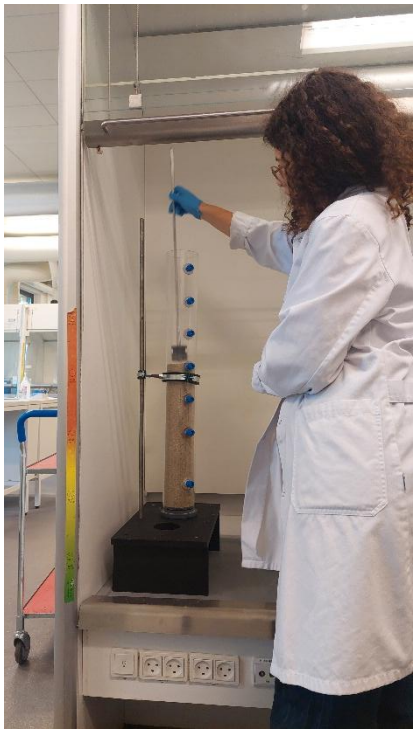

Figure D.5 Packing clean dry sand with a pestle

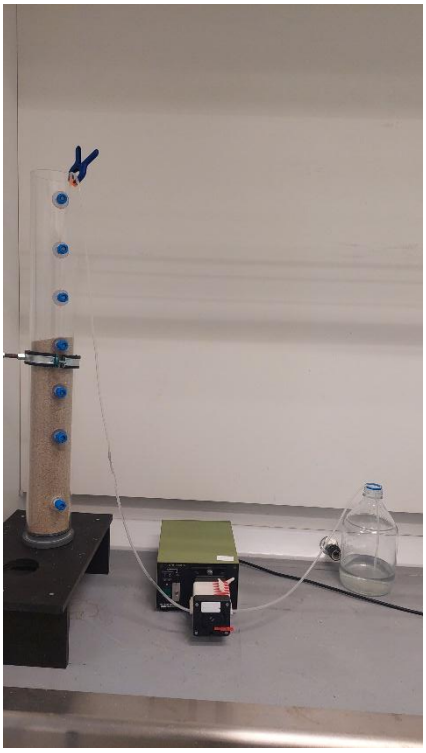

Figure D.6 Saturating the column from the top with tap water through a peristaltic pump

The column is then saturated with tap water from the top using a peristaltic pump (Fig. D.6). Once full saturation is achieved, an additional layer of clean, dry sand is placed on top to simulate the vadose zone and compacted with the pestle.

Finally, the column is connected to the flowmeter (Fig. D.7), and the air flow is initiated.

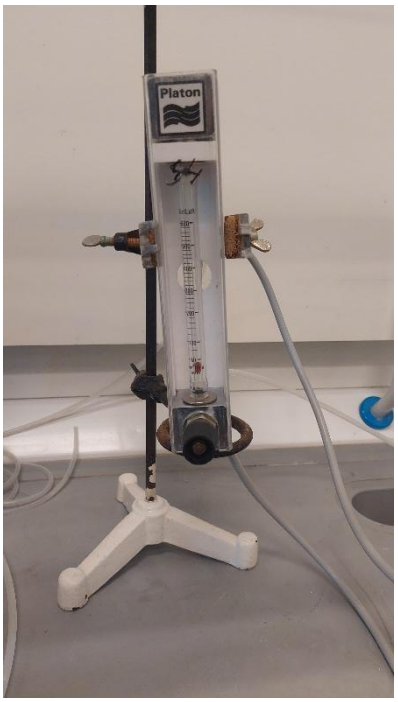

Figure D.7 Platon flowmeter 60-600 cm^3/min

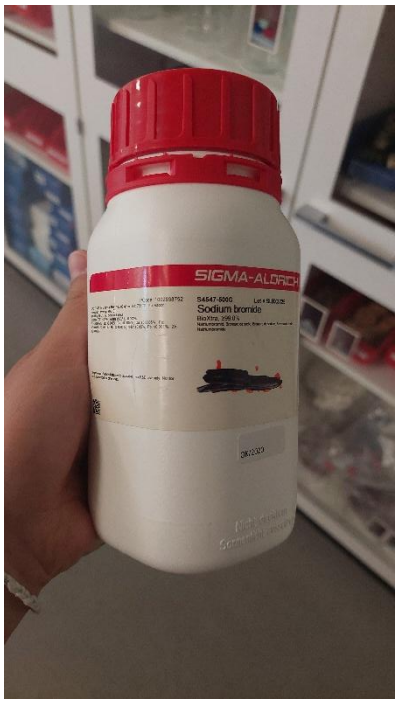

Figure D.8 Sodium bromide used in the experiment with fine sand

In the experiment with fine sand, sodium bromide (Fig. D.8) is added to the PFAS solution as a tracer.

APPENDIX E: Sodium bromide calibration curve

The calibration curve was used to establish the relationship between NaBr concentration and EC, allowing for the indirect estimation of tracer concentration during the column experiments.

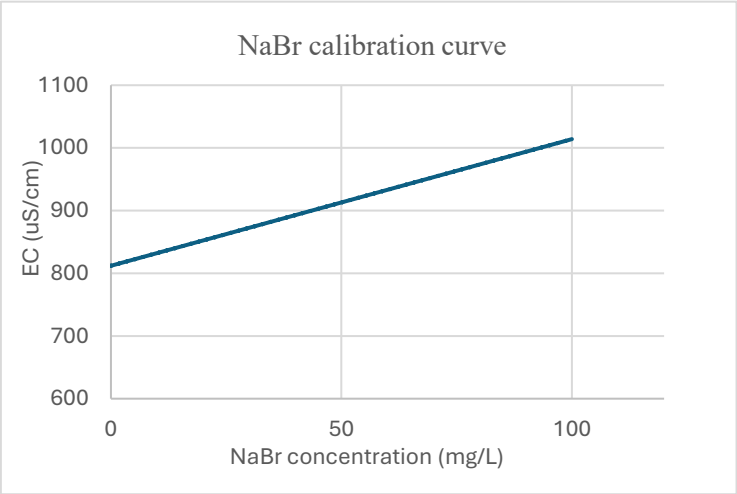

Figure E.1 NaBr calibration curve

APPENDIX F: Sampling port volumes

An investigation is conducted to explore the influence of the selected port volumes on the accuracy of the calculated mass balance. By varying volumes assigned to each sampling port, the goal is to evaluate whether this would lead to more precise or representative results. Two cases are considered: the first assumes that the saturated section of the column is divided into four different volumes, each corresponding to one of the four sampling ports (Fig. F.1). In the second case, four equal volumes are assigned to each port, while for the remaining sections, the pore water concentration is assumed to be the average of the concentrations measured at adjacent ports (Fig. F.2). The concentration in the volume between port 1 and the bottom of the column is considered equal to the one of the first port. Smaller volumes are considered in an attempt to improve the accuracy of the concentration analysis. This decision is based on the observation that the small sample volumes collected are assumed to represent relatively large volumes within the column. Assuming a uniform concentration over such large volumes is a strong simplification and may not accurately reflect the actual spatial variability of PFAS distribution system.

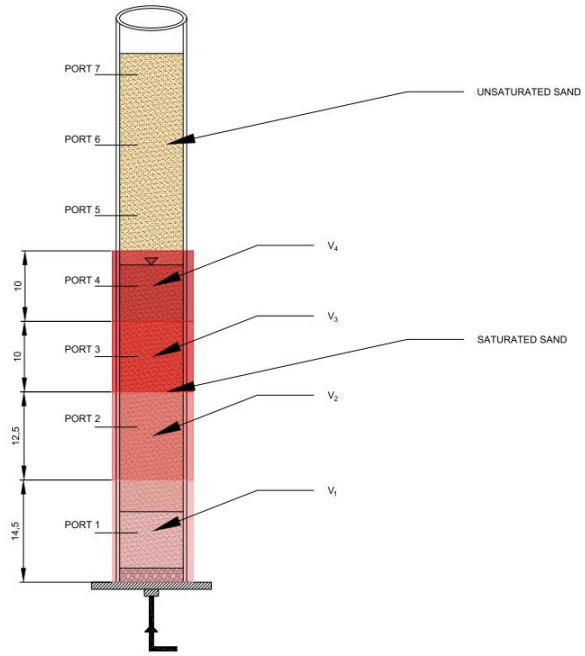

Figure F.1 Case 1: saturated column divided in four volumes

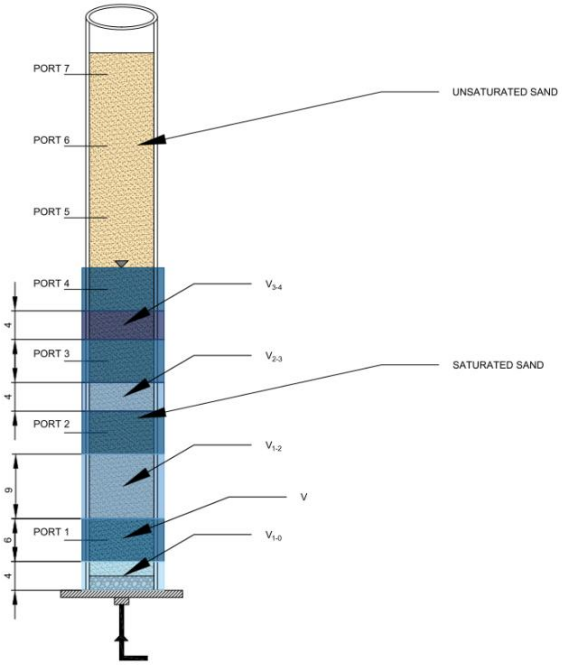

Figure F.2 Case 2: saturated column divided in eight volumes

From this analysis, the difference in mass values between the two approaches was found to be minimal. Therefore, the first case – using four different volumes for each sampling port – is selected for further calculations, as it is more practical to apply.

APPENDIX G: Concentration of each PFAS in space and in time

Concentration variation of each PFAS is represented in Figures G.1-3 for the experiment with coarse sand and in Figures G.4-6 for the experiment with fine sand.

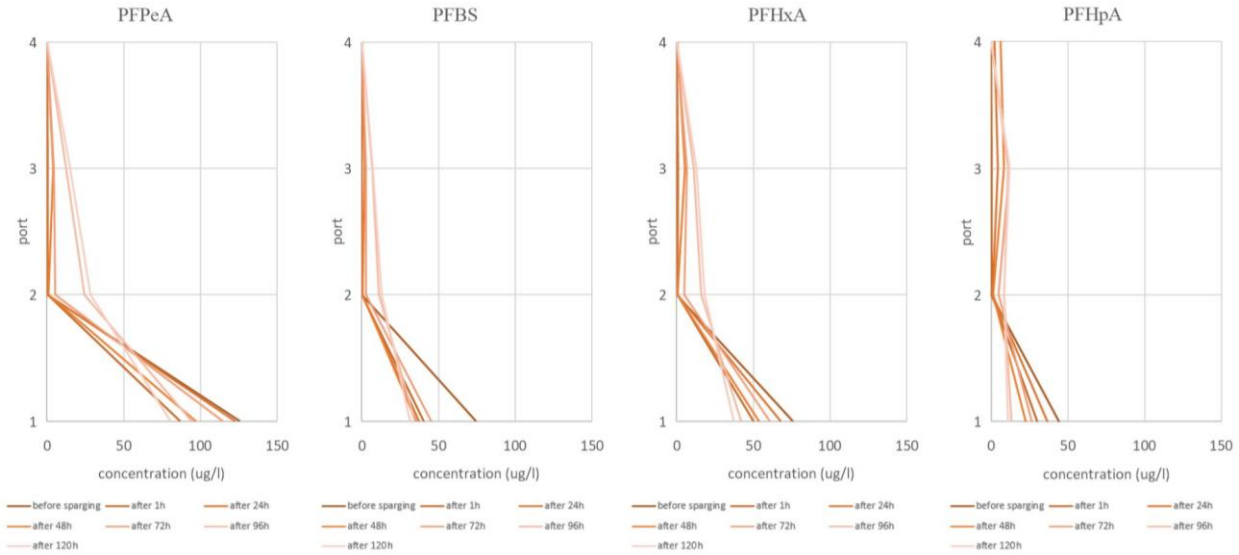

Figure G.1 Short-chained PFAS concentration variation before sparging and during sparging at different height of the column. Experiment with coarse sand.

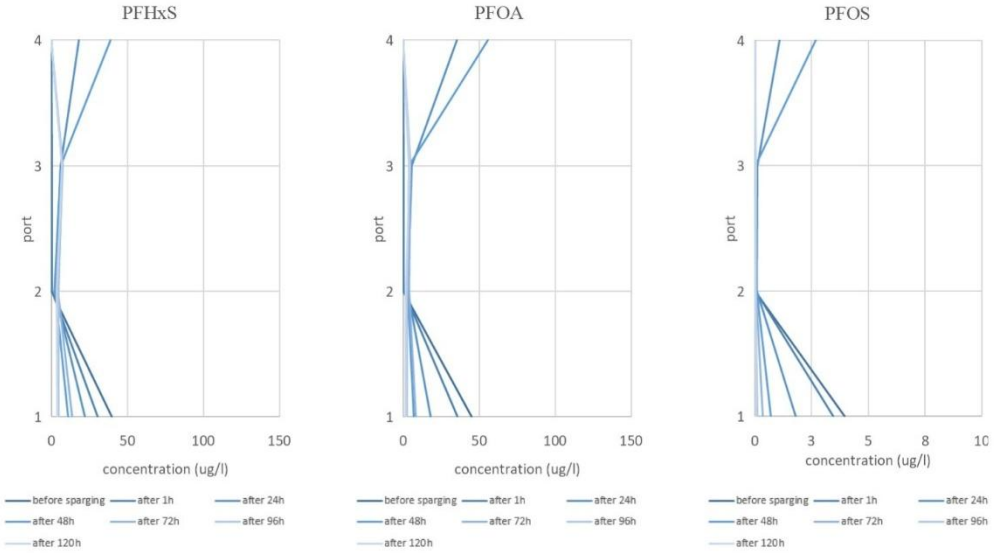

Figure G.2 Long-chained PFAS concentration variation before sparging and during sparging at different height of the column. Experiment with coarse sand.

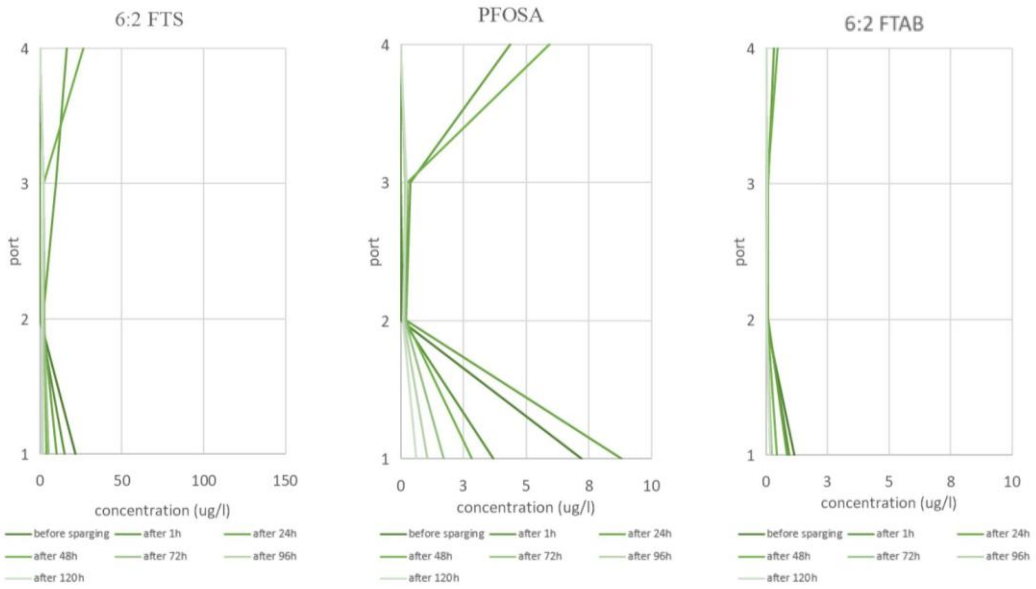

Figure G.3 Precursors concentration variation before sparging and during sparging at different height of the column. Experiment with coarse sand.

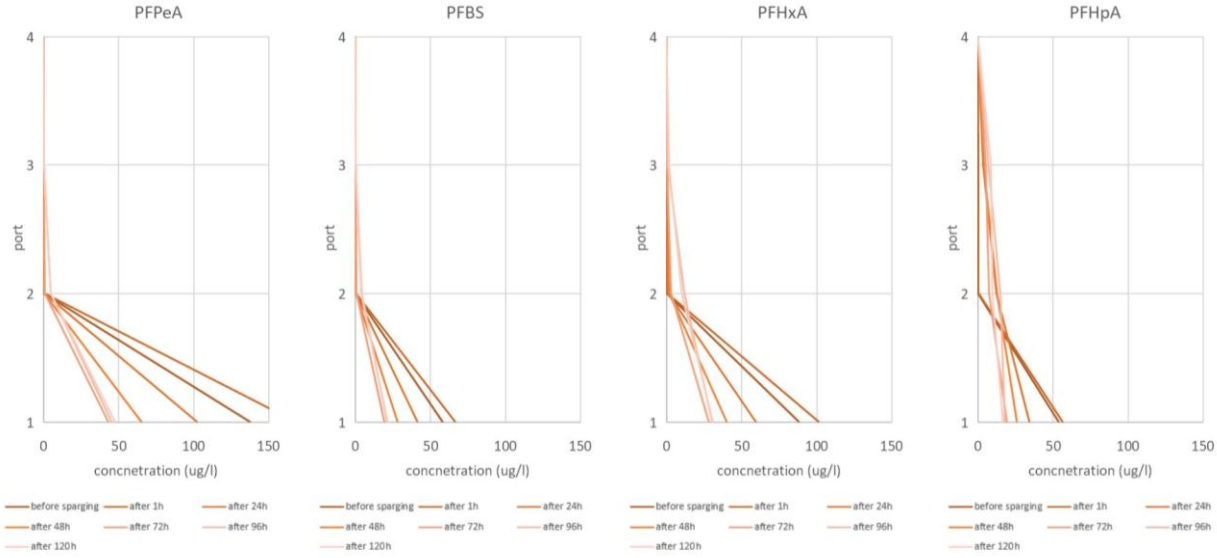

Figure G.4 Short-chained PFAS concentration variation before sparging and during sparging at different height of the column. Experiment with fine sand.

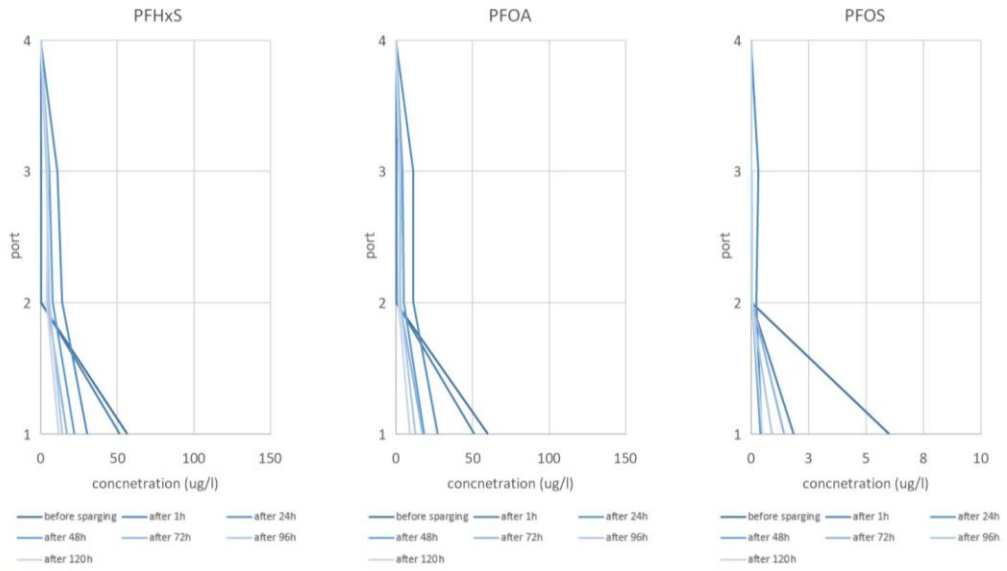

Figure G.5 Long-chained PFAS concentration variation before sparging and during sparging at different height of the column. Experiment with fine sand.

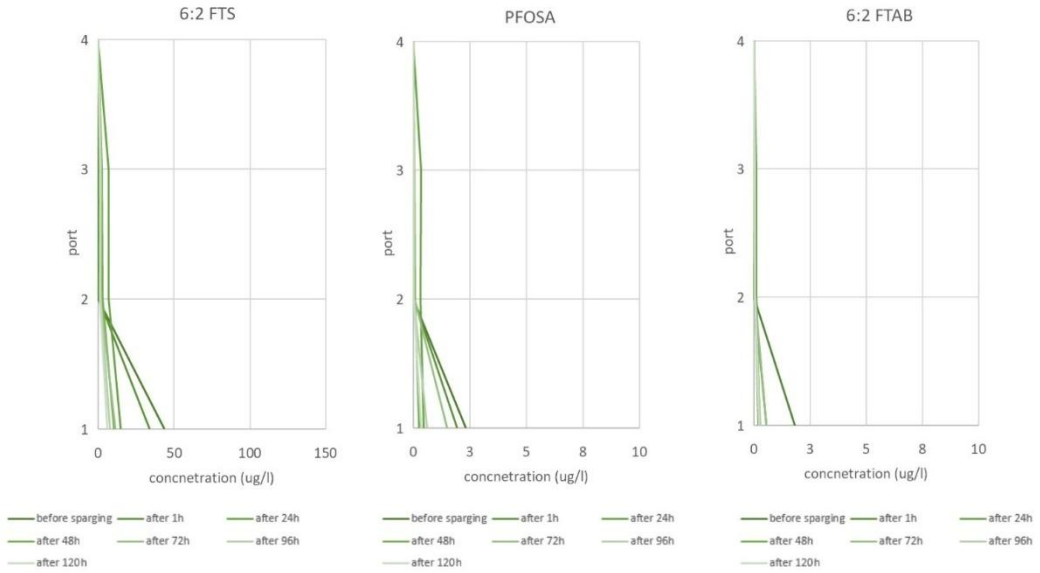

Figure G.6 Precursors concentration variation before sparging and during sparging at different height of the column. Experiment with fine sand.

APPENDIX H: Electronic files

H.1 POROSITY AND SATURATION CALCULATION

H.2 MASS BALANCE CALCULATION

H.3 PFAS PORE WATER CONCENTRATIONS, TOTAL CONCENTRATIONS AND BROMIDE CONCENTRATIONS